Leonardo Teixeira Dall'Agnol
Bacharel em Biologia e Mestre em Genética e Biologia Molecular

Deeper insights into SRB-driven biocorrosion mechanisms

Dissertação para obtenção do Grau de Doutor em Química Sustentável

Orientador: Doutor José João Galhardas de Moura, Professor Catedrático Aposentado da Faculdade de Ciências e Tecnologia da Universidade Nova de Lisboa

Juri
Presidente: Doutora Maria D'Ascenção Carvalho F. Miranda Reis
Arguentes: Doutora Marie-Françoise Libert
Doutora Ana Rosa Leal Lino
Vogais: Doutora Maria de Fátima Grilo da Costa Montemor
Doutora Cristina Maria Grade Couto da Silva Cordas
Doutora Luciana de Jesus dos Santos Peixoto

FACULDADE DE CIÊNCIAS E TECNOLOGIA
UNIVERSIDADE NOVA DE LISBOA

Julho 2013

2013

Deeper insights into SRB-driven biocorrosion mechanisms

Leonardo Teixeira Dall'Agnol

Leonardo Teixeira Dall'Agnol
Bacharel em Biologia e Mestre em Genética e Biologia Molecular

Deeper insights into SRB-driven biocorrosion mechanisms

Dissertação para obtenção do Grau de Doutor em Química Sustentável pela Universidade Nova de Lisboa, Faculdade de Ciências e Tecnologia

Orientador: Doutor José João Galhardas de Moura, Professor Catedrático Aposentado da Faculdade de Ciências e Tecnologia da Universidade Nova de Lisboa

Juri
Presidente: Doutora Maria D'Ascenção Carvalho F. Miranda Reis
Arguentes: Doutora Marie-Françoise Libert
Doutora Ana Rosa Leal Lino
Vogais: Doutora Maria de Fátima Grilo da Costa Montemor
Doutora Cristina Maria Grade Couto da Silva Cordas
Doutora Luciana de Jesus dos Santos Peixoto

Lisboa
2013

Deeper insights into SRB-driven biocorrosion mechanisms

“(…) Enquanto houver você do outro lado
Aqui do outro eu consigo me orientar
A cena repete a cena se inverte
Enchendo a minh'alma d'aquilo que
[outrora eu deixei de acreditar
Tua palavra, tua história
Tua verdade fazendo escola
E tua ausência fazendo silêncio em todo lugar

Metade de mim
Agora é assim
De um lado a poesia, o verbo, a saudade
Do outro a luta, a força e a coragem
[pra chegar no fim
E o fim é belo incerto... depende de como você vê
O novo, o credo, a fé que você deposita
[em você e só

Só enquanto eu respirar
Vou me lembrar de você
Só enquanto eu respirar (…)”

O Teatro Mágico

Acknowledgments

First I would like to thanks the BIOCOR project. BIOCOR ITN is a Marie Curie Action funded by the European Community's Seventh Framework (FP7) 2008 "People" Programme, under grant agreement n° 238579. Project website: www.biocor.eu.

I am very grateful to my supervisor, Prof. José Moura, who accepted to host me at his laboratory and always gave me his full support and encouragement, not only at the work but also for daily life. This made the adaptation (to a new country and “language”) much easier and pleasant. Also has taught to me that life at the faculty is much broader than just science and that a bit of art and music also gives us news perspectives.

I am also grateful to Prof. Isabel Moura for all the helpful discussions, support and delicious dinners over this time.

I thank all the researchers at the biological chemistry group, Marta, Patrícia, Gabi Almeida, Sofia for the all the support and discussions.

To Pablo Gonzalez and Gabi Rivas who have proved to me that not all argentines are bad people, although Pablo is still under debate. Thanks for all the pleasant discussions, lunches and for the basketball matches.

Especial thanks to Ana Teresa Lopes, the angel at the 4th floor lab, who always helped me with all my questions, requests, bureaucratic problems, laboratory training and bioreactor assembling.

I am deeply grateful to my office friends, Célia (Dra. Chefinha) and Luisa, who always listened to me, helped me with all my “dumb biologist” and “brazilian” doubts, all the rides and lunches at the sushi. Thanks for your kindness which made me feel welcome.

I express my appreciation to all my colleagues (past and present) from the lab: Raquel, Catarina, Luis, Simone, Susana, Rui Almeida, Americo, Cristiano, Alexandra, Maiti, Rute, Rashmi, Claudia, Magdalena, Patrícia, Humberto, Florina, Cintia, Diego, Rafael and Diana thanks for everything.

Thanks to Dr. Cristina Cordas who helped with the bioelectrochemistry training and experiments.

I would like to thank all my BIOCOR partners/friends who provided many memorable meetings and special moments. All my appreciation to Vincent and Jenny who have been the best managers we could ever have. To Omar, Marko (Don Corleone, wait to see you in Brazil), Madga, Yang Yi (thanks for the badmintons matches) and Oystein, thanks for your friendship and pleasant conversations during this time.

I am grateful to Prof. Wolfgang Sand and the UDE group in Essen, who hosted me for my EPS extraction and analysis training. Especial thanks to Agata with her endless energy and friendship, have shown to me that anything is possible with determination.

I really appreciated the support from Prof. Christine Dupont and her group in UCL, Louvain-la-Neuve, who helped me with the surface analysis and allowed me to stay in Belgium for 3 amazing and productive months. Thanks to Prof. Paul Rouxhet, Michel Genet, Claude, and all the friends I have made during this period. Chocolates (and beers) will never be the same again.

A really especial thanks to my lab friends and “portuguese family” Jacopo and Nathália, who in these 3 years have provided unforgettable moments in a daily basis in our “República dos Boludos”. A real friendship that will last wherever we may be.

I am grateful to my family whom always gave me their full support and love. They always have been a safe port I could count on, no matter where I am.

Finally, I could not be thankful enough to my wife Hivana, whom since the first moment, has given her love, respect, kindness and companionship. She always backed my professional and personal growth and has endured (most of) my manias. She always kept our love alive, even with an ocean apart, and I hope that this is just the beginning of a long and exciting journey together. “Só enquanto eu respirar…”

Abstract

Microbially Influenced Corrosion (MIC) is recognized as an important category of corrosion and represents one of the most challenging to study and prevent. In biocorrosion, Sulphate Reducing Bacteria (SRB) are the best suited organisms because its ability to produce biogenic hydrogen sulphide. Still little is known about the mechanisms related to corrosion involving those microorganisms. In that regard, this thesis describes the analysis of the interactions, and its consequences, between *Desulfovibrio desulfuricans* ATCC 27774 and metal surfaces using electrochemistry, of surface analysis and biochemical techniques.

The Open Circuit Potential (OCP) showed that the equilibrium of sulphide in the solution/gas phases is a key factor on determining the evolution of the corrosion process. Also it have been demonstrated that, although the trend in the behaviours remains, long measurements periods are necessary to avoid overestimations when dealing with biocorrosion. Our results also indicate that the nitrate injection strategy in oil fields has to be considered carefully as it can increase the uniform corrosion and the SRB population growth rate.

High-throughput analysis techniques were used to characterize the surface of metal plates after incubation with SRB with different respiratory substrate. The precipitation of inorganic salts as calcium and phosphates, has been detected in the samples incubated in sulphate and could be related to iron dissolution areas in the metal surface. Also micropitting underneath the bacteria cells could be observed when the bacteria were incubated. In nitrate medium, a high concentration of precipitated chloride ions was observed on the surface which could be responsible for the enhanced corrosions rates observed.

The Extracellular Polymeric Substance chemical composition corroborated the previous results regarding the iron uptake and the influence of phosphates and other functional groups in the corrosion process. The protein profile characterization has demonstrated heterogeneity of the expressed proteins depending on the respiratory substrate.

Keywords: biocorrosion, EPS, iron uptake, SRB, surface analysis.

Resumo

A biocorrosão é reconhecida como uma importante categoria de corrosão e representa uma das mais desafiantes no que toca ao seu estudo e prevenção. Em biocorrosão, as Bactérias Redutoras de Sulfato (BRS) são os organismos mais estudados devido a sua habilidade em produzir sulfureto de hidrogénio biogênico. Pouco ainda é conhecido sobre os mecanismos relacionados à corrosão envolvendo estes micro-organismos. Nesse sentido, esta tese descreve as análises das interações, e suas consequências, entre *Desulfovibrio desulfuricans* ATCC 27774 e as superfícies metálicas usando eletroquímica, ciência de superfícies e técnicas bioquímicas.

O Potencial do Circuito Aberto (PCA) mostrou que o equilíbrio do sulfureto na fase solução/gasosa é um fator chave para determinar a evolução do processo corrosivo. Também demonstrou que, apesar da tendência no comportamento se manter, medições de longa duração são necessárias para evitar superestimações quando se tratar de processos de biocorrosão. A injeção de nitrato em poços de petróleo deve ser considerada com cautela já que a mesma pode causar um aumento na corrosão do tipo uniforme e nas taxas de crescimento da população de BRS.

Técnicas de alto rendimento em análise de superfícies foram usadas para caracterizar a superfície de placas metálicas após a incubação com BRS em diferentes substratos respiratórios. A precipitação de sais inorgânicos como o cálcio e fosfatos foi detetada nas amostras incubadas em sulfato e pode estar relacionada com as áreas de dissolução de ferro observadas na superfície do metal. Em meio nitrato, a alta concentração des iões de cloro na superfície, os quais podem ser responsáveis pelo aumento das taxas de corrosão detetados quando a bactéria foi incubada nesse meio de cultura.

A composição bioquímica das Substâncias Exopoliméricas (EPS) corroborou os resultados prévious em relação à quelação de ferro e a influência dos fosfatos e outros grupos funcionais no processo corrosivo. A caracterização do perfil proteico demonstrou a heterogeneidade das proteínas expressas dependendo do substrato respiratório.

Palavras-chaves: análise de superfície, biocorrosão, BRS, EPS, quelação de ferro.

Table of Contents

Figure Index

Table Index

List of abbreviations and symbols

2DE	two-dimensional gel electrophoresis
A	Area
Abs	absorbance
AES	atomic emission spectrometer
APS	adenosine 5'-phosphosulfate
ATCC	American Type Culture Colection
ATP	adenosine triphosphate
βa	anodic Tafel constant
βc	cathodic Tafel constant
BDL	below detection limit
BSA	bovine serum albumin
CE	counter electrode
CV	cyclic voltammogram
cyt	cytochrome
Da	Dalton
DNA	deoxyribonucleic acid
DNase	desoxyribonuclease
e	electron
E	potential
E_{corr}	corrosion potential
EDX	energy dispersive x-ray spectroscopy
EIS	electrochemical impedance spectroscopy
EPR	electron paramagnetic resonance spectroscopy
EPS	Extracellular Polymeric Substances
ET	electron transfer
ETC	electron transfer chain
EVAP	evaporated
FWHM	full width at half maximum
HFR	high flow rate
HPLC	high performance liquid chromatography
HV	high vacuum
I	current
i_{corr}	corrosion current
ICP	inductively coupled plasma
ID	identification
IOB	iron oxidizing bacteria

j	current density
j_{corr}	corrosion current densities
KDO	2–keto–3–deoxyoctonate
LFR	low flow rate
µ	specific growth rate
M	metal atom
MALDI	matrix-assisted laser desorption ionization
MIC	microbially influenced corrosion
MOB	manganese oxidizing bacteria
MS	mass spectrometry
MVA	multivariate statistical analysis
MW	relative molecular weight
v	scan rate
n	number of electron transferred
NA	not applicable
NAP	periplasmic nitrate reductase
NIR	nitrite reductase
ND	not determined
NHE	normal hydrogen electrode
NM	not measured
NMR	nuclear magnetic resonance spectroscopy
MWM	molecular weight marker
m/z	mass to charge ratio
NCIMB	national collections of industrial, marine and food bacteria
OCP	open circuit potential
OD	optical density
ox	oxidized
PAGE	polyacrylamide gel electrophoresis
PCA	principal components analysis
pmf	peptide mass fingerprint
Q	charge
RE	reference electrode
red	reduced
Ref	reference
RNA	ribonucleic acid
RNAse	ribonuclease

rpm	rotation per minute
SCE	saturated calomel electrode
SDS	sodium dodecyl sulphate
SEM	scanning electron microscopy
SIMS	secondary ion mass spectrometry
SRB	sulphate reducing bacteria
Td	doubling time
ToF	time of flight
Tris	tris(hydroxymethyl)aminomethane
UV-vis	ultra violet – visible
VMN	vitamin medium
WE	working electrode
WL	weight loss
XPS	x-ray photoelectron spectroscopy

Preface

This thesis is based in a PhD project undertaken under the research project BIOCOR ITN, a Marie Curie Initial Training Network, and performed at the biological chemistry group at REQUIMTE/CQFB, Departamento de Química, Faculdade de Ciências e Tecnologia, Universidade Nova de Lisboa, from May 2010 to June 2013. This thesis is composed of an introduction and 3 publications in scientific journals.

(1) **Dall'Agnol, L.T.**, Cordas, C.M., Moura, J.J.G. (2013) "Influence of respiratory substrate in carbon steel corrosion by a SRP model organism" (Accepted in Bioelectrochemistry journal).
(2) **Dall'Agnol, L.T.**, Yang, Y., Dupont-Gillian, C. and Moura, J.J.G. "Surface Analysis of a mild steel corroded by a SRB model organism using ToF-SIMS, SEM-EDX and XPS." (In submission process).
(3) **Dall'Agnol, L.T.**, Yang, Y., Rouxhet, P., Dupont-Gillian, C. and Moura, J.J.G. "Analysis of SRB extracellular polymeric substance chemical composition and iron uptake and its relation to biocorrosion." (In submission process).

Some publications are closely related to the topic of the thesis, however are not totally comprised here or co-authored and are listed below:

Book Chapter

Dall'Agnol, L.T., Moura, J.J.G. (2013) "Sulphate Reducing Bacteria and Microbially Induced Corrosion - Bringing together H, S, N biocycles". In: Greenbook in Understanding Biocorrosion: Fundamentals & Applications. (Under review by the editors)

Journal manuscript

Yang, Y., Wikiel, A., Dall'Agnol, L.T., Eloy, P., Genet, M.J., Moura, J.J.G., Sand, W., Dupont-Gillain, C.C., Rouxhet, P.G. (2013) "Proteins dominate in conditioning layers formed by extracellular polymeric substances (EPS) from bacteria". (In submission process Colloids and Interface B: Biointerface).

Oral Communications

(1) **Dall'Agnol, L.T.**, Almeida, M. G. Cordas, C.M., Moura, J.J.G. "Bacterial diversity and influence SRB activity in metal induced corrosion within oil & gas industry" 2011. EUROCORR 2011, Stockholm, Sweden, 4-8 September 2011.
(2) **Dall'Agnol, L.T.**, Maia, L. Almeida, M. G. Cordas, C.M., Moura, J.J.G. "Influence of Respiratory Substrate in Carbon Steel Corrosion by a SRP model organism" EUROCORR 2012, Istanbul, Turkey, 9-13 September 2012
(3) **Dall'Agnol, L.T.**, Yang, Y., Dupont-Gillian, C.C., Moura, J.J.G. "Influence of Respiratory Substrate in Iron Uptake by SRB Exopolymeric Substance" EUROCORR 2013, Estoril, Portugal, 1-4 September 2013.
(4) **Yang, Y.,** Wikiel, A., Dall'Agnol, L.T., Eloy, P., Genet, M.J., Moura, J.J.G., Sand, W., Dupont-Gillain, C.C., Rouxhet, P.G. (2013) "Extracellular polymeric substances (EPS) from bacteria: chemical nature and surface activity" EUROCORR 2013, Estoril, Portugal, 1-4 September 2013.

Chapter 1

General Introduction and Objectives

Chapter 1 – General Introduction

1.1. Corrosion

1.1.1. Definition and general mechanism

Corrosion is a general word that encompasses a vast number of processes related to the deterioration of materials, although in this text we will focus on the ones that affects metals and its alloys. From the point of view of thermodynamics, corrosion is a natural and spontaneous phenomenon as all metals are refined during the extraction procedure from its ore or mineral compounds. This refinement is attained by giving more electrons to the metal atoms present in the ore, by reducing methodologies, breaking its bonds with oxygen, water and other compounds and producing a pure metal formation that is in a thermodynamically unstable state. With exception of noble metals, all others tend to return to its more stable energy conformation by the dissipation of this stored energy, which is the basis for its oxidation also known corrosion. According to ISO 8044 standard [1], corrosion is defined as:

"Physicochemical interaction (usually of an electrochemical nature) between a metal and its environment which results in changes in the properties of the metal and which may often lead to impairment of the function of the metal, the environment, or the technical system which these form a part".

In electrochemical corrosion there are three basic components in the system (with exception of galvanic corrosion that has only the two first components): the anode (where the metal is oxidized and the dissolution occurs), the cathode (where the released electrons are utilized) and the electrolyte (a conductor solution that allows the flow of energy in the system). The representative reactions are presented below:

$$M \rightleftharpoons M^{2+} + 2\,e^{-} \tag{1.1}$$

This oxidation reaction represents the metal dissolution at the anode with the released electrons being transported to the cathode by the electrolyte where they will reduce an electron acceptor, like H^{+} in reaction (1.2):

$$2H^{+} + 2e^{-} \rightleftharpoons 2H \rightleftharpoons H_2 \tag{1.2}$$

The cathodic reagent can differ according to the pH, electrolyte composition, although hydrogen is the most common in acidic conditions.

The combination of the two half reactions lead to the formation of metallic oxides/hydroxides at the interface in a phenomenon known as passivation, which tends to slow down the rate of corrosion [2, 3].

1.1.2. Types of corrosion

Corrosion is a complex phenomenon with several possible causes and mechanisms. In this section we try to illustrate a few major categories.

When two metals with different potentials are in contact and immersed in an electrolyte, there is the formation of a galvanic cell, with the flow of electrons from the less noble material (see Fig. 1.1). The presence of concentration gradients at the surface can also trigger the development of an electrochemical cell. The uniform corrosion is characterized by the dissolution of the metal when in contact with an aggressive solution as acids, seawater and others. The erosion corrosion is a especial type of corrosion as it is not electrochemical; instead the corrosion process is physically driven by a flow and friction [2].

The pitting corrosion is one of the most problematic, since it is very difficult to detect and can evolve very quickly to deep holes leading, for example, to leakages in pipes. Some studies have shown that it can be related to inclusions in the microstructure of the metal (as Mn inclusions in carbon steel), which constitute the attack initiation site [4].

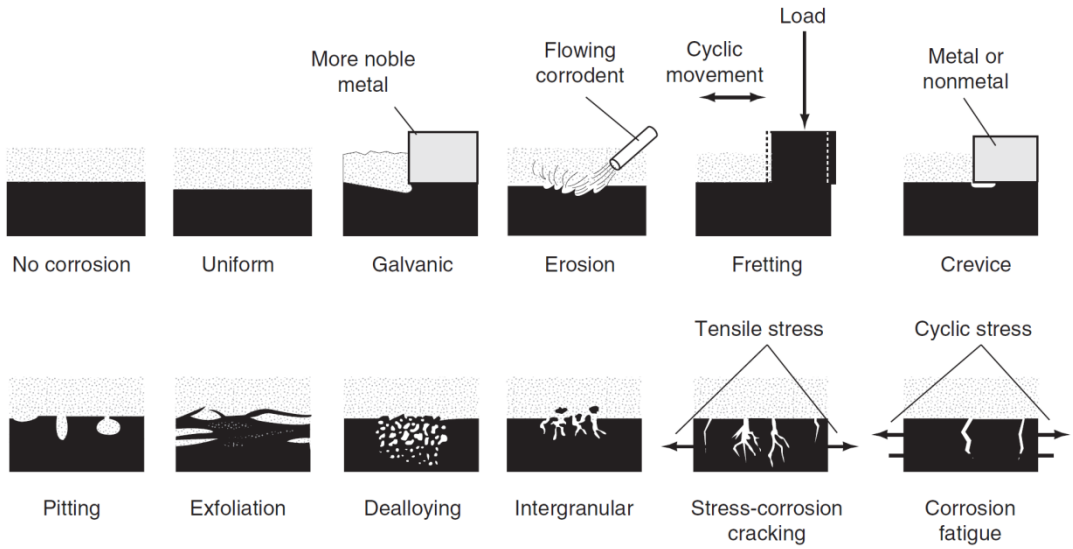

Figure 1.1: Schematic of the common forms of corrosion (From Davis, 2000).

A common tool used for the prediction of corrosion in a given system are Pourbaix diagram(s) (See Fig. 1.2). These diagrams are used to preview the thermodynamic possibility of certain reactions to occurs in a determined condition, although other variables have to be considered that can also influence the occurrence of the corrosion process. Some

of those variables are diffusion limitations, kinetics and also the local conditions as it can differ(s) substantially from the bulk medium, which is used to build the diagram. Pourbaix diagrams are representations of potential versus pH where the lines delimit the passivation and prone to corrosion areas. These diagrams are helpful to follow tendencies, but to determine the rates and reactions that actually happen it is necessary to study their kinetics by electrochemical tools such as polarization curves or electrochemical impedance spectroscopy (EIS) that will be discussed later in this chapter [3, 5].

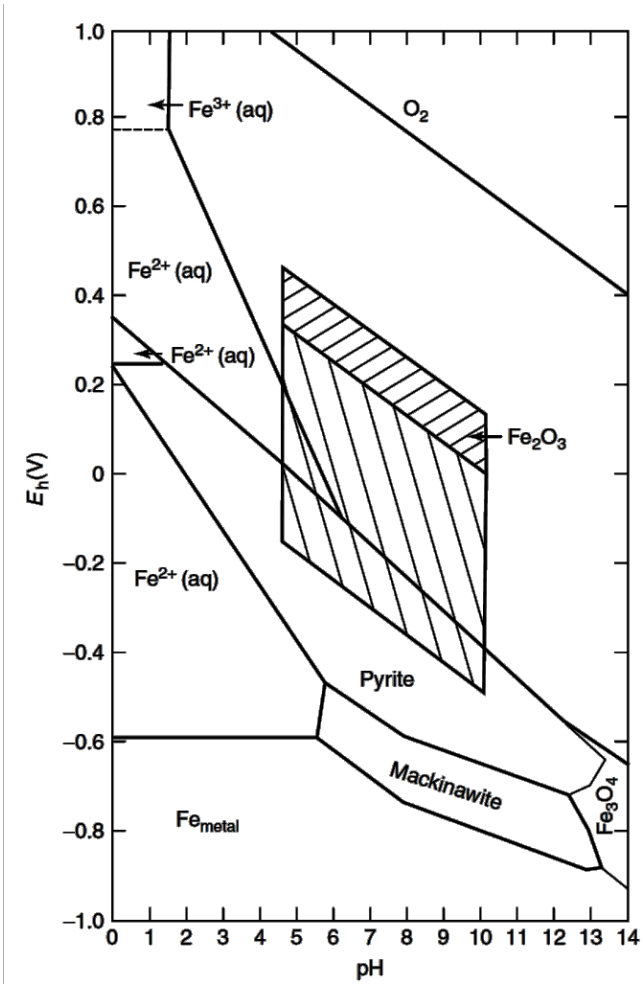

Figure 1.2: Iron stability Pourbaix diagram: water without chloride ions; total sulfide 10–2 M. (From Little and Lee, 2007).

1.2. Microbially Induced Corrosion (MIC) or Biocorrosion

MIC refers to an accelerated deterioration of metals due to the presence of microorganisms and biofilms in their surfaces. Since very early, biocorrosion has been progressively acknowledged as an important cause of material failure [6]. Biocorrosion is not restricted to a sole type of corrosion mechanism, rather it can produce localized attacks like pitting, crevice corrosion, dealloying, underdeposit corrosion, enhance erosion and galvanic corrosion, hydrogen embrittlement and stress corrosion cracking [5].

Although the electrochemical processes are the same from normal corrosion cases, the detailed mechanisms related to the microorganism influence corrosion are still poorly understood. Several authors gave protagonism to biomineralization processes and the impact of extracellular enzymes, active within the biofilm matrix, that may enhance electrochemical reactions at the biofilm-metal interface and in the biofilm matrix itself [7, 8]. The complexity of the multiple possible interactions between the microorganisms, material and environment are illustrated in Fig. 1.3:

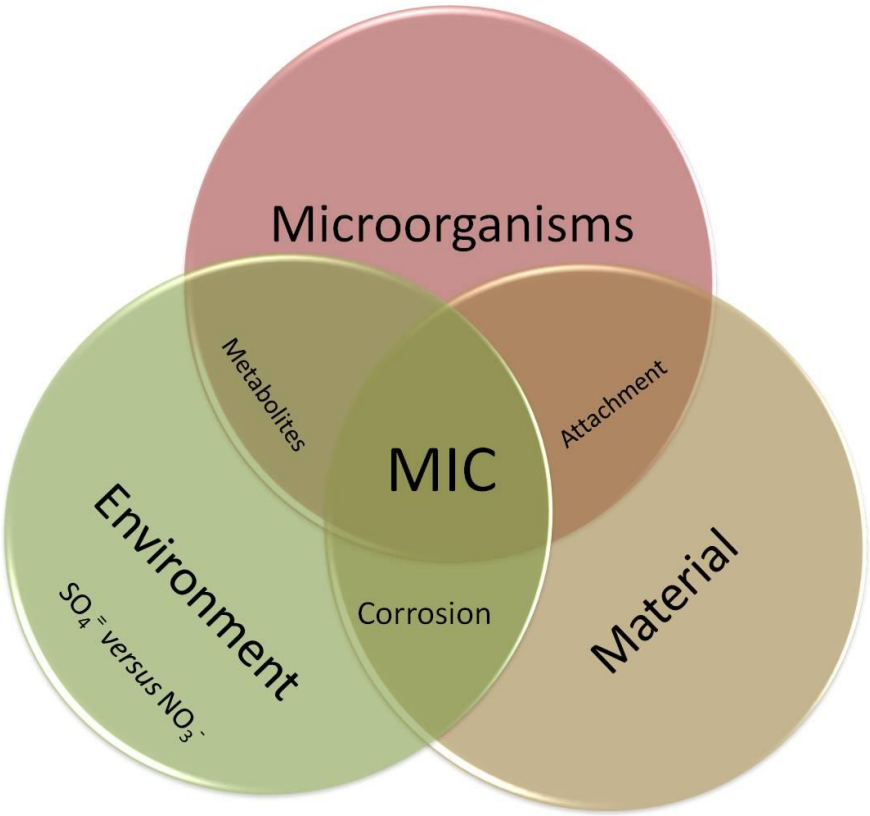

Figure 1.3: Venn diagram of variables influencing MIC.

Within the bacterial consortia present at the biofilms, SRB are considered as one of the main responsible for iron corrosion in anoxic environments (e.g pipelines) with consequent formation of black crusts related to iron sulphide and also severe localized corrosion [9, 10]. Accumulated evidence demonstrated the importance of the presence of iron sulphides produced by the SRB, in corrosion evolution [11, 12]. This observation was of fundamental importance for the Oil and Gas industry where sulphate is usually in abundance. On of the most common strategy to avoid localized corrosion and souring consists of injecting nitrate in the water to avoid sulphate reduction to occur [13].

Other groups of prokaryotes have been also acknowledged as important in biocorrosion such as manganese oxidizing bacteria (MOB), methanogens, iron oxidizing bacteria (IOB), acid producer bacteria and fungi, as seen in Table 1.1 [5, 14-19].

Table 1.1: Common microorganisms identified with MIC

Genus or specie	pH	Temperature (ºC)	Oxygen requirement	Metals affected	Metabollic process
Bacteria					
Desulfovibrio	4–8	10-40	Anaerobic	Iron and steel, stainless steels, aluminum, zinc, copper alloys	Use hydrogen in reducing SO_4^{2-} to S^{2-} and H_2S, promote formation of sulfide films
Desulfotomaculum	6-8	10-40 (some 46-74)	Anaerobic	Iron and steel, stainless steels	Reduce SO_4^{2-} to S^{2-} and H_2S
Desulfomonas		10-40	Anaerobic	Iron and steel	Reduce SO_4^{2-} to S^{2-} and H_2S
Acidithiobacillus thiooxidans	0.5-8	10-40	Aerobic	Iron and steel, copper alloys, concrete	Oxidize sulfur and sulfides to form H2SO4; damages protective coatings
Acidithiobacillus ferrooxidans	1-7	10-40	Aerobic	Iron and steel	Oxidize Fe (II) to Fe (III)
Gallionella	7–10	21-40	Aerobic	Iron and steel, stainless steels	Oxidize Fe (II) and Mn (II) to Mn (IV); promotes tubercle formation
Siderocapsa	-	-	Microaerophilic	Iron and carbon steel	Oxidize iron
Leptothrix	6.5–9	10-35	Aerobic	Iron and steel	Oxidize Fe (II) and Mn (II) to Mn (IV)
Sphaerotilus	7–10	21-40	Aerobic	Iron and steel, stainless steels	Oxidize Fe (II) and Mn (II) to Mn (IV); promotes tubercle formation
Sphaerotilus natans	-	-	-	Aluminum alloys	-

Table 1.1 (cont.): Common microorganisms identified with MIC

Genus or specie	pH	Temperature (ºC)	Oxygen requirement	Metals affected	Metabollic process
Pseudomonas	4-9	21-40	Aerobic	Iron and steel, stainless steels and Aluminum alloys	Some strains reduce Fe3+ to Fe2+
Fungi					
Hormoconis resinae	3–7	10-45	Aerobic	Aluminum alloys	Produce organic acids when metabolizing certain fuel constituents

(Adapted from Little and Lee, 2007).

The microorganisms can enhance the corrosion process by breaking the passive layer and stimulating anodic or cathodic reactions as a result of:

a. Production of acids and other corrosive compounds like ammonia and sulphide [20];
b. Consumption or degradation of the passive layer or protective coating layer [21];
c. Secretion of redox enzymes (like hydrogenases) or electrically active molecules (like cytochromes and flavins) [22-25];
d. Production of exopolymeric substances that possesses binding sites for metal ions [7, 26];
e. Creation of gradients at the surface by biofilm formation [27].

The first attempt to create a model for MIC was done by the pioneer work of von Wolzogen and van der Flugt that established the cathodic depolarization theory [28]. This theory gives key importance to the SRB capability of catalyzing hydrogen evolution by the hydrogenases enzymes, and evolved hydrogen was considered responsible for the polarization of the cathode and therefore passivation of the metal. Moreover, it is possible to establish a direct electron transfer between the enzyme and steel surface, since hydrogenase can remain active in biofilm for months even if the bacteria are not viable [29-31].

More recently, some authors have focused on the role of oxygen as final electron acceptor and consequently accelerating the global cathodic reaction. It was noted that when surfaces with an iron sulphide layer were exposed to oxygen, severe corrosion occurred. Considering this interaction between the biotic/abiotic systems, the Unifying Electron Transfer Hypothesis was proposed [32]. Both models were contested and supported by susequent studies and there are still debates about their application in the field [8, 33].

SRB have been used as experimental model for transferring laboratory conditions in real biocorrosion field cases. A special interest has been put on strains able to switch from sulphate to nitrate reduction, in order to understand the role of the sulphide vector and the influence of nitrate mitigation processes, on the metabolism of SRB at molecular level. The study of field samples before and after treatment with nitrate helps understanding the mechanisms that can inhibit the enzymes responsible for SRB contribution to biocorrosion [34-37]. This is particularly important because the biomolecules identified as being involved in electron transfer mechanisms can be used as targets for the development of more eco-efficient biocides and to evaluate, at the molecular level, the use of nitrate as a mitigation strategy.

Oxygen tolerance and adaptation to stressful conditions of SRB are important for the understanding the role of SRB in the global sulfur cycle and for controlling microbial activities and further developing biotechnological applications for environmental remediation, control of biocorrosion, energy production, wastewater treatment and mineral recovery [38-41].

1.3. Sulphate reducing bacteria - bringing together S, N and H biocycles

Comprehensive descriptions, visiting and revising of the assimilatory and dissimilatory sulphate reduction pathways, have been published in the past as on as on the impact of SRB on corrosion of metals [34, 39, 42-46].

1.3.1. Sulphate respiration

Anaerobic respiration using sulphate as the terminal electron acceptor is a central component of the global sulfur cycle. Sulphate Reducing Bacteria and the biological sulfur cycle (in parallel to the utilization of H, O, C, and N) have a major role in the interface of this element between Geology and Biology [47, 48]. SRB perform dissimilatory reduction of sulfur compounds such as sulphate, sulphite, thiosulphate and sulfur into sulphide. These organisms show metabolic flexibility and cover a high range of thermal stability. SRB are able to use lactate, pyruvate, malate, simple aromatic compounds (benzene or phenol), amino acids or high molecular weight fatty acids as carbon sources. Some species can use nitrate or molecular hydrogen as alternative respiratory substrate [38, 49, 50].

Despite they were historically classified as anaerobic microorganisms, today it is known that some genera tolerate oxygen and even grow in its presence, which reinforces its ubiquity in different environments around the globe [38].

Sulfur undergoes extensive metabolic transformations in order to be used by biological systems (see Fig. 1.4). S can be utilized in the form of sulphate produced by a series of oxidative reactions from S_2^-, S^0, and $S_2O_3^{2-}$ [34, 42]. Oxidized and reduced forms of sulfur can be interconverted by various organisms. In the biological sulfur cycle we are particularly

interested in the dissimilatory sulphate reduction: SO_4^{2-} → APS (SO_4^{2-} activated form) → $S_2O_3^{2-}$ → S_2^{-}. Three enzymes have key roles: ATP sulfurylase, APS and Sulphite reductases [39, 51]. Keller and Wall have built a very accurate model for the electron flow during sulphate reduction in *Desulfovibrio* as can be seen in Fig. 1.5.

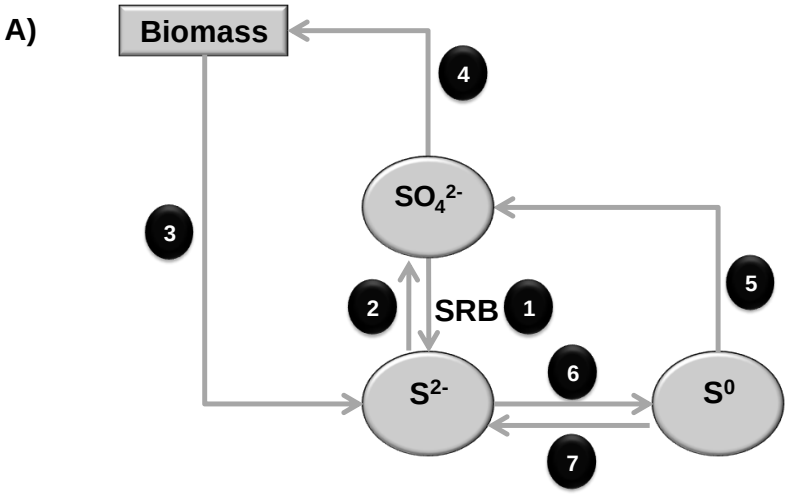

1. **Dissimilatory reduction**
2. **Biological & abiotic oxidation**
3. **Decomposition**
4. **Assimilatory reduction**
5. **Biological & abiotic oxidation**
6. **Biological & abiotic oxidation**
7. **Dissimilatory reduction**

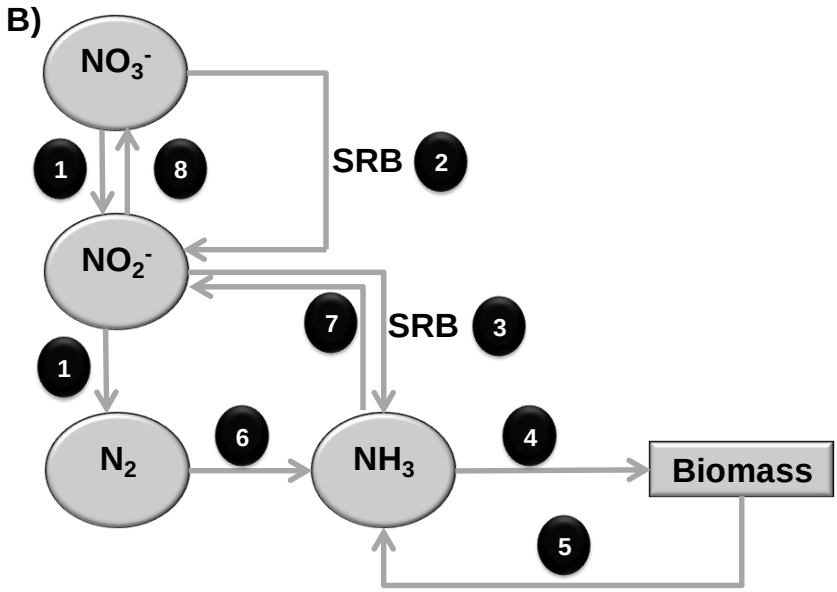

1. **Denitrification**
2. **SRB nitrate reduction**
3. **SRB nitrite reduction**
3. **Nitrification**
5. **Decomposition**
6. **Nitrogen fixation**
7. **Amines oxidation**
8. **Nitrite oxidation**

Figure 1.4: Scheme of sulphur and nitrogen biocycle. A) Sulphur cycle; B) Nitrogen cycle.

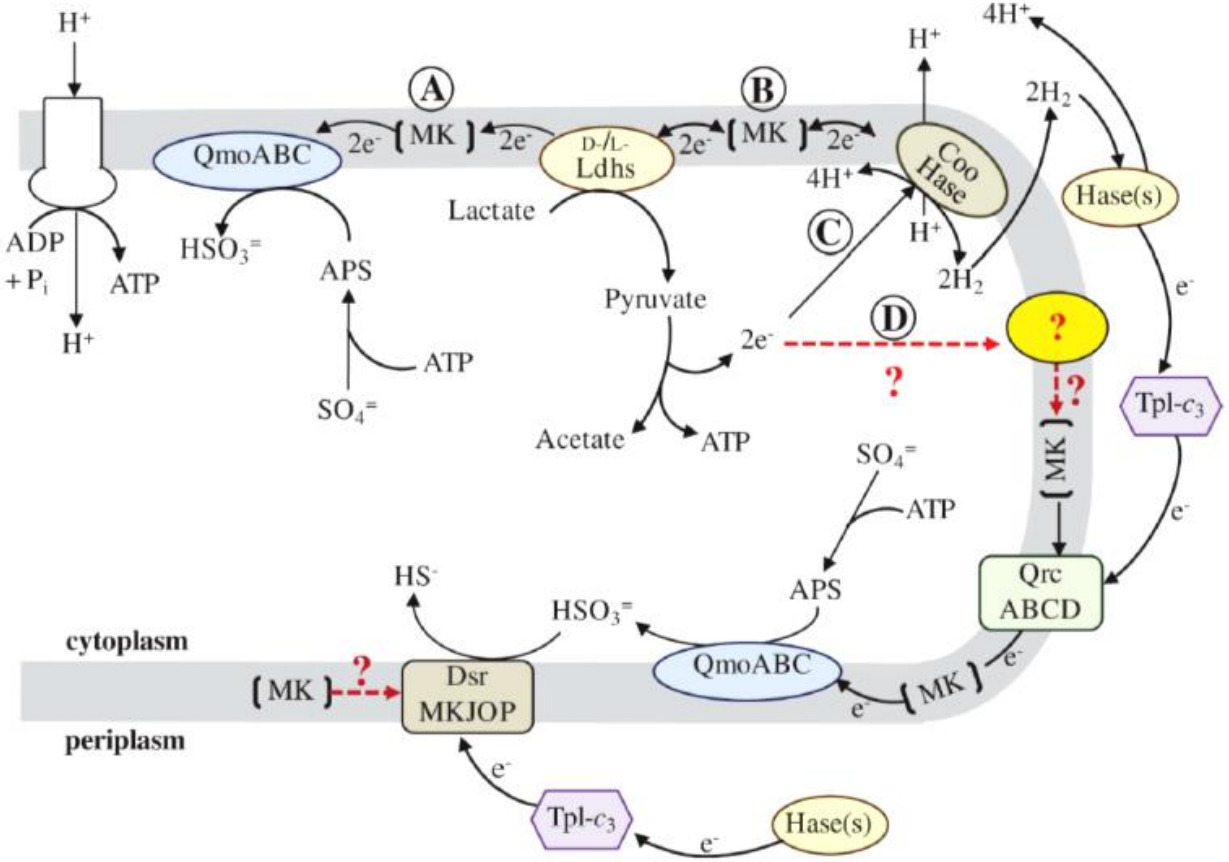

Figure 1.5: Proposed model for the flow of electrons during sulphate reduction in *Desulfovibrio vulgaris* Hildenborough. Abbreviations: QmoABC, Quinone-interacting membrane-bound oxidoreductase (DVU0848–0850); Ldhs, lactate dehydrogenases (nine annotated); CooHase, CO-induced membrane-bound hydrogenase (DVU2286–2293); Hase(s),periplasmic hydrogenases(four annotated);TpI-c3, Type-1 tetraheme cytochrome c3 (DVU3171); QrcABCD,Type-1 cytochrome c3: menaquinone oxidoreductase, formerly molybdopterin oxidoreductase (DVU0692–0695); DsrMKJOP, (DVU1290–1286);and MK, Menaquinone pool. Red, dashed lines and (?) indicate metabolic pathways for which less evidence is available. There action arrows were drawn as unidirectional for clarity of the model and electron flow. From [51].

For a long time, sulphate reducers were considered as a specialized group of bacteria that grow anaerobically reducing sulfur compounds. However, the successive discovery of many other inorganic compounds that can also serve as final electron acceptors attested the high flexibility of the energy metabolism of these organisms, especially in the case of *Desulfovibrio* species, allowing them to easily adapt to rapid environmental changes [35, 36].

In the MIC context some sulphate-reducing organisms have been scrutinized and used as model systems: *Desulfovibrio gigas (D.g.)*, a system where our group has an extended knowledge on ET components [29, 52, 53], *Desulfovibrio alaskensis (D.a.)* [10], and *Desulfovibrio desulfuricans (D.d.)* ATCC 27774. Additionally, a switch from sulphate to nitrate as respiratory substrates) [25, 54], enabling an increased dimension on the study of the mechanisms involved and of the metabolic problem.

In the biological S cycle there is particular interest in the dissimilatory sulphate reduction and the production of sulphide, one of the vectors of biocorrosion. We have been taking advantage on the information accumulated, on well characterized purified ET components using biochemical methodologies and spectroscopic tools. The role of small ET carriers has been extensively discussed (ferredoxin, flavodoxin and cytochromes, etc) [22, 55-58].

Electron transfer from pyruvate via pyruvate dehydrogenase to multiheme cytochrome c3/Hydrogenase complex with consequent hydrogen evolution, as well as the transfer of electron from molecular hydrogen via cytochrome c3/Hydrogenase complex to the sulphite reductase are relevant metabolic reactions in which small acidic ET proteins (such as ferredoxin) are involved. Hydrogenases seem to have an energetic regulatory role (see below) [22, 39, 59, 60].

Specific macromolecular interactions play a critical role in ET. Molecular recognition studies have been used in crucial proteins involved in the ET pathways of SRBs. Docking between different redox partners (cytochromes, rubredoxin, flavodoxins, ferredoxin and hydrogenase) isolated from SRB demonstrate the functionality of non-covalent protein-protein interactions occurring both in vivo and in vitro. This has been done by using a combination of independent techniques, namely, molecular docking simulations, NMR protein titrations, cross-linking experiments, microcalorimetry. Results from molecular docking can be validated by filtering the experimental data with cross and independent data obtained by site direct mutagenesis and spectroscopy [23, 61-65].

1.3.2. Nitrate *vs* sulphate utilization

As mentioned earlier, SRB reduce (beside sulphate) a number of different terminal electron acceptors (organic and inorganic compounds). The dissimilatory reduction of nitrate and nitrite (also called ammonification) can function as the sole energy-conserving process in

some SRB [66]. Two key enzymes on this metabolic route are nitrate and nitrite reductases. A very interesting example is *D.d.* ATCC 27774 that carries out the dissimilatory reduction of nitrate or nitrite to ammonia, with higher growth yields than sulphate reduction [36]. The metabolic adjustments that enable the switch in oxidizing substrates are still under debate. Little more is known besides that terminal nitrate and nitrite reductases are overexpressed when these compounds are the only electron acceptors. A comparative analysis of the total proteome of cell lysates using differential 2D electrophoresis or Mass Spectrometry, would make possible to identify the global changes on protein expression of *D.d.* ATCC 27774 induced by the alteration of the oxidizing substrate (nitrate vs sulphate), with a special emphasis on the electron transport chains [34, 47, 51, 67].

The dissimilatory nitrate reductase from *D.d.* (NAP) has a key role since all the reductive routes of the N-cycle involve the conversion of nitrate to nitrite. The 3D structure is known; the catalytic site contains Mo coordinated to two MGD cofactors, a S-atom from cysteine 140, and a sulphur ligand. Gene organization and electron pathway for nitrate reduction are available, EPR data are known under different conditions and mechanistic proposals have been advanced [36, 37, 68-70].

The nitrite reductase (NIR) form *D. desulfuricans* is a complex c-type cytochrome. Its 3D structure is known and available. Spectroscopy, reactivity and mechanism were discussed and proposed [71-74]. NIR's role in the mechanism of energy conservation is not absolutely clear and many questions on the structural organization of the electron transfer chain remain. The reduction of nitrite by SRB yields ammonia, a different path carried out by denitrifiers that reduce nitrate and nitrite to dinitrogen as seen in Fig. 1.6 [37, 75].

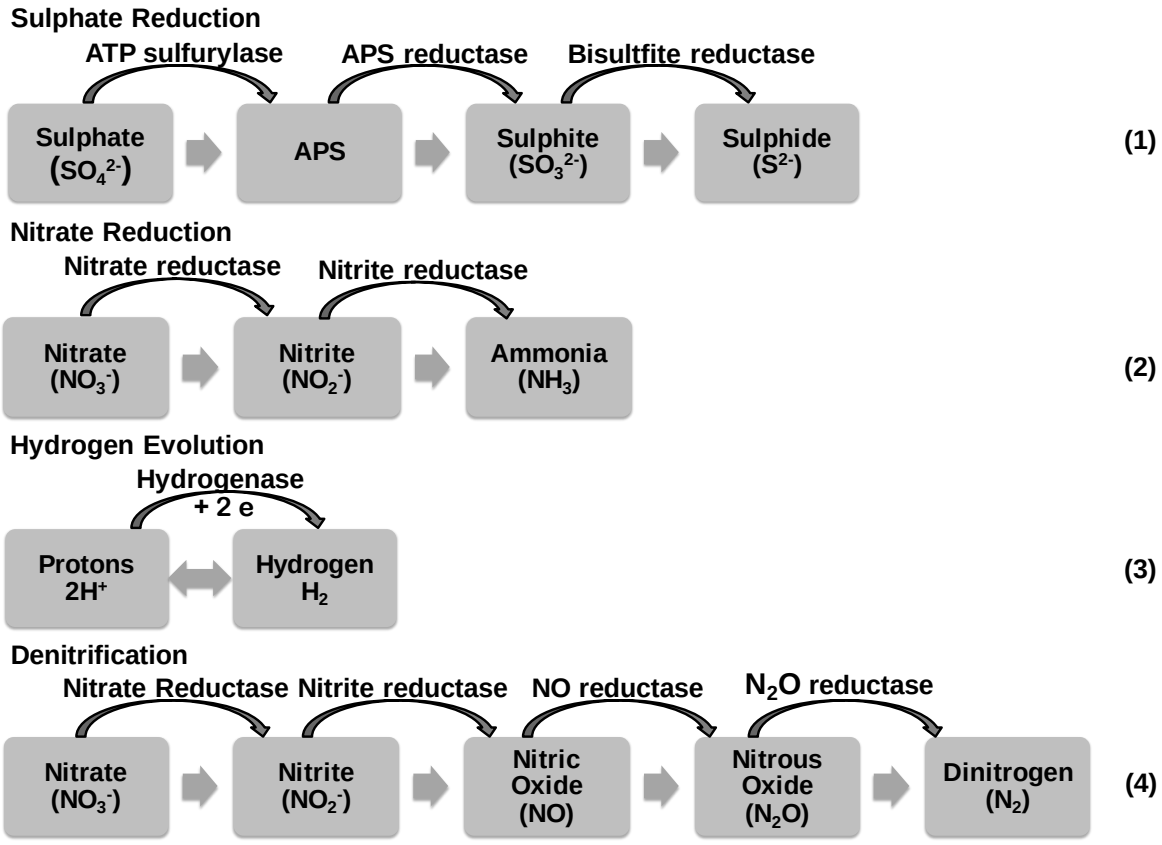

Figure 1.6: Relevant reactions in sulphur and nitrogen metabolism in SRB's.

H and N are the major chemical elements in the chemistry of life. The two biocycles "collide" in many bioenergy aspects, such as BioH2 – the "ideal" fuel, agriculture and food chemistry, energy bioconversion and bioremediation (the "Janus face" of N compounds – its biological relevance and the toxicity and environmental impact).

The microbial wide diversity provide other important links such as: i) sulfur oxidizing bacteria can reduce nitrate to N_2, ii) H_2 can be used instead of sulfur and reduced organic substrates and iii) autotrophic growth under H_2 occurs, since H_2 can be an electron source for denitrification [76, 77].

As indicated above, the dissimilatory nitrate reductase isolated from *D.d.* has a key role since all the reductive routes of the N-cycle involve the conversion of nitrate. When these proteins are expressed, the constitutive enzymes for sulphate reduction are kept.

Another interesting aspect of these microorganisms is the fact that they can either use or produce molecular hydrogen. In this last case, other microbial groups present in the same environment (e.g. methane forming organisms producing methane by reduction of carbon dioxide) may oxidize hydrogen (Interspecies Hydrogen Transfer) [78, 79]. As stated previously hydrogenases seem to have an energetic regulatory role, supplementing reducing power when carbon sources are scarce (i.e., lactate, pyruvate limitation) or receiving

electrons when respiratory substrates are not available (e.g., sulphate limitation) or blocked (e.g., molybdate inhibited respiration) [50, 53]. These metabolic avenues will be explored in relation to microbial induced biocorrosion. The understanding of the mechanisms involved is important for the use of new forms of energy (bioconversion), diverse biotechnological applications and in biocorrosion itself (sees Fig. 1.7).

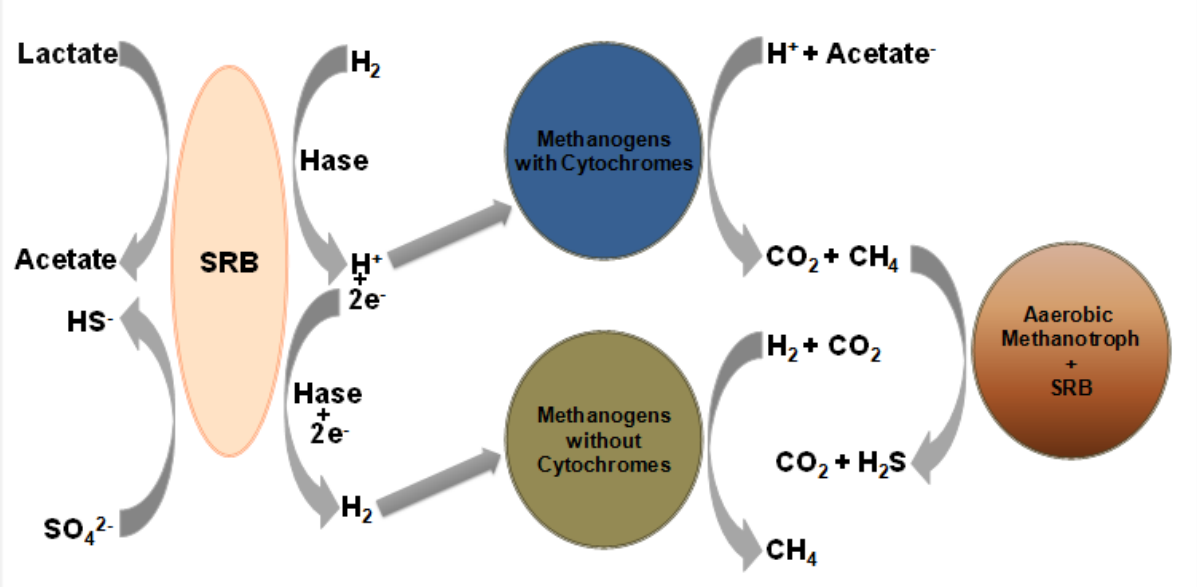

Figure 1.7: Hydrogen regulation in anoxic environments. Relationship between SRB's, methanogenic archea and anaerobic methane oxidizers.

1.4. Electron transfer processes relevant for sulphate reducing bacteria

Sulphate Reducing Bacteria (SRB) have complex electron transfer chains (ETC) which allow the reduction of sulphate by oxidation of either organic compounds or molecular hydrogen. The result of the bacterial activity results in the formation of large amounts of sulphide, which presents serious health and environmental problems. The capability of either use or produce molecular hydrogen by the activity of the Hydrogenase enzyme and the presence of iron sulphide have been indicated as key factors of the SRB deterioration of steel according to the cathodic depolarization theory (see Figure 1.8).

A necessary step for the understanding of the mechanisms involved is the identification and isolation of metalloenzymes involved. More than 30 new metalloproteins have been identified by our group over the years and this has been a general topic of interest [23, 29, 37, 39, 70, 75, 80-88]. A review of all the published data has not been exhaustively made yet, but there are partial accounts.

The active centers that have been studied include iron-sulfur clusters (also in associations with molybdenum and nickel) and hemes. Special relevance has been given to the characterization of bacterial hydrogenases (and to the role of the nickel in hydrogen

evolution/consumption). Hydrogenase catalyses the reversible oxidation of hydrogen and is present in all SRB. Moreover, it is possible to establish a direct electron transfer between the enzyme and steel surface, since the Hydrogenase can remain active in biofilm for months even if the bacteria are no longer viable [24, 89].

The role of small ET carriers in the activity of hydrogenase will be discussed (Ferredoxin, Flavodoxin and Cytochromes). The electron transfer in the **phosphoroclastic reaction** (from pyruvate via pyruvate dehydrogenase to multiheme cytochrome c_3 /hydrogenase complex with consequent hydrogen evolution), as well as the transfer of electron from molecular hydrogen via multiheme cytochrome c_3/Hydrogenase complex to the **sulphite reductase** are relevant metabolic reactions in which small acidic ET proteins (ferredoxin) are involved. Aldehydes can be a relevant substrate linked to hydrogen production [39, 90]

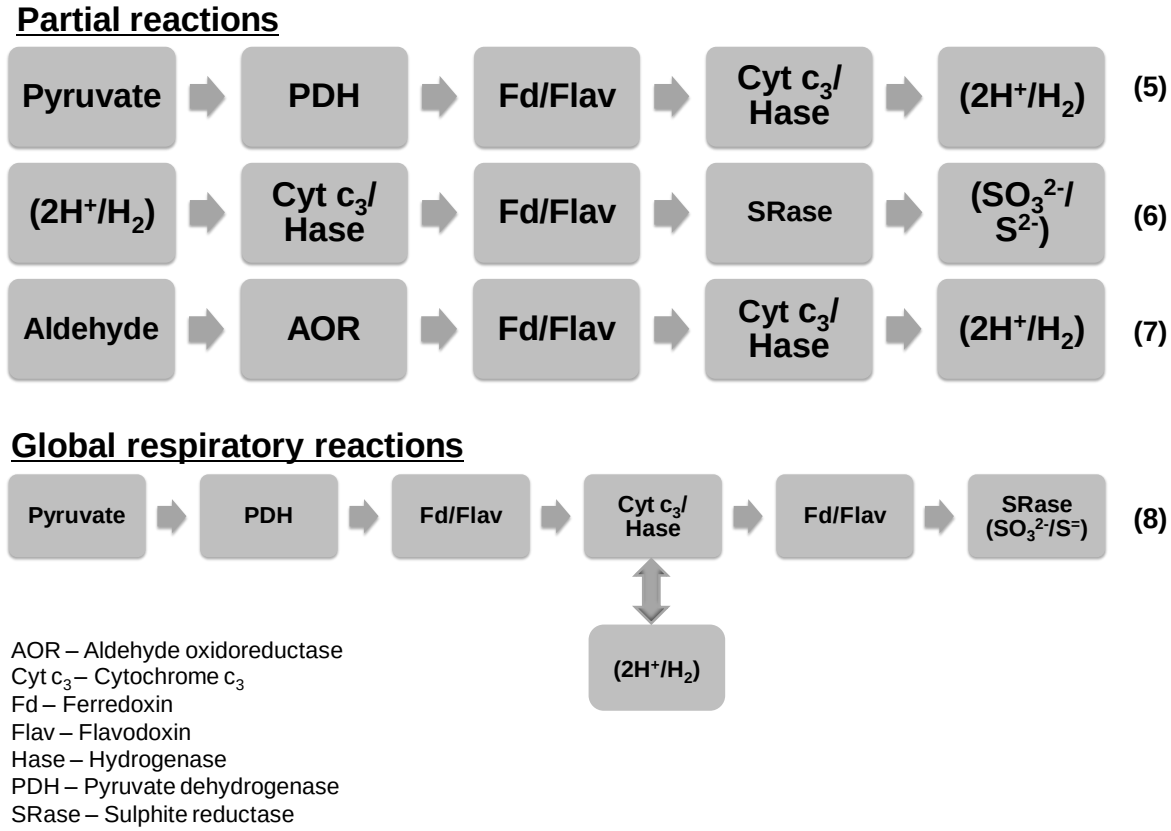

Figure 1.8: Relevant and recognized Electron Transfer Chain in SRB. AOR – Aldehyde oxidoreductase; Fd- Ferredoxin; Flav – Flavodoxin; Hase – Hydrogenase; PDH – Pyruvate dehydrogenase; SRase – Sulphite reductase.

1.5. Bacteria and metal surfaces / Biofilm influence

The interaction of bacteria and metal surfaces is a general accepted phenomenon. The presence of microorganisms at the surfaces can have a profound effect on material performances. Surface associated microbial growth (biofilms) is known to promote biofouling and provide a media where interfacial reactions take place (chemical, physical, electrochemical) that are not favoured under abiotic conditions. Alterations of metal surfaces (generally undesirable) by the presence of biofilms are referred as biocorrosion [7, 91, 92].

Biofilm formation is the primary step in the development of a biocorrosion process, as it produces a markedly different environment from the bulk medium, with distinct properties: pH, dissolved oxygen, and the presence of organic and inorganic species [93]. A biofilm is a complex structure mainly composed by water (95%), bacteria, extracellular polymeric substances (EPS) (polysaccharides, enzymes, proteins, lipids), corrosion products and metals ions (see Fig. 1.9). Microbial produced EPS (which contain different macromolecules) mediate initial cells adhesion to the material surface and constitute the biofilm matrix and lounge a wide range of metabolic activities including enzymes, exopolymers, organic and inorganic compounds, gases (H_2S) [26].

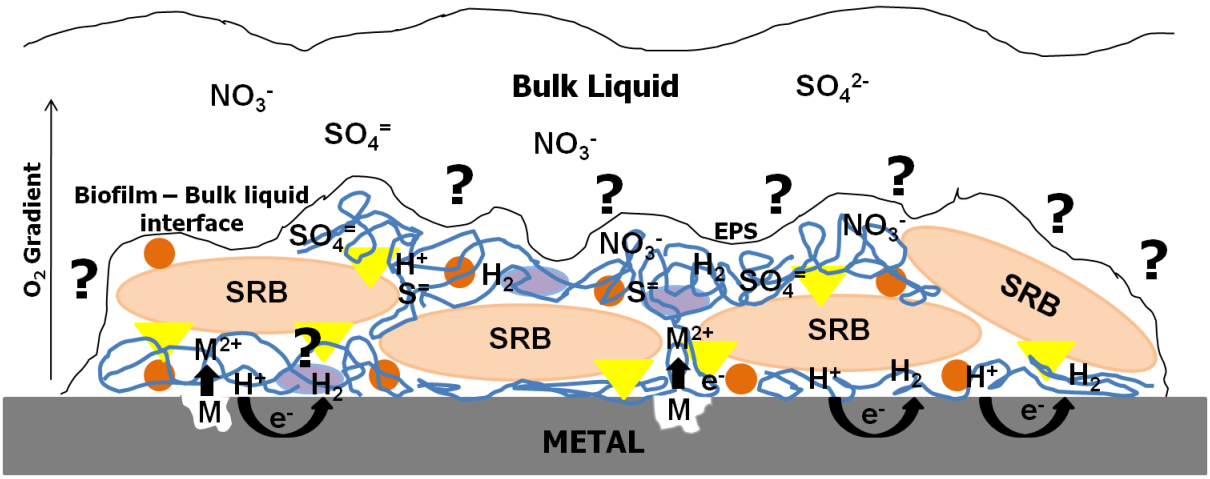

Figure 1.9: Schematic representation of a SRB biofilm chemical complexity at a surface metal and its influence in MIC.

These biopolymers can be classified as capsular (if linked to the cell surface by non-convalents interactions) or lime (if weakly associated to the cell surface). After attachment the biofilm has also an important role on the resistance to biocides and antibiotics, acting as a chemical barrier against the diffusion of substances towards the microorganisms at the metal surface [94]. The 3D structure of the biofilm can also differ substantially and became quite elaborated with channels with liquid flow, voids, just as a “microbial city” [95, 96] as seen in Fig. 1.10:

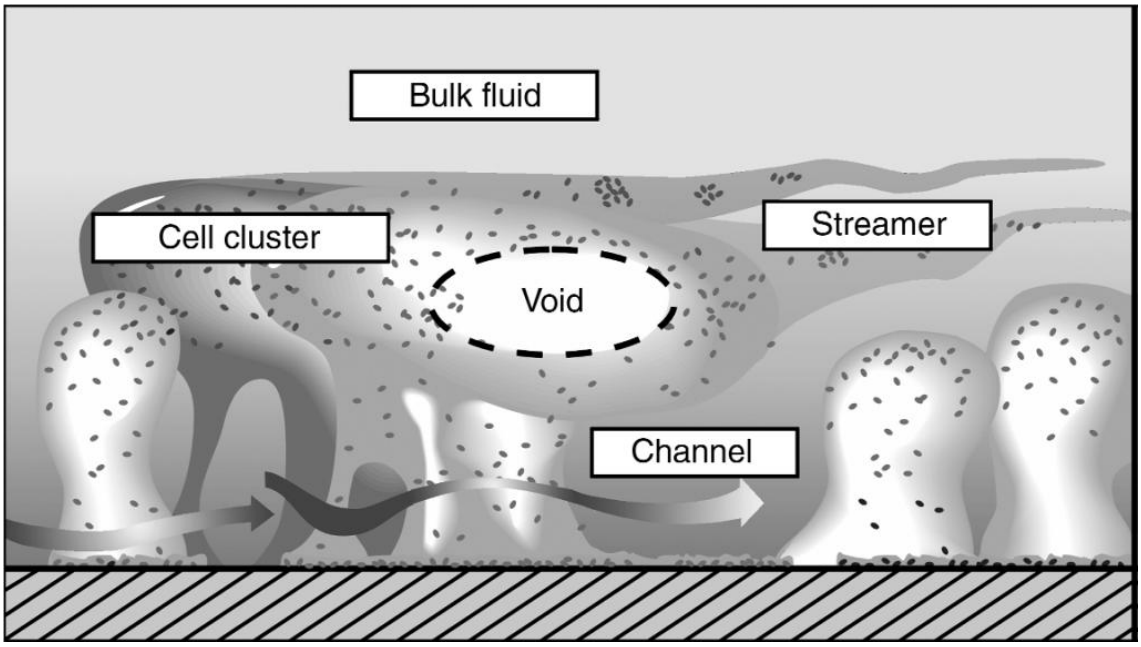

Figure 1.10: Conceptual illustration of the heterogeneity of biofilm structure, with labeled bacterial clusters, streamers, and water channels. (From Little and Lee, 2007).

SRB have been implicated in pitting corrosion of ferrous metals in several anoxic habitats. SRB activity is of great concern to many industrial operations, in particular, oil and gas industries [40, 85].

Under discussion is still the question of other possible roles for the contribution of EPS to the general biocorrosion picture. Actually, “green” oriented strategies for preventing or mitigating MIC, excluding the more traditional technologies such as biocides, propose the use of biofilms to inhibitor prevent corrosion. Another approach is the manipulation (removal or addition) of an electron acceptor (oxygen, sulphate, and nitrate) to influence the microbial populations. In both strategies the composition of the microbial populations may be influenced and tuned by environmental factors – for example temperature, nutrients, flow, pH, etc [97].

Of fundamental and biotechnological interest is the possible direct or indirect (mediated) electron transfer between bacteria and electrodes. For technological applications like biosensors, electrodes are seen as the transducer of the biological counterpart supplementing or receiving electrons from the biological partner. Most work has been done on electroactive biofilms studied in different environment [29, 30, 80, 98]. The modulation and limitation of electron transfer from (to) electrodes to bacteria is shown in Fig. 1.11.

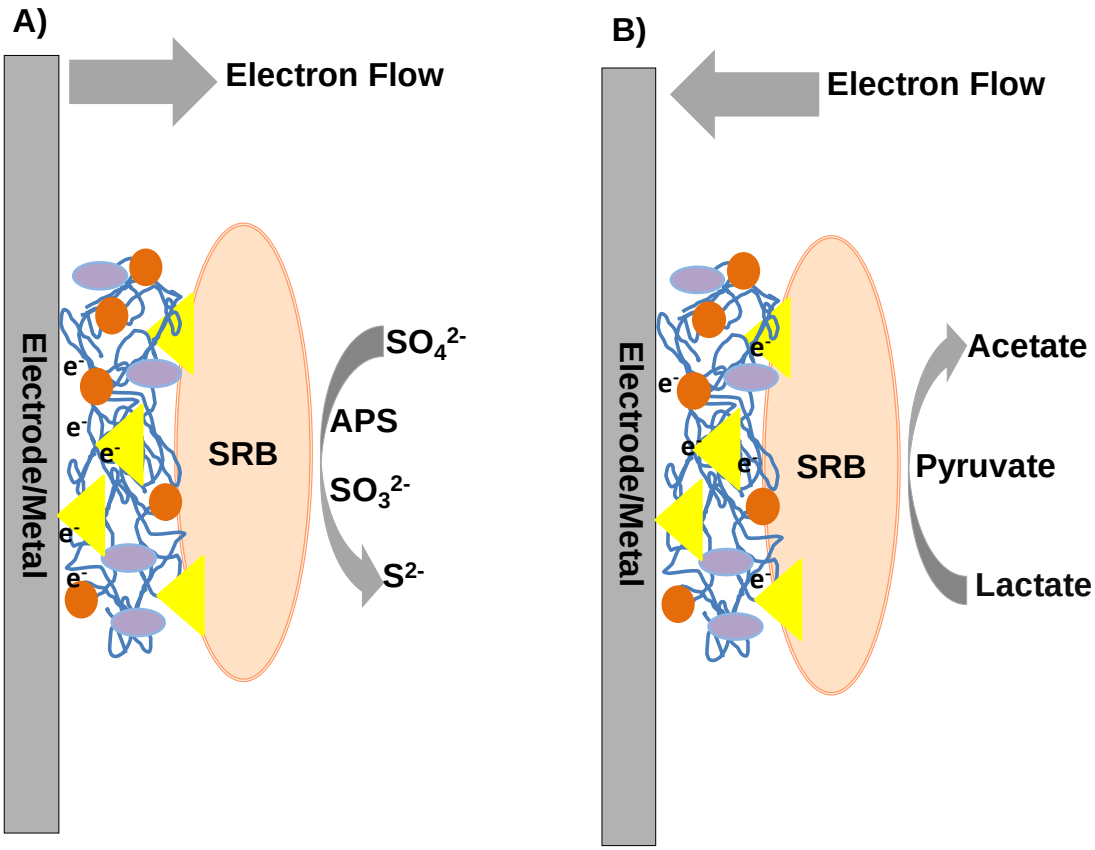

Figure 1.11: Direct and reverse electron flow between SRB's and electrode/metal surface.

The way the biological counterpart interacts with the metal surface various widely and can take different nuances: *direct electron transfer* as a consequence of cell adhesion (biofilm), or *mediated electron transfer* by fermentation products, secondary metabolites or redox components (proteins, organic and inorganic compounds). The direct electron transfer via membrane bound cytochromes and electron conducting nanowires (pili), multiheme cytochromes present in outer membranes, shuttling and mediation by extracellular ET Flavins, hydrogenase and c-type cytochromes facilitate reduction of inorganic compounds [31, 55-58, 60, 99]. The involvement of "pili" is an exciting proposal and may tune different modes of recognition of surfaces by cells implicating adhesion, DNA transfer, motion and communicating electric nanowires [100-103].

From the wealth of information available it is clear that the extracellular polymeric substances (EPS) are crucial actors in the MIC phenomena, the main component of biofilm. And have an important role in the metabolism of planktonic bacteria. Several studies have shown that the EPS composition has an influence in the bacterial attachment, biofilm formation, resistance to antibiotics and biocorrosion, and that there is a remarkable influence of respiratory substrate in the EPS composition and its corrosiveness on carbon steel [104]. The EPS can also function as an external digestive system and recycling centre, as it keeps

all the components of dead cells available [96]. But most excitingly the biofilm creates a confined space where molecules (small and large) can enhance and establish a clear communication between bacteria and metal surface. Several of those components are redox active and will have a net participation on the electrochemical reactions that promote MIC. EPS and ET components (namely Hydrogenase, cytochromes and flavins, metals, etc) are a prior aim of research as well as the understanding of the role of EPS on cell adhesion and core-sensing / biosensing [26, 92].

Metabolomics and proteomics in particular on the switch nitrate / sulphate may provide a better understanding of the regulation / expression / repression of the key molecules involved [93, 105].

1.6. Extracellular Polymeric Substances (EPS) composition

The composition of EPS can vary accordingly to the environmental conditions, microbial community and time. The general components are proteins, polysaccharides, nucleic acids, lipids, water and ions. EPS is formed by active secretion, detachment from the cell surface, cell lyses and adsorption of surrounding molecules. From now on we will describe the main components characteristics.

1.6.1. Proteins

There is a large diversity of extracellular proteins present in the EPS with different roles from structural proteins to enzymes, with different roles. In what concerns structural proteins, for example, the negatively charged amino acids can interact with divalent ions helping to stabilize the structure of the biofilm [106]. Many studies have demonstrated the importance of cell surface and carbohydrate-binding proteins (also known as lectins) in the build up and stabilization of the biofilm matrix network. Examples include LecB, a galactose-specific lectin of *Pseudomonas aeruginosa* and glucan-binding proteins of the dental pathogen *Streptococcus mutans* [107, 108].

Biofilm-associated surface protein, Bap proteins, from *Staphylococcus aureus* have also been implicated in the biofilm formation in many bacterial species. This high-molecular–mass proteins, located in the cell surface, have a core domain of tandem repeats with functions related to biofilm formation and host infection processes [109]. Functional amyloids have also been involved in bacterial adhesion to material surfaces and host cells; they have an additional feature of working as cytotoxins to host and biofilm competitors. These molecules have been found in different habitats like lakes, drink-water reservoirs and waste-water treatment plants [110].

The last group of structural proteins is related to cell appendixes like fimbriae, pili, flagella and nanowires. These can work by helping to strengthen the biofilm structure and

also allowing the cell interaction with other elements in the EPS matrix like eDNA or electron transfer proteins [100, 111].

Most of the enzymes secreted to the EPS or to the aqueous media, are related to the extracellular degradation of macromolecules allowing them to be transported to the inner part of the cells to be used as carbon source and for energy production. The targets can be water-soluble polymers like polysaccharides, or also water-insoluble compounds such as chitin and cellulose (see table 1.2 below). One of the most common class of exoenzymes present in EPS are hydrolases such as: proteases, polysaccharases, glucosidases, lipases, esterases, phosphatases, and others [95, 112-114].

Table 1.2: Biofilm enzymes in natural and man-made environments.

Enzyme	Type of biofilm
Protein-degrading enzymes	
Protease	River biofilms and activated sludge
Peptidase	Drinking-water biofilms, river biofilms, waste-water biofilms, sewer biofilms, marine aggregates and activated sludge
Polysaccharide or oligosaccharide-degrading enzymes	
Endocellulase	River biofilms
Chitinase	River biofilms and estuarine-sediment biofilms
α-glucosidase	River biofilms, sewer biofilms, stream sediment biofilms, lake sediment biofilms, waste-water biofilms, marine aggregates and activated sludge
β-glucosidase	River biofilms, biofilms from trickling biofilters, sewer biofilms, stream sediment biofilms, lake sediment biofilms, marine aggregates and activated sludge
β-xylosidase	River biofilms and lake sediment biofilms
N-acetyl- β-D-glucosaminidase	River biofilms, marine aggregates and activated sludge
Chitobiosidase	Marine aggregates
β-glucuronidase	Activated sludge
Lipid-degrading enzymes	
Lipase	Marine aggregates and activated sludge
Esterase	River biofilms, lake sediment biofilms, drinking-water biofilms, sewer biofilms, stream sediment biofilms and activated sludge
Phosphomonoesterases	
Phosphatase	River biofilms, sewer biofilms, stream biofilms, marine aggregates and activated sludge
Oxidoreductases	
Phenol oxidase	River biofilms
Peroxidase	River biofilms
Extracellular redox activity	Activated sludge

(From Flemming and Wingender, 2010)

The polysaccharases deserve special attention as they are implicated in one important feature of the microbial biofilm: microbial detachment and dispersion [115, 116]. Due their activity, the microorganisms can reduce the polymerization of the polysaccharides and lead to the release of cells located in the biofilm as shown in Fig. 1.12.

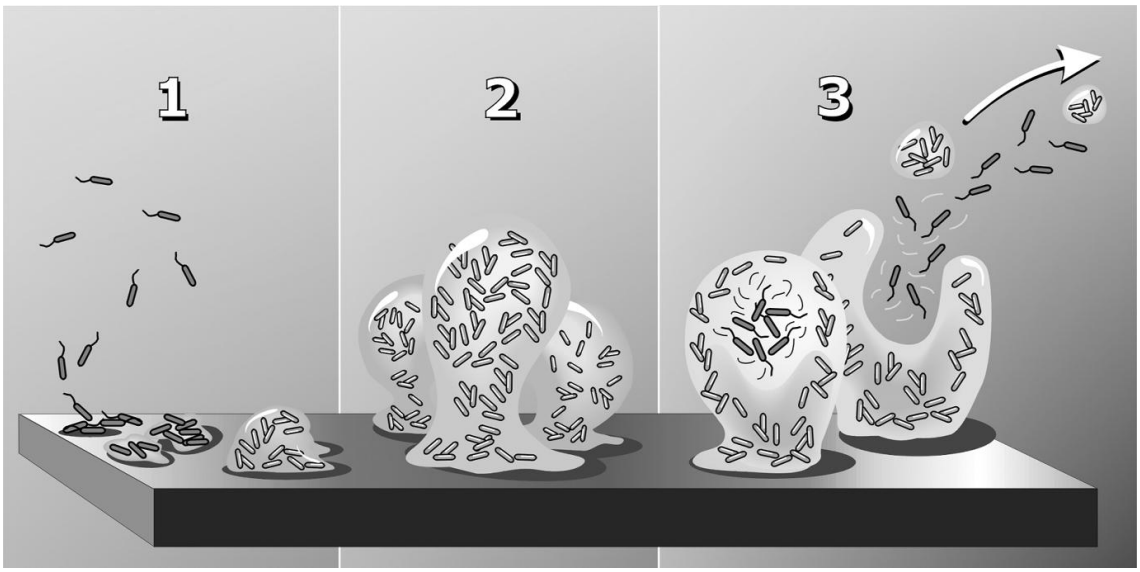

Figure 1.12: The biofilm life cycle in three steps: (1) attachment, (2) growth of colonies, and (3) detachment in clumps or "seeding dispersal." (From Little and Lee, 2007).

Exoenzymes have commercial interest due to their potential applications in treatment of waste-waters and production of synthetic polymers. Some enzymes may also have biosynthetic functions, as glycotransferases, related to synthesis of dextranes [117]. Some redox proteins can be also involved in the electron transfer between biofilm and metal or with metal uptake and thus play a role in biocorrosion [11, 118]

1.6.2. Polysaccharides

Polysaccharides are heterogeneous long molecules with an average size of 10^3 to 10^8 kDa. Their physical properties are related to the chemical composition and also the existing bonds between the monomers. Links α-1,6- or α-1,2- produce polysaccharides more soluble and flexible, while types 1,3- or 1,4- (α or β) bonds produce insoluble polymers, rigid and very appropriate for the structural stability of the biofilm [117].

The (associated) negative charge of these polymers is due to the carboxyl group of uronic acids and organics and inorganics substituents (like pyruvate, sulphate and phosphate) as can be found in alginate and xanthan [114]. However, there are some

polycationic polysaccharides, like intercellular adhesions, that were discovered in *Staphylococcus epidermidis* and *S. aureus*, which are important nosocomial pathogens [96].

The composition of the produced polysaccharides present in EPS can differ significantly even between strains of the same species; the ratios, chemical composition, molecular mass are greatly influenced by the conditions of growth. Variables like temperature, carbon source, pH, metal presence and phase of growth can be determinant to the quantity and overall composition [115, 119, 120].

Many studies involving the mutants that lack central genes in the biosynthesis of important carbohydrates have shown that polysaccharides are fundamental for the biofilm formation. Although some mutants could still attach to the surface and form limited microcolonies. This feature can be compensated in the field as others EPS producing bacteria can supply the missing feature of other inhabitants of the biofilm [95, 121].

1.6.3. Extracellular DNA (eDNA)

Initially the DNA found in the EPS was thought to be a residue of the lysed cells during extraction protocols, nowadays it has been proved that it is part of the matrix and that it has an important role in the biofilm development [122, 123]. In *P. aeruginosa* biofilms, eDNA is a major component and works as an intercellular connector [124]. This DNA can act as an adhesin, antimicrobial by chelating important cations at the surface of bacterial outer membrane [96, 125]. There is still debate about the eDNA origin, wheter it come from lyzed cells or is actively secreted.

1.6.4. Lipids and other components

Besides all the previous components, EPS can also comprise lipopolysaccharide (LPS), phospholipids and humic substances. The lipopolysaccharides have been demonstrated to be very important to the attachment of *Thiobacillus ferrooxidans* to pyrite surface [126]. This hydrophobic characteristic can be important to the adhesion of specific surfaces like Teflon by *Rhodococcus* sp. strains. Little is known about the function of lipids in EPS mainly because it is quite hard to extract these compounds from the EPS.

This diversity of components function and the relevance for the biofilm are listed in the Table 1.3.

Table 1.3: Functions of extracellular polymeric substances in biofilm.

Function	Relevance for biofilms	EPS componentes involved
Adhesion	Allows the initial steps in the colonization of abiotic and biotic surfaces by planktonic cells, and the long-term attachment of whole biofilms to surfaces	Polysaccharides, proteins, DNA and amphiphilic molecules
Aggregation of bacterial cells	Enables bridging between cells, the temporary immobilization of bacterial populations, the development of high cell densities and cell–cell recognition	Polysaccharides, proteins and DNA
Cohesion of biofilms	Forms a hydrated polymer network (the biofilm matrix), mediating the mechanical stability of biofilms (often in conjunction with multivalent cations) and, through the EPS structure (capsule, slime, or sheath), determining biofilm architecture, as well as allowing cell–cell communication	Neutral and charged polysaccharides, proteins (such as amyloids and lectins), and DNA
Retention of water	Maintains a highly hydrated microenvironment around biofilm organisms, leading to their tolerance of dessication in water-deficient environments	Hydrophilic polysaccharides and, possibly, proteins
Protection	Confers resistance to nonspecific and specific host defences during infection, and confers tolerance to various antimicrobial agents (for example, disinfectants and antibiotics), as well as protecting cyanobacterial nitrogenase from the harmful effects of oxygen and protecting against some grazing protoza	Polysaccharides and proteins
Sorption of compounds	Allows the accumulation of nutrients from the environment and the sorption of xenobiotics (thus contributing to environmental detoxification)	Charged or hydrophobic polysaccharides and proteins
Sorption of inorganic ions	Promotes polysaccharide gel formation, ion exchange, mineral formation and the accumulation of toxic metal ions (thus contributing to environmental detoxification)	Charged polysaccharides and proteins, including inorganic substituents such as phosphate and sulphate
Enzimatic activity	Enables the digestion of exogenous macromolecules for nutrient acquisition and the degradation of structural EPS, allowing the release of cells from biofilms	Proteins
Nutrient source	Provides a source of carbon-, nitrogen- and phosphorus-containing compounds for utilization by the biofilm community	Potentially all EPS components
Exchange genetic information	Facilitates horizontal gene transfer between biofilm cells	DNA

Table 1.3 (Cont.): Functions of extracellular polymeric substances in biofilm

Function	Relevance for biofilms	EPS componentes involved
Electron donor or aceptor	Permits redox activity in the biofilm matrix	Proteins (for example, those forming pili and nanowires) and, possibly, humic substances
Export of cell components	Releases cellular material as a result of metabolic turnover	Membrane vesicles containing nucleic acids, enzymes, lipopolysaccharides and phospholipids
Sink for excesso energy	Stores excess carbon under unbalanced carbon to nitrogen ratios	Polysaccharides
Biding of energy	Results in the accumulation, retention and stabilization of enzymes through their interaction with polysaccharides	Polysaccharides and enzymes

(From Flemming and Wingender, 2010)

1.7. Useful methods and tools for MIC assessment

MIC is a very complex phenomenon. The “tip of the iceberg” is starting to be revealed and it is clear that an intense program is required using a wide range of complementary tools to identify the vectors involved in the process and to make possible to go deeper into the understanding of the participating mechanisms. It is fundamental to link the studies from the field through the laboratory and back to the field, bringing industry and fundamental research together and training researchers to answer field problems. In this way, the prevention and mitigation of MIC can be achieved, mechanisms tested and solutions to the main problem envisaged in the near future.

Microbial consortia and the role of extracellular polymeric substances (highly emphasized) can be better tackled by the contributions of modern analytical methods that are called to give partial answers to this complex problem.

A list of such techniques, now available and adapted to MIC, is presented in the Table 1.4 below:

Table 1.4: Techniques available for MIC Assessment.

Category	Advantage/Disadvantage	References
Electrochemical methods		
• Open Circuit Potential (OCP)	Easy, can be used both at the lab and the field/Only access trends and general corrosion.	[50, 66, 91, 127]
• Tafel Polarization	Easy interpretation of data/Needs a stable system; not useful in SS at seawater.	[8, 50, 92]
• Potentiodynamic sweep techniques	Simple and good correlation with biofilms/Very dependent on experimental conditions	[66, 98, 128]
• Electrochemical Impedance Spectroscopy (EIS)	More precise and allow to explain the mechanism/Difficult to interpret the data; needs one stable system.	[128, 129]
• Polarization techniques	Rapid and easy interpretation/Not useful for localized corrosion; biofilm interference	[11, 19]
• Electrochemical Noise	Able to identify the type of corrosion/Difficult to interpret the data.	[129, 130]
Surface analysis methods		
• Time of Flight-Secondary Ions Mass Spectrometry (ToF-SIMS)	Highly sensitive and accurate; Link chemical and visual analysis/Needs vacuum and generate huge amount of results requiring data treatment	[104, 131, 132]
• X-ray Photoelectron Spectroscopy (XPS)	Quantitatively evaluate surface chemistry/Needs Vacuum; Time consuming	[104]
• Atomic Force Microscopy (AFM)	Possible to analyze wet samples to atomic resolution/No chemical information	[133]
• Confocal Laser Scanning Microscopy (CLSM)	Possible to analyze wet samples with 3D images/	[8, 92]

Table 1.4 (Cont): Techniques available for MIC Assessment.

Category	Advantage/Disadvantage	References
Surface analysis methods (Cont.)		
• Quartz Cristal Microbalance with Dissipation (QCM-D)	Allows accurate analysis of adsorption of cells and molecules/Needs very stable conditions	[134]
• Microautoradioagraphy (MAR)	Allows identification of active microorganism and mechanisms/Laborious and time consuming	[135]
• Fluorescent In Situ Hybridization (FISH)	Fast and specific; Link of metabolic pathways, identification and cell location/Needs probe design; relatively expensive	[135]
Molecular Biology methods		
• Polymerase Chain Reaction (PCR)/ Quantitative PCR (qPCR)	Easy and inexpensive/Needs previous knowledge of the target groups	[15, 136]
• Denaturing Gradient Gel Electrophoresis (DGGE)	Gives an overview of the community diversity/Poor reproducibility and no identification	[127, 137]
• DNA Microarray	Fast results; metabolic and identification assessment/Only detect already known microorganisms	[51]
• Sequencing	Allows identification, quantification and metabolic analysis/More expensive and time consuming	[14, 138, 139]
Microbiology/Bulk/Biochemistry methods		
• Culturing	Simple and cost effective/Maximum 10% of the diversity can be cultured; time consuming	[91, 140]
• Enzyme Linked Immunosorbent Assay (ELISA)	Very specific and fast/ few kits available; do not distinguish live or dead cells	[8, 94]
• Fatty acid analyze	Good precision/Relatively expensive and limited library	[8, 94]

Table 1.4 (Cont): Techniques available for MIC Assessment.

Category	Advantage/Disadvantage	References
Microbiology/Bulk/Biochemistry methods		
• Protein analysis Mass Spectrometry (MALDI-ToF)	Specific and precise/Relatively expensive and time consuming	[92]
• ATP assay	Fast and cost effective/Unspecific	[3]
• Microscopic examination	Good estimation of total microorganisms/Not very accurate	[3]
• Scanning Electron Microscopy - Energy dispersive X-ray analysis (SEM-EDX)	Allows semi-quantitative surface chemistry analysis; Good image resolution/Needs vacuum; conductive sample or coating.	[9, 98]
Other Spectroscopies		
• Raman Spectroscopy	Monitoring of Electron Transfer molecules in vivo/Time consuming and requires a lot of data treatment	[141]
• Fourier transform infrared spectroscopy (FTIR)	Allows identification and metabolism behaviour analysis/Still needs comparison of known patterns	[142]
• Electron paramagnetic resonance (EPR)	Analyze paramagnetic molecules related to Electron Transfer/Time consuming; relatively expensive	[54]

1.8. Objectives

This thesis is dedicated to the development of a SRB driven corrosion model on carbon steel using *Desulfovibrio desulfuricans* ATCC 27774 as a model organism. The characterization of the influence of the respiratory substrate in the corrosion evolution was performed using electrochemical techniques aided by scanning electron microscopy [134] and weight loss tests.

We were also interested in understanding the alterations caused at metal plate surfaces by the incubation of carbon steel coupons in the presence of the model organism in different conditions. Again, the role of the respiratory substrate was used for comparison. For this purpose high-throughput surface analysis techniques were employed like Time of Flight – Secondary Ion Mass Spectrometry (ToF-SIMS) and X-ray Photoelectron Spectroscopy (XPS).

Finally, the Extracellular Polymeric Substances (EPS) general composition and iron uptake was investigated using the previously mentioned techniques and SDS-PAGE for protein profile assessment.

Chapter 2

Influence of the respiratory substrate in carbon steel corrosion by a SRB model organism

Chapter 2 – Influence of the respiratory substrate in carbon steel corrosion by a SRB model organism

2.1. Introduction

Corrosion is a natural process that leads to the deterioration of metals and alloys, causing release of the metal ions to the environment. It is an electrochemical phenomenon that occurs by the transfer of electrons, in the presence of an electrolyte, through a series of anodic (metal oxidation) and cathodic (electron acceptor reduction) reactions [91]. The process can take place between two different metals (galvanic coupled since they present different electrochemical potentials) or at the same metal if it possess two areas with distinct aeration conditions due to the presence of a water drop, a biofilm, superficial imperfections, etc. The most common electron acceptor is oxygen, however, in acidic conditions, protons may also work as final electron acceptors [32].

Microbiologically Influenced Corrosion (MIC) or biocorrosion was recognized as an important category of corrosion almost 50 years ago. Microbes can influence the deterioration of metals by a variety of ways, reflecting their physiological diversity [143]: (i) production of aggressive/corrosive metabolic products towards the protective layer or the metal itself; [144] secretion of enzymes that promote reduction processes at cathodic sites; (iii) degradation of chemical compounds that inhibit or enhance corrosion; [21] production of Exopolymeric Substances (EPS) that act as a matrix for binding of metal cations; biofilm formation that can create an anaerobic zone at the metal surface.

Biofilm formation is the primary step to develop a biocorrosion process, as it produces a markedly different environment from the bulk medium with distinct properties: pH, dissolved oxygen and the presence of organic and inorganic species [93, 145]. A biofilm is a complex structure mainly composed by water (95%), bacteria, exopolymeric substances (EPS) - polysaccharides, enzymes, proteins, lipids -, corrosion products and metal ions. These biopolymers can be classified as capsular (if linked to the cell surface by non-covalent interactions) or lime (if weakly associated to the cell surface). After attachment the biofilm has an important role on the resistance to biocides and antibiotics, acting as a chemical barrier against the diffusion of substances towards the microorganisms at the metal surface [26]. Some studies already have established a relationship between EPS from biofilm and metal ion chelating in the biocorrosion process [98, 104].

Sulphate-reducing Bacteria (SRB) are a morphologically and taxonomically diverse group (mostly bacteria, although some archaea have been identified already) being the most studied microorganisms associated to biocorrosion in both aquatic and terrestrial environments [92]. SRB performs dissimilatory reduction of sulphur compounds such as sulphate, sulphite and thiosulphate into sulphide. Some species from the *Desulfovibrio* genus

(*D. desulfuricans*, for example) can use nitrate as alternative respiratory substrate. High concentration of nitrite is also known to inhibit sulphate reduction and is a key factor to other microorganisms to out compete SRB's, being frequently considered as a strategy to control oil field souring [146]. Although they were historically classified as anaerobic microorganisms, today it is known that some genera tolerate oxygen and even grow in its presence, which reinforces its ubiquity around the globe [147].

SRBs have been implicated in pitting corrosion of ferrous metals in several anoxic habitats and its activity is of great concern to many industrial operations, in particular, oil and gas industries (O&G) [8]. The presence of hydrogenase enzymes and also the presence of iron sulphide have been indicated as key factors of steel deterioration by SRB according to the cathodic depolarization theory. Hydrogenase catalyses the reversible oxidation of hydrogen and is present in all SRB. Moreover, it is possible to establish a direct electron transfer between the enzyme and steel surface, since hydrogenase can remain active in biofilms for months even if the bacteria are not viable [29, 30]. Besides other molecules like flavin groups and the MtrC protein family (deca-haem cytochromes) have been implicated in extracellular electron transfer [56, 57].

Thermodynamics are used to predict the occurrence of corrosion in a given system by the variation of the Gibbs free energy, ΔG_{cel}. When this variable has negative values it means that the corrosion process is likely to take place. Considering that Gibbs free energy is related to the equilibrium potential E^{Θ}_{cel}:

$$\Delta G_{cel} = -nF\, E^{\Theta}_{cel} \tag{2.1}$$

and that

$$E^{\Theta}_{cel} = E^{c}_{e} - E^{a}_{e} \tag{2.2}$$

which means

$$\Delta G_{cel} < 0 \rightarrow E^{\Theta}_{cel} > 0 \rightarrow E^{c}_{e} > E^{a}_{e} \tag{2.3}$$

These equations tell us that in the case of the cathodic process being more positive than the anodic one, the equilibrium potentials are determined by the Nerst equation below:

$$E_e = E^{\Theta}_{cel} + RT/nF\, ln\, a_{Red}/a_{Ox} \tag{2.4}$$

In the above equations, "n" corresponds to the number of electrons involved in the process, "F" is the Faraday constant, "R" is the ideal gas constant, "T" the absolute

temperature and a_O and a_R are related to the activity of the oxidized and reduced species, respectively.

Besides the thermodynamics that can be use to predict corrosion occurrence, by using Pourbaix diagrams for example, the kinetics of the reactions can also be determined. For this the methodology is based on the Butler-Volmer equation:

$$i = i_0 \cdot \left\{ \exp\left[\frac{\alpha_a n F \eta}{RT}\right] - \exp\left[-\frac{\alpha_c n F \eta}{RT}\right] \right\} \quad (2.5)$$

where i represents the current density observed, i_o is related to the current density of the corrosion, α_a and α_c represents the anodic and cathodic charge transfer coefficient, respectively and "η" activation overpotential.

The available methods for corrosion assessment have been detailed in the general introduction. In our study we were more interested in the measurement of the Open Circuit Potential (OCP) and methods of polarization (potentiodynamics).

Potentiodynamic methods consist in the performance of a linear potential sweep, measuring the current resulting through a pontetiostat. Using a Cyclic Voltammetry (CV) that is one of the above mentioned techniques is possible to plot the potential (E) versus current (i) [2].

By using the logarithm of the Butler-Volmer equation it is possible to calculate the Tafel slopes which are regions where we can observe a linear variation of log i vs η (= E - E_{corr}) and that the extent depends on the kinetics of the charge transfer mechanisms associated to the corrosion. From the analysis of the Tafel slopes is possible to infer the i_{corr}, E_{corr}, β_a (Tafel anodic slope), β_c (Tafel cathodic slope).

The objective of this chapter is to compare the influence of respiratory substrate, on D. desulfuricans growth in metal plates, in order to understand the role of the sulphide vector and the influence of nitrate treatment on the metabolism of SRB and its consequences to the biocorrosion evolution. Electrochemical, weight loss (WL) and surface analysis (Scanning Electron Microscopy) techniques were used for this purpose.

2.2. Experimental

2.2.1. Bacterial strain and growth conditions

For the development of the model organism and standardization of growth conditions, cells culture of *Desulfovibrio desulfuricans* ATCC 27774 were grown in two semi-defined culture media, Vitamin (VMN) Sulphate and VMN Nitrate [148], which differ only in the electron acceptor substrate. VMN base was composed of (g/l distilled water): KH_2PO_4, 0.5; NH_4Cl, 1.0; $CaCl_2 \cdot 2H_2O$, 0.04; sodium lactate, 6.0; sodium citrate, 0.3; casamino acids, 2.0; tryptone, 2.0; modified Wolfe's mineral elixir (0.1% volume/volume) and vitamin solution (0.2% volume/volume). The sulphate complement was (g/l distilled water): Na_2SO_4, 4.5; $MgSO_4 \cdot 7H_2O$, 0.06; $FeSO_4 \cdot 7H_2O$, 0.004. The nitrate complement was (g/l distilled water): $NaNO_3$, 2.4; $MgCl_2 \cdot 6H_2O$, 0.05; $FeCl_2 \cdot 4H_2O$, 0.003. The Vitamin solution was composed of (g/l distilled water): riboflavin, 0.1; nicotinic acid, 0.25; thiamine, 0.3; pentatonic acid, 0.3; pyridoxine, 0.3; cyanocobalamin, 0.025; ascorbic acid, 1; biotin, 0.005. The composition of the modified Wolfes Elixir was (g/l distilled water): Nitrilotriacetic acid, 1,5; $MgSO_4 \cdot 7H_2O$, 0.06; $MnSO_4 \cdot H_2O$, 0.5; NaCl, 1; $FeSO_4 \cdot 7H_2O$, 0.1; $CoSO_4 \cdot 7H_2O$, 0.1; $NiCl_2 \cdot 6H_2O$, 0.1; $CuCl_2 \cdot 2H_2O$, 0.1; $ZnSO_4 \cdot 7H_2O$, 0.1; $CuSO_4 \cdot 5H_2O$, 0.01; $AlK(SO_4)_2 \cdot 12H_2O$, 0.01; H_3BO_3, 0.01; $Na_2MoO_4 \cdot 2H_2O$, 0.01; $Na_2SeO_3 \cdot 5H_2O$, 0.001.

All the chemicals were p.a. grade purchased form Sigma-Aldrich. After weighting and mixing all components, the pH value was adjusted with KOH (5 M) to a final value of 7.45 - 7.55. The medium was then deoxygenated with argon flux to ensure anoxic conditions and sterilized by autoclaving for 20 minutes at 120ºC and 1 atm pressure. The vitamin solution, sterilized by filtration (0.22 µm cellulose, Millipore) was added after, just before the inoculation in a concentration of 0.2% (volume/volume) of the final volume of the culture.

The inocula were performed with cell suspensions in the exponential phase in the proportion of 10% (volume/volume) in the presence of a Bunsen burner to ensure sterile conditions. The growth curve was made in the presence of a metal coupon of carbon steel (St52-3N) simultaneous to the electrochemical assay at 30ºC. The planktonic cell growth was followed by optical density at 600 nm, using a Shimadzu® UV-VIS Spectrophotometer model UV-1800, as an indicative parameter of the metabolic phase and cell availability for the biofilm formation. Aliquots were taken every 8h of culture growth for the first 24h and them once per day (48, 72, 96, 120 and 144h) in order to further evaluate the lactate, sulphate and nitrate consumption by High Performance Liquid Chromatography (HPLC), ICS3000 (DIONEX) using an Ionpac AS11 HC column and an AG11 HC pre-column. Sulphide production was measured by a colorimetric assay modified from elsewhere [149]. The pH was also monitored every 24h with a CRISON micropH 2001 (Crison Instruments). All studies described here were performed in triplicate.

2.2.2. Exopolymeric substances extraction

For the extraction of the colloidal and capsular EPS a protocol described elsewhere was used [150]. The bacteria was grown in 5 L VMN Sulphate and VMN Nitrate for 3 days at 30ºC until they reached a minimum cell concentration of 10^8 cells per ml. Then the cultures were centrifuged at 8,000 x g for 15 min. The supernatant was collected and filtered with a 0.22 µm pore cellulose membrane to remove contaminant cells. All samples were dialyzed against deionized water for 16h and then twice for 2h changing the water.

2.2.3. Electrochemical experiments with model organism and EPS

The working electrode (WE) was a carbon steel St52-3N coupon (geometric area of 0.4 cm^2), composed of the following elements with mass ratios of 0.2% C, 1.6% Mn, 0.55% Si, 0.025% S, 0.025% P. The WE were prepared by polishing in an oxide-silicon carbide sandpaper grit 600 (P1200) and flushed with dry air in order to avoid any alteration in the oxide layer of the surface. Sterility was assured with one hour exposure to UV light (253.7 nm) in an Airflow workstation. The counter electrode (CE) was a graphite rod. The reference electrode (RE) was a saturated calomel electrode (SCE), which was in contact with the system through a bridge tube that was filled with the same electrolyte of the experiment.

All electrochemical measurements were registered using an Autolab/PGSTAT30 potentiostat/galvanostat, in a one compartment (1L) MultiPort™ Corrosion Cell (Gamry®) in a three electrode configuration. The data acquisition was performed using the GPES version 4.9 software (AUTOLAB, EcoChemie B.V).

The electrolyte was the culture media, VMN Sulphate or Nitrate. The sterile electrolytes were purged with sterile humidified argon for one hour prior to the experiment. To maintain strict anoxic conditions and avoid contaminations, a permanent flow of sterile humidified argon was kept in the headspace of the cell to ensure a positive pressure during all tests. For the nitrate negative control, a final concentration of 10 µg/mL Ampicillin and 50 µg/mL of Kanamycin were added daily to prevent contaminations. All experiments were performed at 30ºC, to reproduce the same temperature at the oil field platform from where the metal coupons were obtained. In sulphate, cellulose membranes with 0.22 µm pore sizes were attached to the working electrode in order to evaluate the influence of biofilm attachment to the corrosion process. In sulphate incubations, two different flow pressures were tested: a Low Flow Rate (LFR), an argon flow at the headspace of equivalent to 0.3 L per minute; and a High Flow Rate (HFR), an argon flow at the headspace of equivalent to 3 L per minute. Also, in sulphate cultures a 2 M zinc acetate trap was placed in the gas exit to precipitate the H_2S produced.

After inoculation of the electrolyte with the model organism, Open Circuit Potential (OCP) and Cyclic Voltammetry (CV) tests were performed. All potential values are referenced to SCE. The OCP were measured for a period of 144 hours (6 days) with an interval time of 90 seconds. The parameters for CV were as follow: scan rate, 1 mV/s (quasi-stationary state condition); E_i, -0.750; E_f, -0.750 V; Upper vertex, -0.350 V; Lower vertex, -1 V.

For the EPS only CV assays were performed in the same conditions as referred for biofilm experiments.

2.2.4. Weight loss and surface analysis experiments

For the weight loss (WL) and surface analysis by scanning electron microscopy [151], VMN Sulphate and VMN Nitrate were used as the growth media. Metal plates (rectangles) with measures of 20x10x2 mm were used as coupons. The St37 carbon steel used is composed of the following elements with mass ratio of 0.17% C, 1.4% Mn, 0.045% S, and 0.045% P. The plates were cleaned as described above. In both cases there was no degrease so the material had a similar treatment as the oil field pipes. A hole of 1.5 mm area was drilled to hang the coupon using a nylon thread, having each coupon a total area of 3.7 cm^2. All coupons were weighted in a precision scale just before being hanged at the rubber stopper and placed in an empty 100 mL anaerobic bottle. After closing the bottles, with 4 coupons each, they were exposed for 1h to UV light (253.7 nm) in an Airflow workstation to assure sterility of the coupons. A previously prepared medium was transferred from anaerobic bottles to the ones containing the hanged coupons through nitrogen pressure. The bottles for negative control had a final concentration of 1µg/mL Ampicillin to prevent contaminations. The assembled set-up were flushed again with nitrogen for 5 more minutes, and then inoculated with *Desulfovibrio desulfuricans* ATCC 27774 (10% volume/volume of 24 h culture growth) and then incubated at 30ºC for 6 and 30 days in a total of four conditions per period.

2.2.4.1. Carbon steel weight loss

When the incubation time was over, the bottles were opened and the coupons removed. One of the coupons was dried in a desiccator and preserved in a falcon tube flushed with argon to be used in the surface analysis. The other three coupons were dried and weighted, cleaned in a solution of 18.5% HCl plus 5 g/L Hexamethylenetetramine for 30 s, rinsed with deionized water and acetone, dried in desiccators and then weighted again. An aliquot of each medium was stored for further quantification of Iron by Inductively Coupled Plasma-Atomic Emission Spectrometer (ICP-AES), Ultima (Horiba Jobin-Yvon, France).

The corrosion rate was calculated using the formula below using the formula from the ASTM G31-72 standard. Basically, it is related to the mass lost during the incubation and considering the density of the specific metal. The mass loss measurement is done by weighting the coupons before the experiment and after removing the corrosion products from its surface as described above. We applied the conversion factor defined in the mentioned standard to present the results in mm/y.

2.2.4.2. SEM images

The samples were examined by scanning electron microscopy [151] using a high resolution FEG Digital Scanning microscope 982 Gemini (Leo Electron Microscopy) operating at 1 or 2 kV, without any metal coating.

2.3. Results and Discussion

2.3.1. Growth and metabolic changes

The growth curve of *D. desulfuricans* ATCC 27774, here referred as the mass increase with time measured by turbidity in the bulk media, in VMN Sulphate and VMN Nitrate is presented in Fig. 2.1.

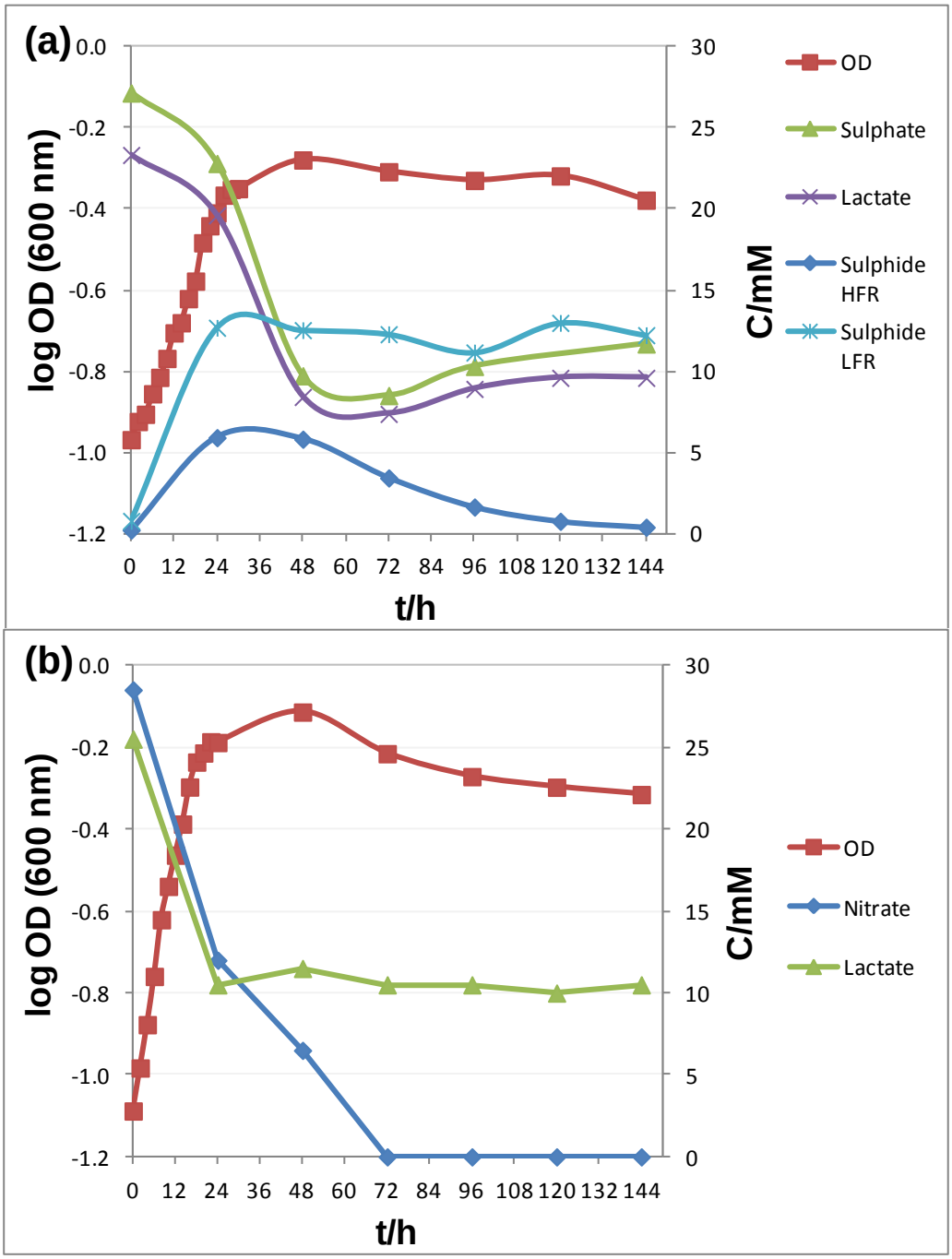

Figure 2.1: Growth curve of *D. desulfuricans* ATCC 27774 in: (a) VMN Sulphate with lactate and sulphate consumption, and sulphide production during the different assays. (b) VMN Nitrate with lactate and nitrate consumption. OD: Optical Density; HFR: High Flow Rate.

For the determination of the kinetic parameters from the growth curve the equations below were applied:

$$\mu = 2.303 (\log OD_2 - \log OD_1 / (t_2-t_1) \quad (1)$$

and

$$t_d = 0.693\mu \quad (2)$$

Where:

μ refers to specific growth factor that is defined as the increase in cell mass per unit time;

OD is optical density in the exponential phase;

t is time; and

t_d refers to "doubling time" that is related to the necessary time to a given population to duplicate itself.

The kinetic parameters of each growth curve are presented in Table 2.1:

Table 2.1. Kinetic parameters of the growth curves presented in Figure 2.1:

Culture medium	**μ/h**	**t_d**
VMN Sulphate	0.059	11.66
VMN Nitrate	0.105	6.57

μ: specific growth rate per hour; t_d: doubling time of the microbial population in hours.

The analysis of the growth curves permited to determine the end of the exponential phase, around 30h for sulfate and 24h for nitrate in the conditions tested. This has important consequences to the electrochemical experiments and corrosion prevention, because it is reported in the literature [93, 152, 153] that the metabolism is heavily influenced by the growth phase and that specially the bacterial attachment and biofilm development is controled by quorum sensing and enhanced during the stationary phase. Our results corroborate this findings as the increase of the potential is more pronounced after the exponential phase ends when there was no membrane protecting the electrode in both media (see Fig. 2.1 and 2.2).

The results indicate that lactate is in excess of concentration because is not completely consumed and that in the presence of nitrate a higher specific growth rate (μ) is achieved (table 2.1). The observed difference in the yeld of cell growth when both media are compared, is in agreement with other studies reported in the literature [13]. There are some explanations for the results, mainly the citotoxicity of the H_2S produced by the bacteria when grown in the presence of a rich source of sulphate. Also, the presence of sulphides produced by the metabolism of the SRB's can lead to the precipitation of iron and other important trace metals by forming metal sulphides, like FeS. This feature is easily observed in *D. desulfuricans* ATCC 27774 cultures in VMN Sulphate, where black precipitates can be seen after 18-24h of incubation. Another result indicating inhbition by sulphide production is the fact that the sulphate is not totally reduced, unlike what occurs in nitrate medium where this substrate is not detected after 48h of growth. Other key factor to consider is that nitrate consists in a much more energetically favorable molecule for reduction and thus permits a higher growth rate as seems by our results [154].

The pH in the bulk media was also monitored during the experiment; it presented an increase from 7.4 to 8.9 in sulphate and from 7.4 to 8.6 in nitrate. Although the pH value in the biofilm/metal interface was not measured, it can differ tremendally from the bulk as already shown in different studies [32, 91].

In our work, it was observed that the flow of argon in the headspace of the electrochemical cell has a critical role by altering the equilibrium of the hydrogen sulphide in the direction of the gas phase. When a high flow rate of argon was kept the concentration of H_2S reached a maximum after 24h and started to decrease after 48h returning to the values of the beginning of the experiment. With a low flow rate, a three times higher concentration of H_2S in solution was achieved and this was mantained until the end of the growth curve. This difference in concentration in solution has serious implications in the metal behavior and passivation of the surface and will be discussed with the electrochemical results.

2.3.2. Chronopotentiometry of the SRB cultures

The results of the 6 days monitoring of the Open Circuit Potential (E_{corr}) in the different conditions (with and without the presence of *D. desulfuricans* ATCC 27774) are presented in Fig. 2.2. As mentioned before, all potential are referenced to SCE.:

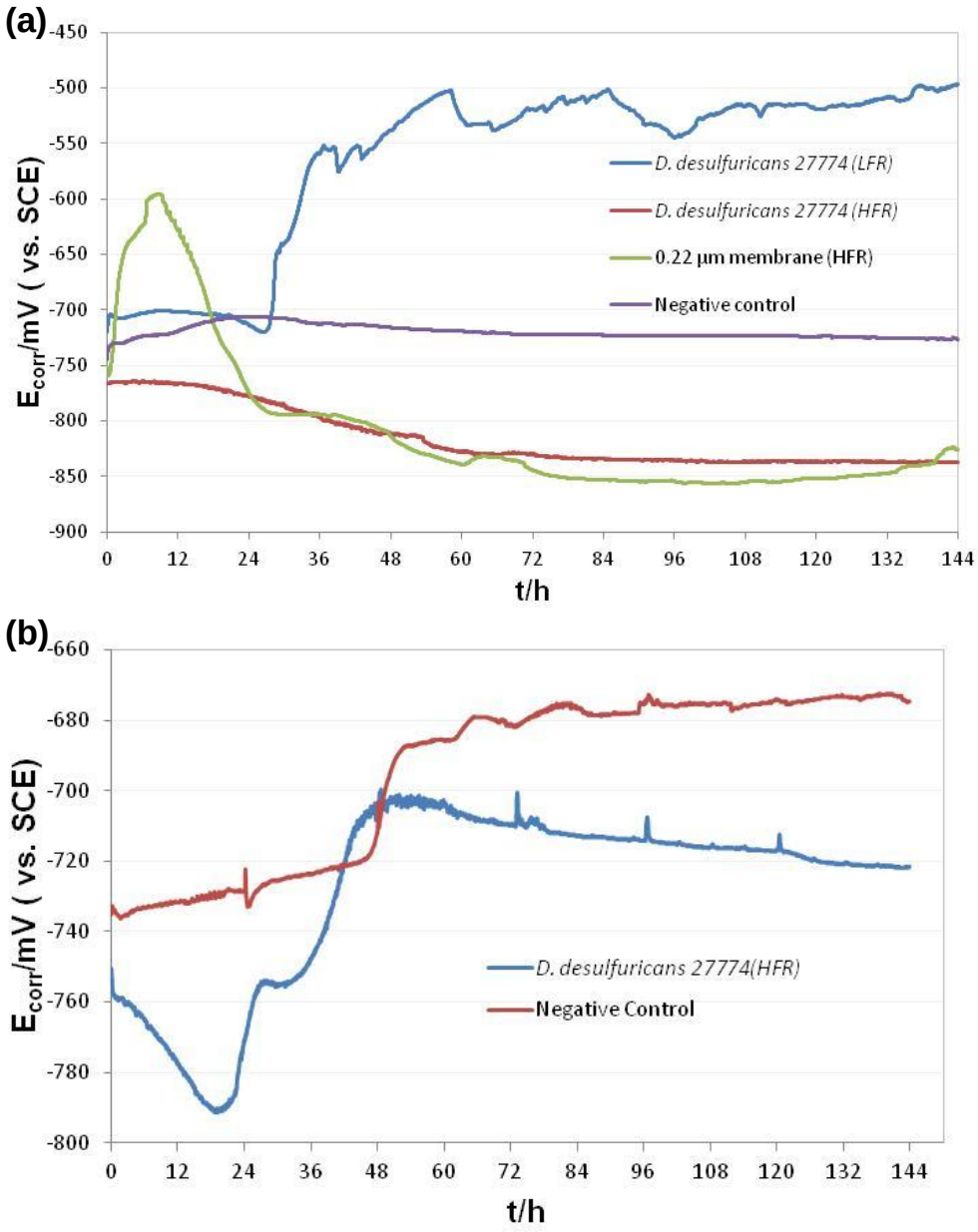

Figure 2.2: Open Circuit Potential measurements (*versus* SCE) in: (a) VMN Sulphate and *D. desulfuricans* ATCC 27774 in different conditions. (b) VMN Nitrate and *D. desulfuricans* ATCC 27774 and respective negative control. HFR: High Flow Rate; LFR: Low Flow Rate.

In the case of sulphate medium with the bacteria in a low flow rate (LFR) it was observed an increase in the potential of 200 mV. The potential is stable for the first 30 hours and then it starts to rise, which is probably related to the end of the exponential phase. According to the litterature where studies have shown that there is an increase of attachment and secondary metabolism products as acids, for example, that could lead to a deterioration of the metal surface [51, 67, 120]. However, when a high flow rate (HFR) was used, a decrease of aproximately 100 mV occurred in the OCP. In the negative control, with sterile sulphate medium, the E_{corr} is stable around the initial potential. In the case of the membrane

covered electrode, that was a control for comparing the influence of biofilm development at the surface, the potential rises rapidly from -750 mV, until its maximum -600 mV at 12h, and then shifts to more negative values, until -850 mV around 96 hours, and finally starts to show a slow increase at the end of the experiment (144h). Without the formation of the biofilm the iron sulphide layer that is formed from the reaction between the biogenic sulphide and the iron oxides present at the surface, could remain stable, thus shifting the potential to more negative values.

Ma et al [155] have shown that abiotic sulphide can inhibit or accelerate corrosion. The more important factors to be taken into account are the pH and the concentration of dissolved sulphide in the electrolyte. According to these authors, the concentration of sulphide in solution also affects the formation of iron crystals' at the metal surface which have important influence in the outcome of the corrosion process. In our case the flow rate of gas at the headspace of the electrochemical cell probably lead to a removal of the sulphide at this space, promoting the difusion of more sulphide from the electrolyte and thus moving the equilibrium of the sulphide to the gas phase. So the increase of potential observed in the membrane covered electrode may be due to diffusional restrictions. As it takes a longer time to the electrolyte equilibrate between the membrane, and this could lead to a difference in concentration of ions close to electrode surface respective to the bulk, even though a high flow rate is present at the headspace of the electrochemical cell.

When nitrate medium was used, the increase of potential was less pronounced (around 90 mV) and it started with a decrease until the bacteria reached the stationary phase when it raised to its maximum value of -0.7 V. After 48h the potential starts to decrease again following the pattern of the planktonic population as can be seen in the Fig. 2.1. The depletion of the nitrate after 48h can be responsible for the cell death observed, which precipitates, changing the redox properties of the bulk electrolyte.

2.3.3. Electrochemistry of SRB biofilm and EPS

The results of the Cyclic Voltammetry (CV) performed after 144h of bacterial biofilm growth in sulphate and nitrate media are presented in the Fig. 2.3:

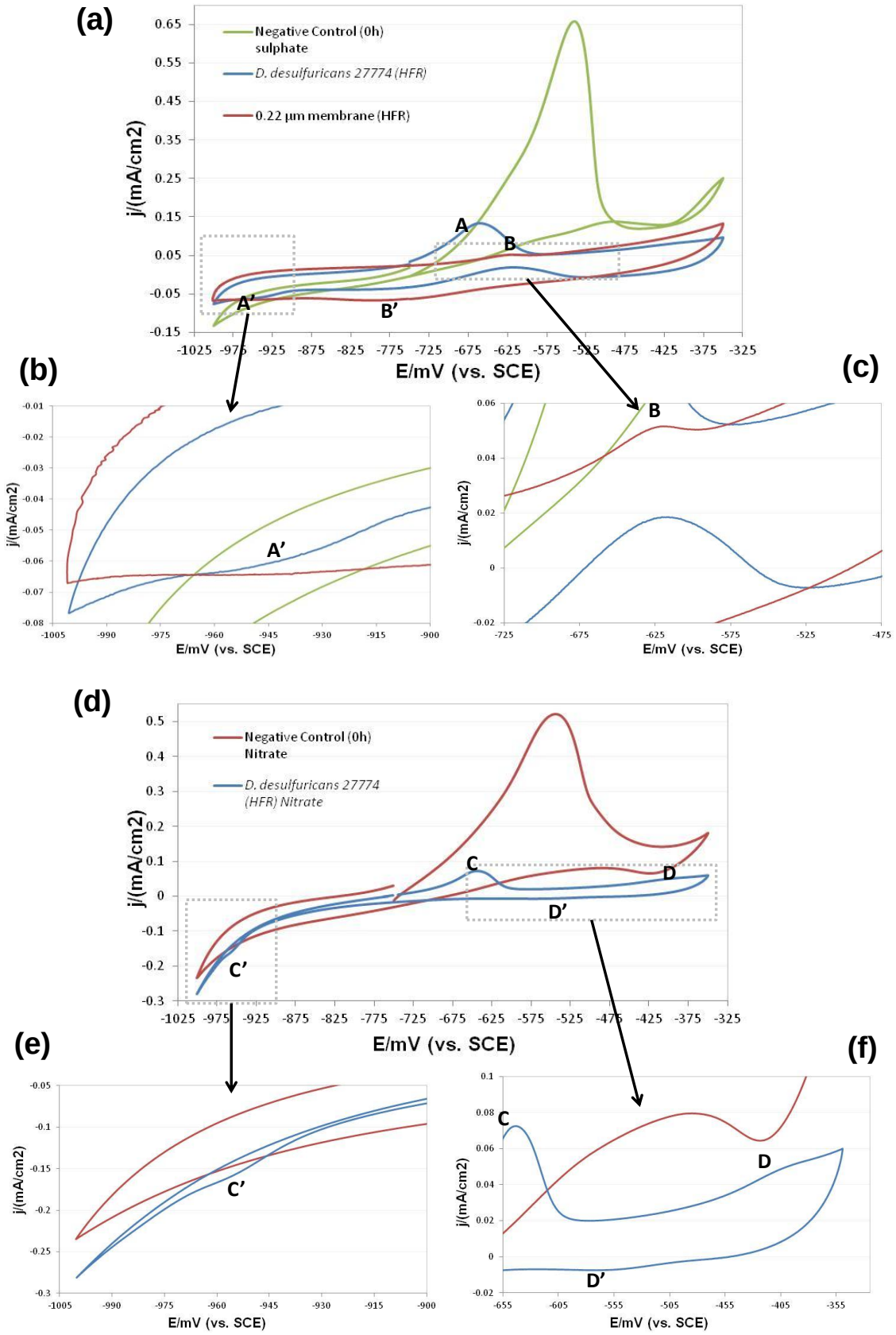

Figure 2.3: Cyclic voltammograms of carbon steel St52 in: (a) VMN sulphate with and without 0.22 µm membrane and respective negative control; (b) and (c) two different detailed area of the respective voltammogram; (d) CV of carbon steel St52 in VMN nitrate and respective negative control; (e) and (f) two different detailed area of the respective voltammogram; initial scan direction: anodic.

In sterile sulphate medium an hysteresis loop is observed in the reverse scan around -425 mV. Other authors [50] state that this is probably due to a high chloride content and that the crossover is indicative of the onset of piting corrosion. In our case, however we have not seen the same occurrence when analysing the nitrate medium. Also we could only confirm pitting by SEM in the samples that were incubated in sulphate (see Fig. 2.6). Other explanation for the hysteresis loop is the formation of an oxide layer on the electrodes, that may be related to the well-defined anodic process occuring approximately at -550 mV, this change in the surface could explain the observed current crossover. This process is probably more visible in sterile medium due to the absence of bacteria or metabolic products attached to the surface that may hinder the electrolyte diffusion towards the electrode.

The cyclic voltammetry results, in presence of sulphate medium and with bacteria, demonstrate an anodic process (A') with the peak maximum at -670 mV versus SCE most probably related to the oxidation of Fe(II) to Fe(III) species or oxide formation as stated earlier. It is also noticeable a cathodic peak at -950 mV (A) that may be related to hydrogen adsorption. In the assay with the membrane, where no biofilm formation at the metal surface occurs, it is possible to see one anodic peak at -625 mV (B) and another cathodic peak around -800 mV (B') similar to the work of Fonseca and co-workers [50]. This indicates that the biofilm formation hinders the electrolyte access to the electrode and can hide electrochemical signals from important reactions occurring at the metal surface. Cordas *et al*. [98] also demonstrated that with time the wave current intensity decreased mostly because of the diffusion barrier that increase as the biofilm develops and gets thicker.

When the cultures were grown in nitrate medium, there is also one main redox process (C), with the maximum redox potential value around -635 mV versus SCE, suggesting an irreversible reaction maybe related to the oxidation of iron. We can also detect an increase in the total cathodic current and a peak at -950 mV (C'), probably due to the adsorption of hydrogen, as observed in the sulphate solution. Other authors [29] have previously proposed that this peak could be related to hydrogen adsorption and that it could be explained by the increase of its catalysis due to the higher availability of iron in solution. Also, in nitrate medium a redox pair at higher potential values, around -400 and -550, respectively D and D', can be observed. This redox process is absent in sulphate medium and may be due to the biofim, or some metabolic products, specific of nitrate media grown bacteria. In the control assays, this process is not observed. However, due to the large currents associated to the equivalent of process "A" in sulphate medium, it is not possible to be certain if it is absent or simply masked. Further assays are necessary to clarify this issue.

When comparing the voltammetric analysis of the EPS extracted from both media (Fig. 2.4), it seems that the one obtained from sulphate medium is more aggressive to the metal,

as it shows a long hysteresis loop indicating a longer time to repassivate and therefore a deep pitting [156]. Coupons exposed to EPS produced in nitrate do not exhibit pitting signals (no crossover are observed), and generally present a decrease in the total current wave when compared to the control.

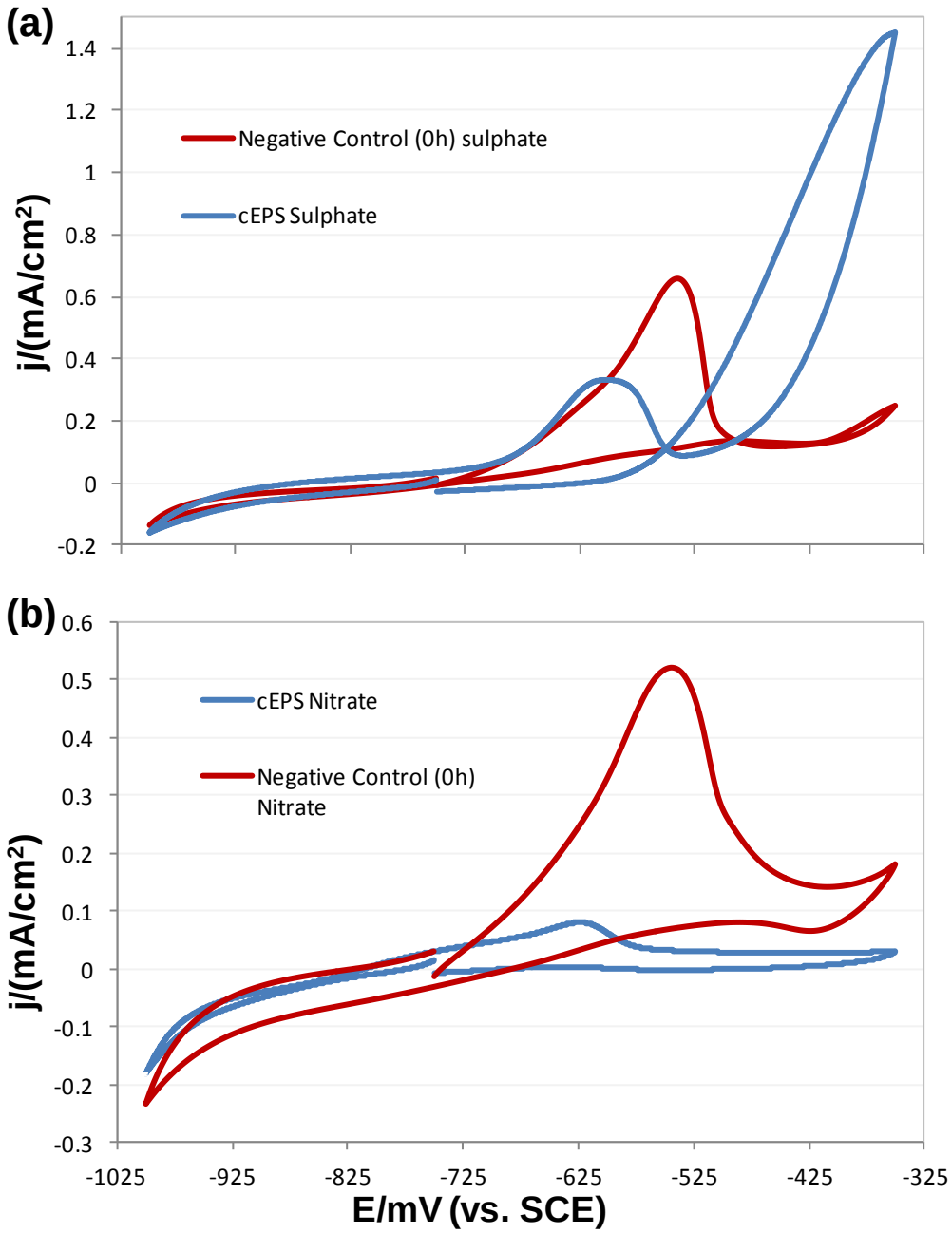

Figure 2.4: Cyclic voltammograms of carbon steel St52 in: (a) Colloidal EPS sulphate and respective negative control; (b) Colloidal EPS nitrate and respective negative control; initial scan direction: anodic.

The quasi-steady state assays allowed to extrapolate the correspondent Tafel's plots (Fig. 2.5) and from this we could calculate the corrosion potentials (E_{corr}), corrosion current densities (j_{corr}) and corrosion rate for the various conditions tested. These results are presented together with the weight loss data in Table 2.2.

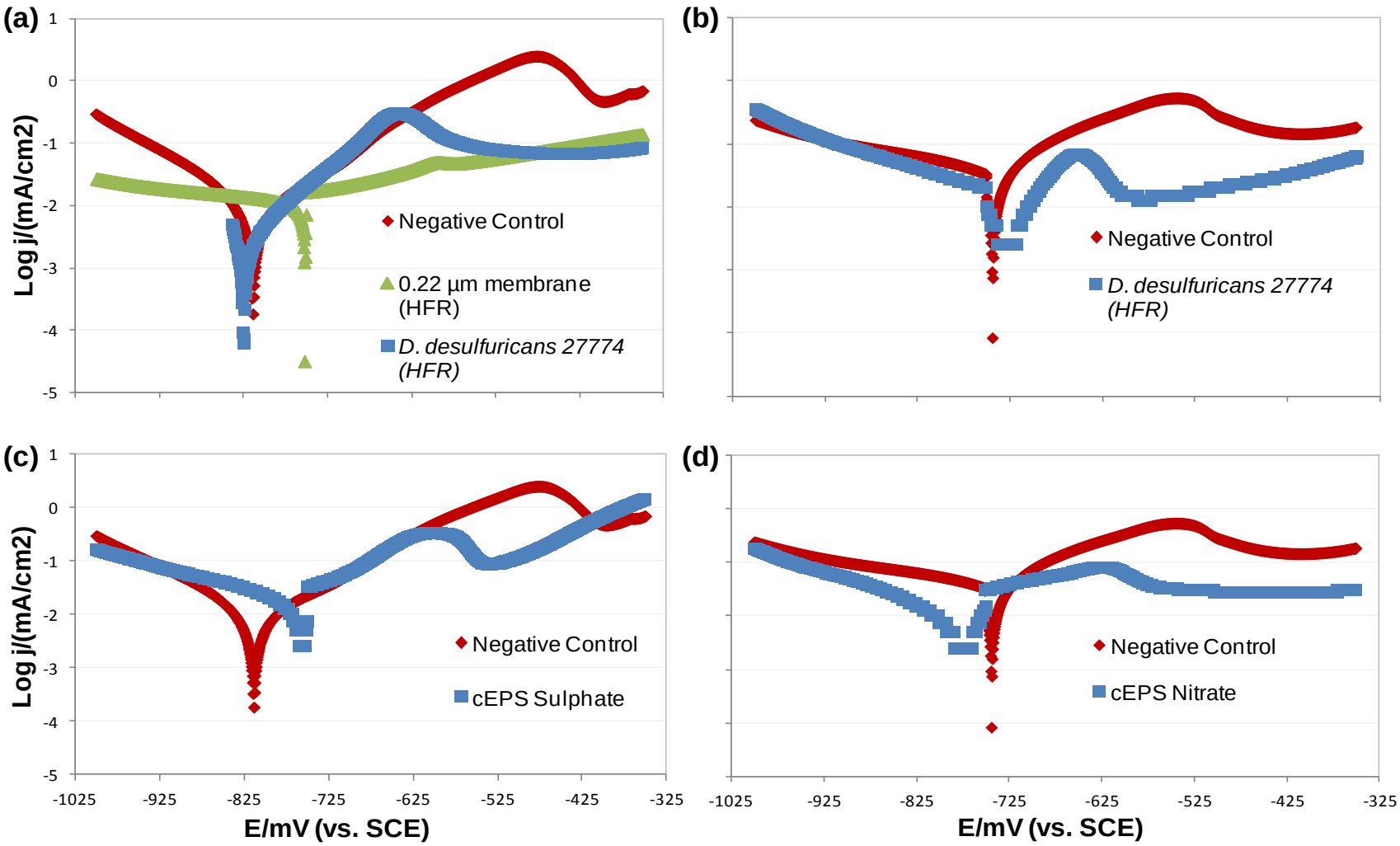

Figure 2.5: Tafel plots of the quasi-steady cyclic voltammetry of carbon steel in: (a) VMN sulphate with and without 0.22 µm membrane and respective negative control. b) VMN nitrate and respective negative control. (c) Colloidal EPS Sulphate and respective negative control. (d) Colloidal EPS Nitrate and respective negative control.

Table 2.2: Electrochemical parameters for corrosion of carbon steel, weight loss and ICP results in different conditions

	Electrochemical measurements					Weight loss test		ICP	
Medium	**E_{corr} (mV)**	**β_a (mV/Dec)**	**β_c (mV/Dec)**	**j_{corr} (µA/cm^2)**	**R^1 /(mm/y)**	**R^1 /(mm/y)**	**R^2 /(mm/y)**	**Dissolved Iron^1 /(mg/L)**	**Dissolved Iron^2 /(mg/L)**
VMN $SO_4^=$	-815.91	35.173	48.094	2.513	0.029	0.02 ± 0.0028	0.005 ± 0.0001	19.04	19.79
SRP in $SO_4^=$	-823.69	19.556	19.749	2.531	0.029	0.009 ± 0.0013	0.002 ± 0.0006	5.82	4.13
cEPS $SO_4^=$	-755.18	7.991	16.343	1.910	0.022	NA	NA	NA	NA
VMN NO_3^-	-743.51	7.247	9.082	2.362	0.027	0.021 ± 0.0015	0.005 ± 0.0007	18.84	14.05
SRP in NO_3^-	-727.77	27.530	20.769	3.716	0.043	0.172 ± 0.0237	0.093 ± 0.0115	158.3	189.4
cEPS in NO_3^-	-778.51	12.660	11.724	1.241	0.014	NA	NA	NA	NA

NA: Not available. All potential mentioned are *vs* SCE; β_a (Tafel anodic slope) = 2.303RT/α_AnF; β_c (Tafel cathodic slope) = 2.303RT/α_CnF. *R* (corrosion rate) = KW/(ρAt); [1]: 6 days incubation; [2]: 30 days incubation.

As the electrochemical data showed, coupons in nitrate media do not display localized corrosion; however these have the higher corrosion rates in accordance with the data from the weight loss and ICP. Our results confirm what has been reported previously that in the presence of sulphate reducing bacteria the electrochemical measurements are not accurate and can only be considered as indicative, as it overestimates the corrosion rate in sulphate and underestimates in nitrate [156]. It is interesting to note that in nitrate medium 27 to 45 times more dissolved iron was detected by ICP tests than in sulphate incubation. Nevertheless, the nature of the corrosion is different according to the medium (localized-sulphate *versus* uniform-nitrate) and pitting propagation analysis should be considered before any further conclusion about the aggressiveness to the metal of each respiratory substrate.

2.3.4. Scanning electron microscopy analysis

Fig. 2.6 shows micrographs of the carbon steel St37 after 6 and 30 days of incubation of *D. desulfuricans* in each inoculated media.

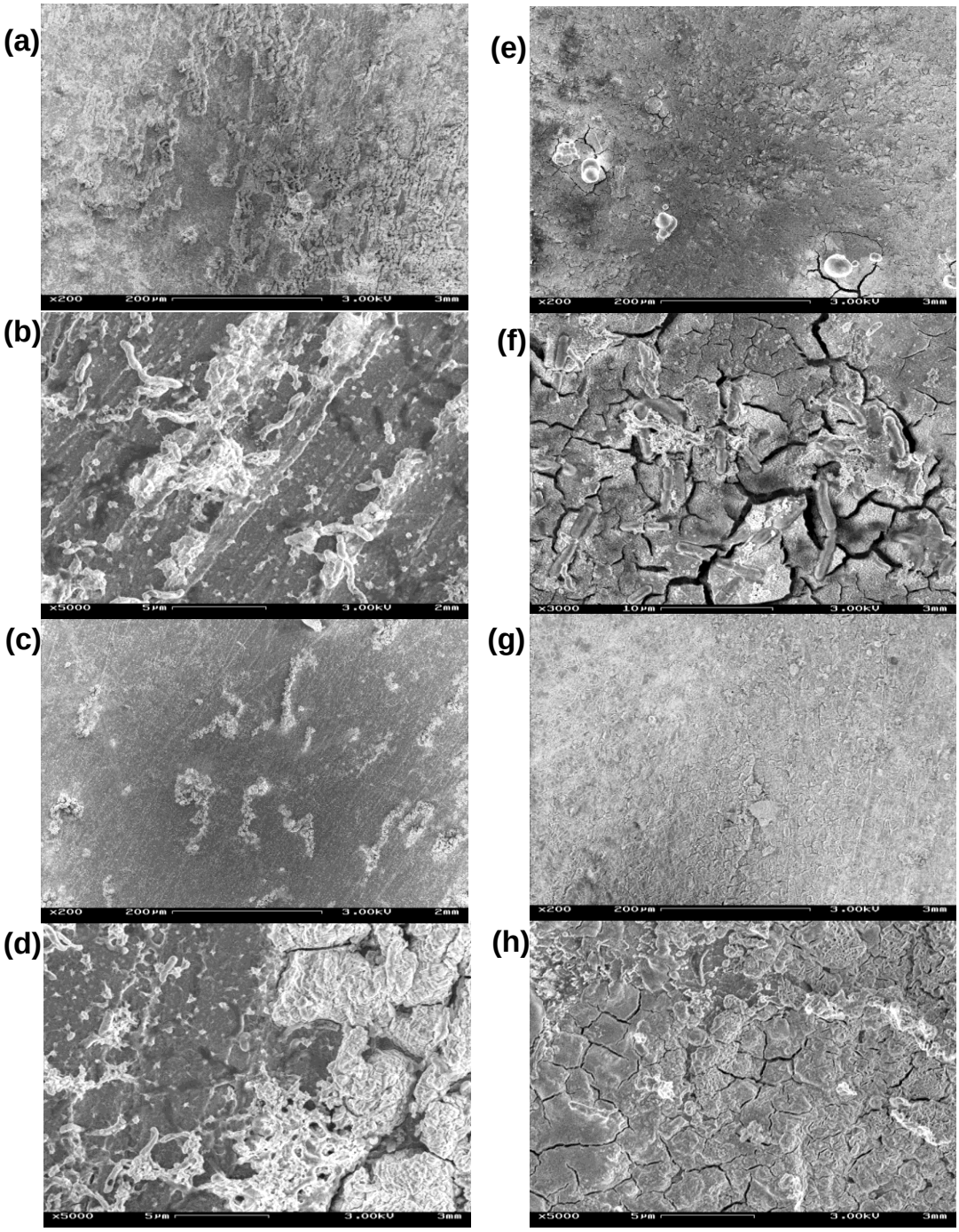

Figure 2.6: SEM micrographs of carbon steel samples after different exposure times and media to *D. desulfuricans* ATCC 27774 culture. VMN Sulphate and correspondant magnification: (a) 6 days, 200x; (b) 6 days, 5000x; (c) 30 days, 200x; (d) 30 days, 5000x. VMN Nitrate and correspondant magnification: (e) 6 days, 200x; (f) 6 days, 5000x; (g) 30 days, 200x; (h) 30 days, 5000x.

The micrographs in sulphate medium clearly show pits distributed on the surface near bacteria cells. The shape indicate that these pits were occurring beneath the cells themselves. After 6 days of incubation the surface is fully covered with a thick biofilm and with 30 days the biofilm bigger structures become more restricted to some areas of the metal, though the rest of the surface is also covered by a thin layer of EPS and cells. In

higher magnifications (data not shown), it is also possible to see many ball and flake shaped deposits that resemble calcium-rich and phosphorous-rich deposits described by previous studies [156]. A further Energy-dispersive X-ray spectroscopy (EDX) analysis is necessary to confirm this hypothesis.

In nitrate medium, the micrographs show huge structures (as the biofilm could be seen by naked eye) and cracks at the surface indicating the formation of rust. It is also clear that with long incubation periods, most part of the cells are dead, as a consequence of the depletion of nutrients that occurs much faster when compared to sulphate medium. Even though the number of viable bacteria is low, it is possible to recognize EPS products as biological material appearing in a lighter shade at the metal surface. This agrees with reported studies which showed that that some electroactive enzymes (like Hydrogenase) remain active even months after all cells died [24]. The composition of the EPS has also to be accounted for the corrosion process as it has already been proven that it can uptake iron from the metal thus increasing the corrosion [104]. Other studies also have shown that the metabolic products of SRB growth have a main role in the corrosion evolution [157] and should be taken into consideration.

2.4. Conclusions

The bulk media and metal interface compositions are strongly dominated and influenced by the SRP biofilm growth. In sulphate medium, the sulphide production as a dual aspect: as a main corrosion vector leading to an increase of the localized corrosion (depending on its concentration in the soluble phase) but can be also responsible for producing a stable protective FeS layer. Moreover, the nitrate medium, which is considered as an alternative to avoid localized corrosion, has serious implications in the general corrosion rate as demonstrated in this study.

The EPS composition differs significantly (data shown in chapter 4) depending on the respiratory substrate, with serious implications to the behaviour of carbon steel surface and type of corrosion observed. We observe that EPS from sulphate medium is more prone to cause localized corrosion. Further studies are on progress to fully characterize the composition of these EPS and to determine which components are mainly responsible for iron dissolution. Also, further surface analysis (such as EDS analysis) will complement the nature of the corrosion products at the surface of the metal, in order to correlate this to the bacteria metabolism.

Chapter 3

Surface Analysis of a mild steel corroded by a SRB model organism: application of surface analysis techniques

Chapter 3 – Surface Analysis of mild steel corroded by a SRB model organism

3.1. Introduction

Microbially Influenced Corrosion (MIC) is becoming an emerging concern in many industrial fields, from oil and gas through naval industry to any production or transportation process that has to rely on metals, as more studies add proofs of its importance from the economical and ecological point of view [8, 94, 97]. Von Wolzogen Kuhr and van der Flugt [28] first proposed a hypothesis to the role of hydrogenase in the evolution of the biocorrosion process with the cathodic depolarization theory. More recently, some studies have shown that the production of thiosulphate/sulphide can be the main responsible for the increase in the corrosion rate [19, 142]. The Unifying Electron Transfer Hypothesis proposed by Hamilton [32] considers a more complex interaction of factors, and covers some recent advances in the understanding of the biocorrosion process. Even though the process of metal degradation remains basically electrochemical, the fundamental problem when studying biocorrosion is the complexity of the system that cannot be explained by a single mechanism or theory. Instead, it should be looked as a synergetic interaction with three overlapping systems: material; environment; and microbial consortia [32, 92].

Although it is still difficult to separate the role of the microorganism from the abiotic variables, the literature agrees that microorganism attachment and consequent biofilm formation is one of the most important steps to speed up the corrosion evolution [11, 27, 91, 98, 143]. The development of a biofilm alters the conditions at the metal/bulk liquid interface allowing the creation of diverse gradients (pH, oxygen, flow, etc), protects the microorganisms from biocides, serves as a support to electrically active enzymes and other biomolecules, and the associated EPS are also able to bind metal cations [19, 96, 158]. There is still some debate about what is the exact role of the EPS in metal dissolution, some studies having shown that its metal chelating ability is the main responsible for iron dissolution [7, 104], and other results have shown that, in some conditions, it can in fact be protective to the surface [158].

Sulphate-reducing Prokaryotes (SRP) is a taxonomically diverse group able to couple the oxidation of a carbon source (such as lactate or fumarate) to the reduction of sulphur compounds to sulphide and was one of the first group to be related to MIC [19, 20, 92]. Although sulphate reduction cannot occur in the presence of oxygen, many SRP are oxygen tolerant or even able to grow in its presence, and so can be found in almost all places on Earth [38, 40]. Nitrate is one of the alternative respiratory substrate s that the SRP may use. The understanding of its metabolism has high importance to biocorrosion mitigation as it is commonly used as an inhibitor of SRP's and to prevent localized corrosion in many industries [13, 37, 49].

Time-of-FlightSecondary Ion Mass Spectrometry (ToF-SIMS) is a fast (from 1 to 15 min per sample), ultra high vacuum (UHV) technique with a high sensitivity and good lateral resolution which make it able to produce from simple spectra to 3D profiling and chemical mapping [159]. It uses a pulsed ion beam to eject secondary ions from the surface (approximately 1 nm depth) and can be used in a non destructive mode [131, 160]. It has been long used by polymer and electronic industry. In recent years, the use of high-throughput surface analysis techniques to characterize biological samples has however started to be more common as the evolution of the computer processing power along the development of bioinformatics tools and dissemination of Multivariate Statistical Analysis (MVA) allowed the study of more complex and large datasets [161-163]. Among the MVA methods available, Principal Component Analysis (PCA) is the most often used with ToF-SIMS data. Jungnickel *et al* used it to discriminate yeast strains and Ingram *et al* were able to successfully identify 28 bacterial strains [164, 165]. Some works have shown the applicability of ToF-SIMS to characterize metal samples exposed to seawater or to differentiate microbially and electrochemically induced pitting and to quantify iron uptake by EPS [4, 104, 132, 166]. The schematic representation of the ToF-SIMS sample analysis is presented in Fig. 3.1 [167].

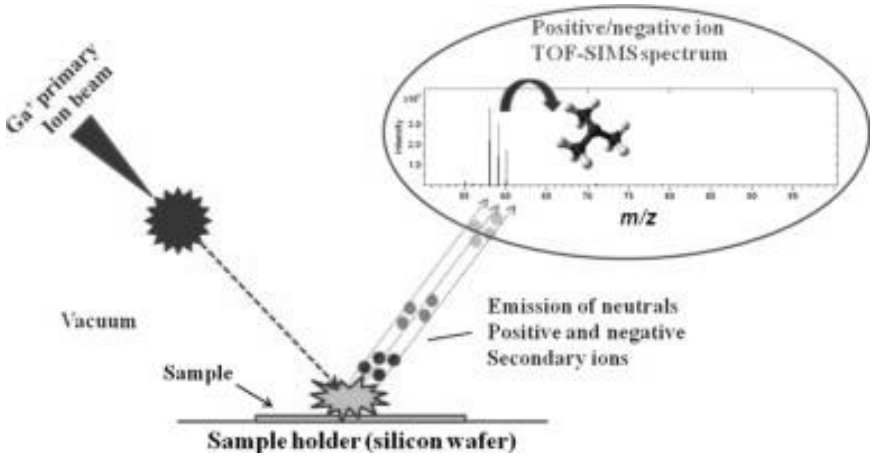

Figure 3.1: Schematic representation of ToF-SIMS sample analysis.

Scanning Electron Microscopy coupled to Energy-dispersive X-ray spectroscopy (SEM-EDX) is a traditional bulk/imaging technique that allows high lateral resolution microscopy of the sample surface along with its semi-quantitative chemical characterization. The probed depth is in 1 nm size. It has been extensively used in biocorrosion studies and to characterize biofilms on solid surfaces [168, 169].

X-ray Photoelectron Spectroscopy (XPS) is also a powerful UHV technique as it can provide direct chemical quantification of elements and functional groups in the outer surface layer probed depth in 10 nm [170]. It uses an X-ray beam to eject photoelectron from the

sample. Their kinetic energy is measured, allowing their binding energy to be determined, and consenquently correlate them to a given element and possibly chemical function. XPS allows a precise elemental quantification and the discrimination of different oxidation states to be achieved.This has been demonstrated to be very important when characterizing corroded surfaces [166, 171, 172]. A Schematic representation f XPS analysis is given in Fig. 3.2.

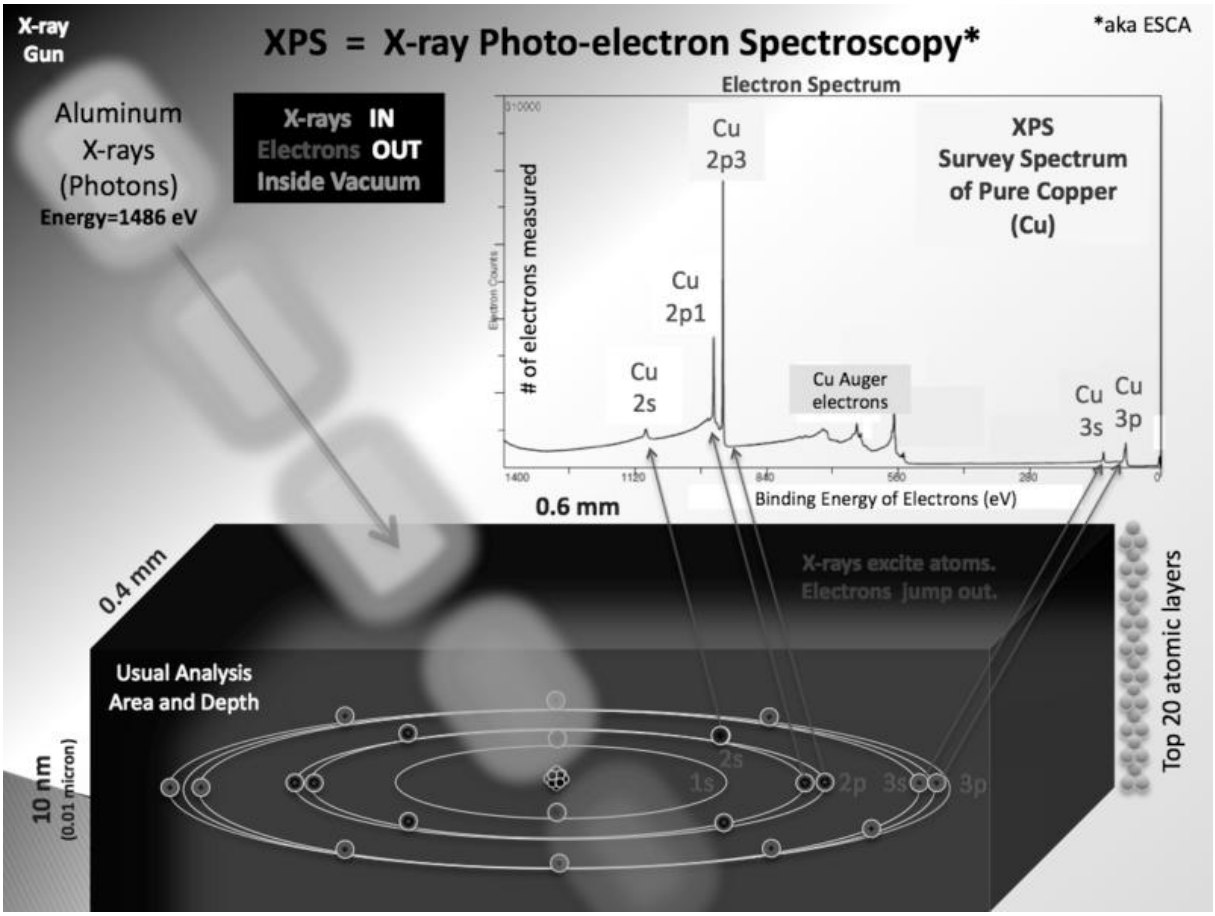

Figure 3.2: Schematic representation of a X-ray irradiation of a sample surface (source: Wikimedia Commons).

This study aims at analyzing the role of the respiratory substrate (sulphate, nitrate) on the corrosion of mild steel by a SRP model organism using high-throughput surface analysis and bulk techniques as ToF-SIMS, XPS and SEM-EDX. PCA was also used to that the generated ToF-SIMS spectra, in order to select ions that could be used as markers to differentiate biocorrosion from abiotic corrosion.

3.2. Experimental

3.2.1. Metal coupons preparation and incubation conditions

Metal plates (rectangles) with measures of 20x10x2 or 10x10x2 mm were used. The St37 carbon steel used is composed of iron and the following trace elements with mass ratio of 0.17% C, 1.4% Mn, 0.045% S, 0.045% P. The plates were polished to 600 grit (P1200) on both sides. A hole of 1 to 1.5mm area was drilled to hang the coupon using a nylon thread, each coupon having a total area of 3.8 cm^2 or 1.7 cm^2, respectively. All coupons were weighted with a precision scale just before being hanged at the rubber stopper of an empty 100 mL glass anaerobic bottle (3 coupons per bottle). Samples were exposed for 1h to UV light (253.7 nm) in a laminar airflow workstation to ensure sterility of the coupons. Two semi-defined culture media, modified from elsewhere [148], VMN Sulphate and VMN Nitrate were used (supplementary material S1). Sterile media were transferred to the bottles containing the coupons by argon positive pressure to keep sterility.

Negative controls which were not inoculated with bacteria were prepared with a final concentration of 1µg/mL of Ampicillin and 5µg/mL of Kanamycin to prevent contaminations. One extra control was prepared with the addition of 150 ppm of Na_2S to the VMN Sulphate medium to compare the influence of abiotic sulphide versus the biogenic one. After the pre-inoculums of *Desulfovibrio desulfuricans* ATCC 27774 reached 24h of growth, they were used as inoculums for the bottles containing the coupons and incubated at 30ºC for 6 and 30 days. A total of five conditions were tested ofr each period. All the experiments were done in duplicate. A list providing sample identification and conditions tested is given in Table 3.1.

Table 3.1: Tested conditions and identification of samples

Sample Number	ID	Respiratory substrate	Presence of bacteria	Incubation time	Exposed to oxygen after incubation
1.	**CS (Negative Control)**	NA	NA	NA	NA
2.	**A6**	Sulphate	No	6 days	No
3.	**B6**	Sulphate	Yes	6 days	No
4.	**C6**	Nitrate	No	6 days	No
5.	**D6**	Nitrate	Yes	6 days	No
6.	**E6**	Sulphate + 150 ppm of Na_2S	No	6 days	No
7.	**A30**	Sulphate	No	30 days	No
8.	**B30**	Sulphate	Yes	30 days	No
9.	**C30**	Nitrate	No	30 days	No
10.	**D30**	Nitrate	Yes	30 days	No

Table 3.1 (Cont.): Tested conditions and identification of samples

Sample Number	ID	Respiratory substrate	Presence of bacteria	Incubation time	Exposed to oxygen after incubation
11.	**E30**	Sulphate + 150 ppm of Na_2S	No	30 days	No
12.	**AO6**	Sulphate	No	6 days	Yes
13.	**BO6**	Sulphate	Yes	6 days	Yes
14.	**CO6**	Nitrate	No	6 days	Yes
15.	**DO6**	Nitrate	Yes	6 days	Yes
16.	**AO30**	Sulphate	No	30 days	Yes
17.	**BO30**	Sulphate	Yes	30 days	Yes
	CO30	Nitrate	No	30 days	Yes
18	**DO30**	Nitrate	Yes	30 days	Yes

N.A.- Not applicable.

3.2.2. Surface analysis

When the incubation time was over, the bottles were opened and the coupons removed. One set of coupons was removed in an anaerobic glove box (with a maximum of 15 ppm of oxygen) to avoid exposure to oxygen and stored in anaerobic bottles with rubber caps and parafilm. The bottles were them flushed with argon to ensure a maximum anoxic atmosphere. The other set of coupons was removed in ambient conditions, placed in a 15 ml tube (falcon) previously flushed with argon for 1 min and stored in a desiccator.

3.2.2.1. Time of Flight Secondary Ion Mass Spectometry (ToF-SIMS)

The corroded metal plates were analyzed by ToF-SIMS with an ION-TOF V (ION-TOF, GmbH, Münster, Germany) spectrometer, using a Bi^{3+} primary ion source. The analyzed area was 500×500μm^2 and the acquisition time for each spectrum was 1 min. Three positive and three negative spectra were acquired on each sample with a pulsed 30keV, 0.67pA primary ion beam in the high current bunched mode. The total ion dose was 1.1×10^{11} Bi^{3+}/cm^2, below the static SIMS limit. Positive ion mass spectra were calibrated using the CH_3^+, $C_2H_3^+$, $C_3H_5^+$ and $C_4H_7^+$ peaks. Negative ion mass spectra were calibrated using the CH_2^-, C_2H^-, C_3^- and C_4H^- peaks. All data analysis was carried out using the software supplied by the instrument manufacturer, SurfaceLab (version 6.1). The intensity of each peak was calculated using the area of the peak that was determined by setting manually a lower and upper m/z ratio. Principal Component Analysis was performed using the software Multi-Ion SIMS (Biophy Research, France). The chosen peak intensities were normalized by the sum of intensities of the selected peaks.

3.2.2.2. Scanning Electron Microscopy - Energy-dispersive X-ray spectroscopy analysis

The samples not exposed to oxygen were observed with a JEOL FEG SEM 7600F equipped with an EDX system (Jeol JSM2300 with a resolution < 129eV), without any metal coating. To determine the morphology, samples were observed with the in-lens detector coupled with the r-filter, which allows the detection of mixed electrons (50% secondary electrons and 50% backscattered electrons). For both analysis (morphology or chemical characterization), the same conditions were used: accelerating voltage of 15keV and working distance of 8 mm. The acquisition time for chemical (EDX) spectra were 300s with a probe current of 1nA.

The semi-quantitative analyses of atomic elements were done with the integrated software Analysis Station. A two-step analysis procedure was necessary to obtain quantitatively reliable results for the elements profiles over the entire cross sections: (i) the subtraction of bremsstrahlung was done with the classical "Top Hat Filter" method [173, 174] and (ii) the quantification of area under each atomic peak was determined by the φ(ρz) model [175-177]. This semi-quantitative determination can be done for the full image or for specific line profiles.

For the samples exposed to oxygen, the scanning electron microscopy analysis was conducted using a high resolution FEG Digital Scanning microscope 982 Gemini (Leo Electron Microscopy) operating at 1 or 2 kV, without any metal coating. No EDX analysis was done on these samples.

3.2.1.3. X-ray photoelectron spectroscopy (XPS)

XPS measurements were carried out only for the samples exposed to oxygen using a Kratos Axis Ultra spectrometer (Kratos Analytical, UK), with a monochromatized Al X-ray source (10mA, 15kV) and an eight-channeltrons detector in high vacuum. The analyzed area was 100 x 100 μm^2. The direction of photoelectron collection was perpendicular to the sample surface (0°). Charge stabilization was achieved by using the Kratos Axis device. Survey spectra were recorded with 160eV pass energy; the narrow scans were done using 40eV pass energy. The binding energy scale was calculated with respect to the aliphatic C-(C,H) component of the C 1s peak that was fixed to 284.8eV. The following sequence of spectra was recorded: survey spectrum, C 1s, O 1s, N 1s, Fe 2p, S 2p, P 2p and Na 1s. C 1s has been analyzed three times (beginning, middle and end) to check for charge stability as a function of time. Molar ratios were calculated after a linear background subtraction using peak areas normalized on the basis of acquisition parameters, experimental sensitivity factors and transmission factors provided by the manufacturer. The spectra were

decomposed with the CasaXPS program (Casa Software Ltd., U.K) with a Gaussian/Lorentzian (70/30) product function.

3.3. Results and Discussion

3.3.1. ToF-SIMS and PCA analysis of corroded carbon steel

A peak list was created with 80 peaks (for positive ions) and 46 (for negative ions), and which was used to treat ToF-SIMS data acquired on all samples. The selection of the peaks was based on previous studies, and was focused on biomolecules (proteins, sugars, etc) and corrosion markers [131, 132, 161, 162, 166, 178]. Chemical maps of the corroded surface were built using the original spectra and choosing 60 and 45 peaks for positive and negative secondary ions, respectively. Table 3.2 presents the 52 peaks related to biomolecules detected on the samples.

Table 3.2: Principal detected peaks attributed to biomolecules

ID	Molecular structure	*m/z*	Corresponding biomolecule	ID	Molecular structure	*m/z*	Corresponding biomolecule
1.	NH_4+	18	Glycan	**27.**	C_4H_6NO+	84.5	Gln, Glu
2.	CH_2N+	28	Ala, Arg, Asn, Glu, Leu, Ser, Trp	**28.**	$C_5H_{10}N$+	85	Lys, Leu
3.	CH_4N+	30	Glycan and/or many amino acids	**29.**	$C_3H_4NO_2$+	86	Asp
4.	C_2H_4N+	42	Ala, Gly, His, Leu, ser	**30.**	$C_5H_{12}N$+	86.2	lle, Leu, Phosphatidycholine
5.	C_2H_3O+	43	Glu	**31.**	$C_3H_6NO_2$+	88	Asn, Asp
6.	C_2H_6N+	44	Ala, Asn, Leu, Glycan	**32.**	C_7H_7+	91	Tyr, Phe
7.	CHS+	45	Cys	**33.**	C_4H_8SN+	102	Met
8.	CH_3S+	46	Cys	**34.**	$C_4H_{10}SN$+	104	Met
9.	C_3H_4N+	54	His	**35.**	$C_5H_8N_3$+	110	His, Arg
10.	C_3H_6N+	56	Lys, Met, Val	**36.**	$C_6H_{10}NO$+	112	Arg
11.	C_2H_4NO+	58.02	Ser	**37.**	$C_4H_7N_2O_2$+	115	Glycine,
12.	C_3H_8N+	58.06	Glu	**38.**	$C_5H_7O_3$+	115	Xylose
13.	C_2H_3S+	59	Cys	**39.**	C_8H_8N+	118	Phe
14.	C_3H_7O+	59.5	Glycan	**40.**	$C_8H_{10}N$+	120	Phe
15.	C_2H_6NO+	60	Ser	**41.**	$C_6H_7O_3$+	127	Glucose
16.	C_2H_5S+	61	Met	**42.**	C_9H_8N+	130	Try
17.	C_4H_6N+	68	Pro, Lys	**43.**	C_9H_7O+	131	Phe
18.	C_4H_5O+	69	Thr	**44.**	$C_5H_9O_4$+	133	Arabinose
19.	C_4H_8N+	70	Pro, Val	**45.**	C_8H_8NO+	134	Tyr
20.	$C_3H_3O_2$+	71	Ser	**46.**	$C_8H_{10}NO$+	136	Tyr
21.	$C_4H_{10}N$+	72	Val	**47.**	$C_6H_{11}O_5$+	163	Glucose

Table 3.2 (cont.): Principal detected peaks attributed to biomolecules

ID	Molecular structure	*m/z*	Corresponding biomolecule	ID	Molecular structure	*m/z*	Corresponding biomolecule
22.	C_3H_8NO+	74	Thr	**48.**	CHO_2-	45	Fatty acids
23.	C_2H_6SN+	76	Cys	**49.**	$C_2H_3O_2-$	59	Fatty acids
24.	C_6H_5+	77	Phe, Tyr	**50.**	$C_3H_3O_2-$	71	Fatty acids
25.	$C_4H_6N_2+$	82	His	**51.**	$C_{16}H_{31}O-$	255	Fatty acids
26.	C_5H_7O+	83	Val	**52.**	$C_{18}H_{35}O-$	283	Fatty acids

As mentioned, all the data were normalized to the sum of the selected peaks. This data treatment is very important considering the type of sample that has been analyzed, since the topography can vary significantly intra and inter sample in the case of biofilms and corroded metal surfaces. This treatment is also useful to eliminate the variance that is due to instrumental conditions and sample charging [131, 163]. In our study, we decided to use PCA only on the spectral results (not on images) and as suggested by the literature the mean-centering was chosen to allow comparison of the variables with a common mean of zero. This allows detecting marked differences between samples which would be hidden by small variation in the case of an auto-scaled data pre-treatment [161].

Figure 3.1 presents the results of the PCA treatment applied to the positive (Fig. 3.1a) and the negative (Fig. 3.1b) spectra. The first PC (PC1) collects 52.7% and the second PC (PC2) answers for about 22.7% of the variance in the case of the positive ions. We can observe in Fig. 31a that PC2 allows the separation of groups of samples according to the exposure to oxygen after the incubation. It must be pointed out that the intra-variation is quite high among all analyzed samples. This is understandable considering the natural variability that is expected for bacterial growth, metal surface microstructure and biofilm 3D structure, even though at least 3 spot per sample were used in the statistical analysis.

In the case of the negative ions (Fig. 3.1b), and the separation of the samples is less clear PC1 collect 39.5% and PC2 35.3% of the total variance. It is not surprising that main differences between samples are better evidenced using positive ions, since most biomolecules and iron oxides produce positive ions, although some important markers such as hydrogen sulphide and phosphate have actually negative charges.

Some carbon contaminations in metal surface are always expected [132]. Although just a few of the peaks related to hydrocarbons were selected for the statistical analysis. In the case of complex samples like the biofilms, a high number of peaks remained unidentified especially on the range of the higher masses, as the possible molecules that can generate each peak increases exponentially. That makes impossible a precise identification without knowing the exact composition of the layer in study.

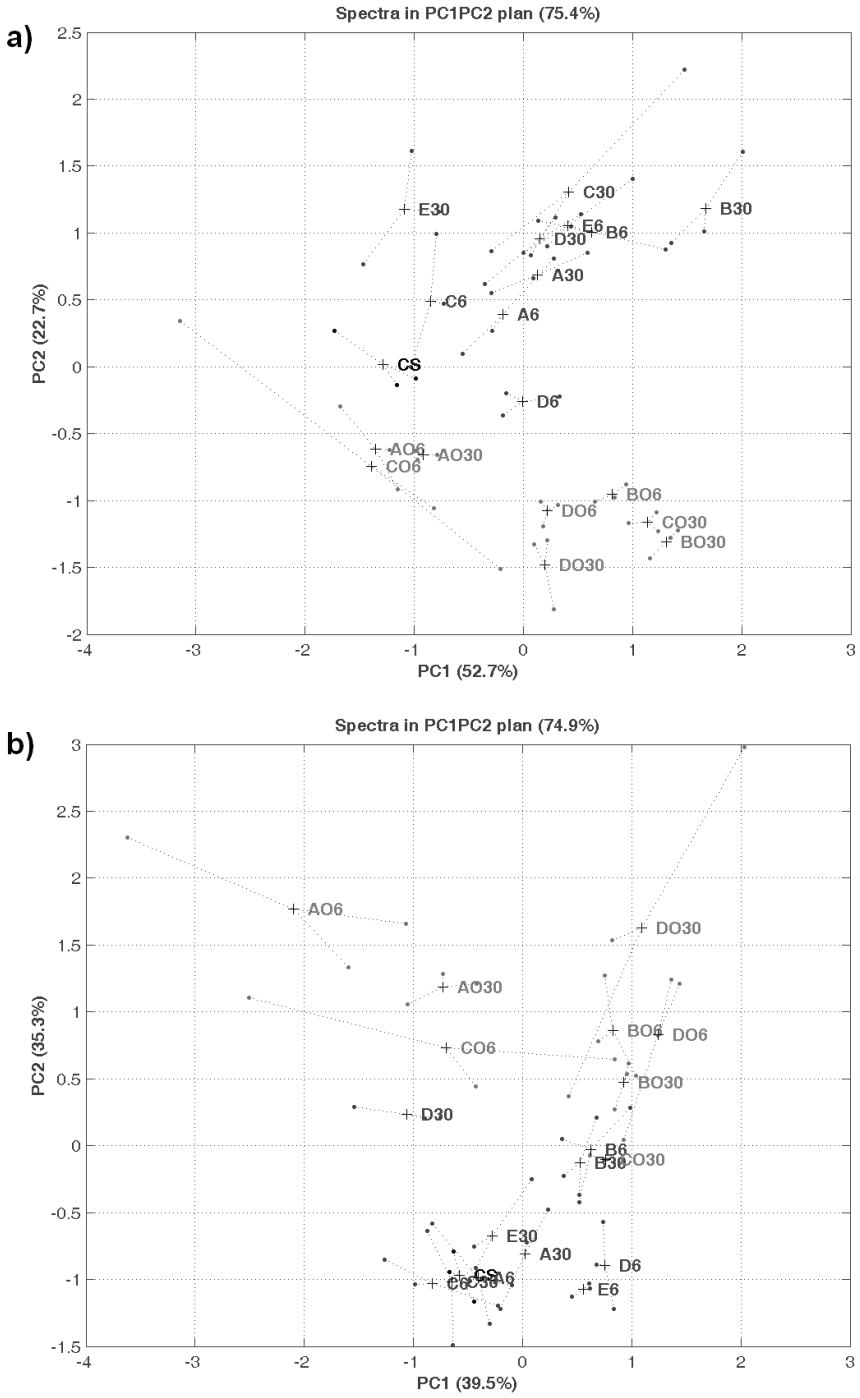

Figure 3.3: Results of PCA treatment performed on ToF-SIMS data. a) Positive ions spectra; (Black) Control Carbon Steel; (Dark gray) Samples unexposed to oxygen after incubation; (Light gray) Samples exposed to oxygen after incubation. b) Negative ions spectra; (Black) Control Carbon steel; (Dark gray) Samples unexposed to oxygen after incubation; (Light gray) Sample exposed to oxygen after incubation.

The analysis of the loading and scores plots, presented in Fig. 3.3 allows further interpretation of the scores presented in Figure 3.1. For loadings, the higher absolute values contribute more to the definition of the PC and the more positive values for a given m/z ratio,

are more strongly correlated to the samples with more positive values in the score plot and conversely for negative values [161, 163].

It appears that for the PC1 obtained on positive ion spectra, the main peaks responsible for the variance between samples are attributed to inorganic ions such as iron, iron hydroxide and some organic compounds. For PC2, besides the previously mentioned peaks, calcium (positive loading values) unexposed to oxygen samples and some protein markers (negative loadings values) would be more present in the samples exposed to oxygen. The important influence of inorganic ions is expected because of the composition of the metal surface, and also of the growth medium is rich in calcium, potassium, phosphate and other inorganic salts which tend to form deposits at the surface as can been seen in the SEM section of this chapter. In the case of the metal samples incubated with bacteria, they tend to exhibit a more complex layer of EPS and/or biofilm in the surface and not only salts, though the amplitude of the variance attributed to such compounds is much smaller than when compared to the one of the inorganic components.

For the negative secondary ions (Fig. 3.2b), the most important ions in PC1 were phosphates, chlorides, hydroxide and some nitrogen markers that could be related to proteins. In the PC2 remain the phosphates, chlorides and some hydrocarbons. The relation between inorganic ions (such as Ca+, PO_3-, Cl-) and the EPS composition and iron uptake will be discussed further in this section. The complete list positive and negative loading lists are available at tables 3.3 to 3.6.

Table 3.3: Top 10 positive and negative loading values for PC1 of positive ions.

N	Load	Mass	Ion	Biological molecule
#40	28903.25	73.05	C_3H_7NO+	
#13	10208.77	43.05	C_3H_7+	
#33	9069.53	70.07	C_4H_8N+	Pro, Val
#14	6156.70	44.05	C_2H_6N+	Ala, Asn, Leu, Glycan
#18	5250.26	46.99	CH_3S+	Cysteine
#41	4330.78	74.05	C_3H_8NO+	Threonine
# 8	4270.08	30.03	CH_4N+	Gly, Arg, Asn, Glu, Leu, Lys, Ser, Glycan
#20	4245.69	55.05	C_4H_7+	
#32	3934.33	69.07	C_5H_9+	
# 5	3841.75	27.98	Si+	
# 9	-2189.15	31.02	CH_3O+	
#80	-2225.37	287.72	Fe_4O_4+	
# 1	-2392.82	15.02	CH_3+	
#79	-3992.60	215.79	Fe_3O_3+	
#34	-4522.39	70.96	CH_3Fe+	
#70	-6081.65	127.87	Fe_2O+	

Table 3.3 (Cont.): Top 10 positive and negative loading values for PC1 of positive ions.

N	Load	Mass	Ion	Biological molecule
#76	-7161.75	144.87	Fe_2O_2H+	
#12	-9575.83	43.02	C_2H_3O+	Glutamic acid
#39	-18844.59	72.94	FeOH+	
#21	-61624.53	55.93	Fe+	

Table 3.4: Top 10 positive and negative loading values for PC2 of positive ions.

N	Load	Mass	Ion	Biological molecule
#40	25405.32896	73.05	C_3H_7NO+	
#21	14464.2177	55.93	Fe+	
#20	14100.30217	55.05	C_4H_7+	
#10	11888.90059	39.96	Ca+	
#18	10644.72282	46.99	CH_3S+	Cysteine
# 5	10063.27453	27.98	Si+	
#13	9700.76177	43.05	C_3H_7+	
#42	5239.1531	75.02	SiC_2H_7O+	
# 7	3721.4321	29.04	C_2H_5+	
#15	3365.76255	44.98	CHS+	Cysteine
#11	-3305.30736	42.03	C_2H_4N+	Ala, Gly, His, Leu, ser
#31	-3408.51198	69.04	C_4H_5O+	Threonine
# 2	-4452.14682	18.03	NH_4+	Glycan
#30	-5018.78252	68.06	C_4H_6N+	Pro, Lys
#39	-5896.63024	72.94	FeOH+	
#12	-6039.17828	43.02	C_2H_3O+	Glu
# 6	-10367.51985	28.02	CH_2N+	Ala, Arg, Asn, Glu, Leu, Ser, Trp
#14	-10575.33493	44.05	C_2H_6N+	Ala, Asn, Leu, Glycan
# 8	-13465.437	30.03	CH_4N+	Gly, Arg, Asn, Glu, Leu, Lys, Ser, Glycan
#33	-15191.97571	70.07	C_4H_8N+	Pro, Val

Table 3.5: Top 10 positive and negative loading values for PC1 of negative ions.

N	Load	Mass	Ion	Biological molecule
#31	29434.72077	78.96	PO_3-	
# 7	29028.62397	26	CN-	
#14	22063.38777	42	CNO-	
#24	17000.8065	62.97	PO_2-	
#10	5282.68386	32.98	HS-	
#21	3713.33222	50	C_3N-	
# 8	3614.80382	31.97	S-	
#27	3310.67917	66	C_3NO-	
# 1	2941.58265	13.01	CH-	Hydrocarbon
#34	2438.16259	90.99	$C_2H_4PO_2$-	
#18	-1311.31197	44.98	SiHO-	
#13	-2389.94912	41	C_2HO-	
# 9	-2645.26162	31.99	O_2-	

Table 3.5 (Cont.): Top 10 positive and negative loading values for PC1 of negative ions.

N	Load	Mass	Ion	Biological molecule
#23	-3640.68968	59.97	SiO_2-	
#22	-6068.38345	59.01	$C_2H_3O_2$-	Fatty acids
# 6	-8343.41939	25.01	C_2H-	Hydrocarbon
#33	-9676.1863	87.92	FeO_2-	
#19	-13400.35726	45	CHO_2-	Fatty acids
# 5	-37896.17846	17	OH-	
#11	-43920.33474	34.97	Cl-	

Table 3.6: Top 10 positive and negative loading values for PC2 of negative ions.

N	Load	Mass	Ion	Biological molecule
#31	41939.17736	78.96	PO_3-	
#11	25826.10115	34.97	Cl-	
#24	23780.82401	62.97	PO_2-	
#19	7494.10767	45	CHO_2-	Fatty acids
#22	6445.95314	59.01	$C_2H_3O_2$-	Fatty acids
#33	4603.25709	87.92	FeO_2-	
# 9	1614.33139	31.99	O_2-	
#28	1542.69392	71.01	$C_3H_3O_2$-	Fatty acids
#36	1171.19738	96.96	SO_4H-	
#32	920.91725	79.96	SO_3-	
# 2	-1741.07725	14.02	CH_2-	
#14	-2908.74693	42	CNO-	
#30	-2994.42259	74.99	$CHNO_3$-	
#21	-3250.46005	50	C_3N-	
#23	-3887.2217	59.97	SiO_2-	
#13	-5917.30496	41	C_2HO-	
#20	-10228.85877	49.01	C_4H-	Hydrocarbon
# 1	-16140.82089	13.01	CH-	Hydrocarbon
# 7	-20937.76749	26	CN-	
# 6	-40886.17196	25.01	C_2H-	Hydrocarbon

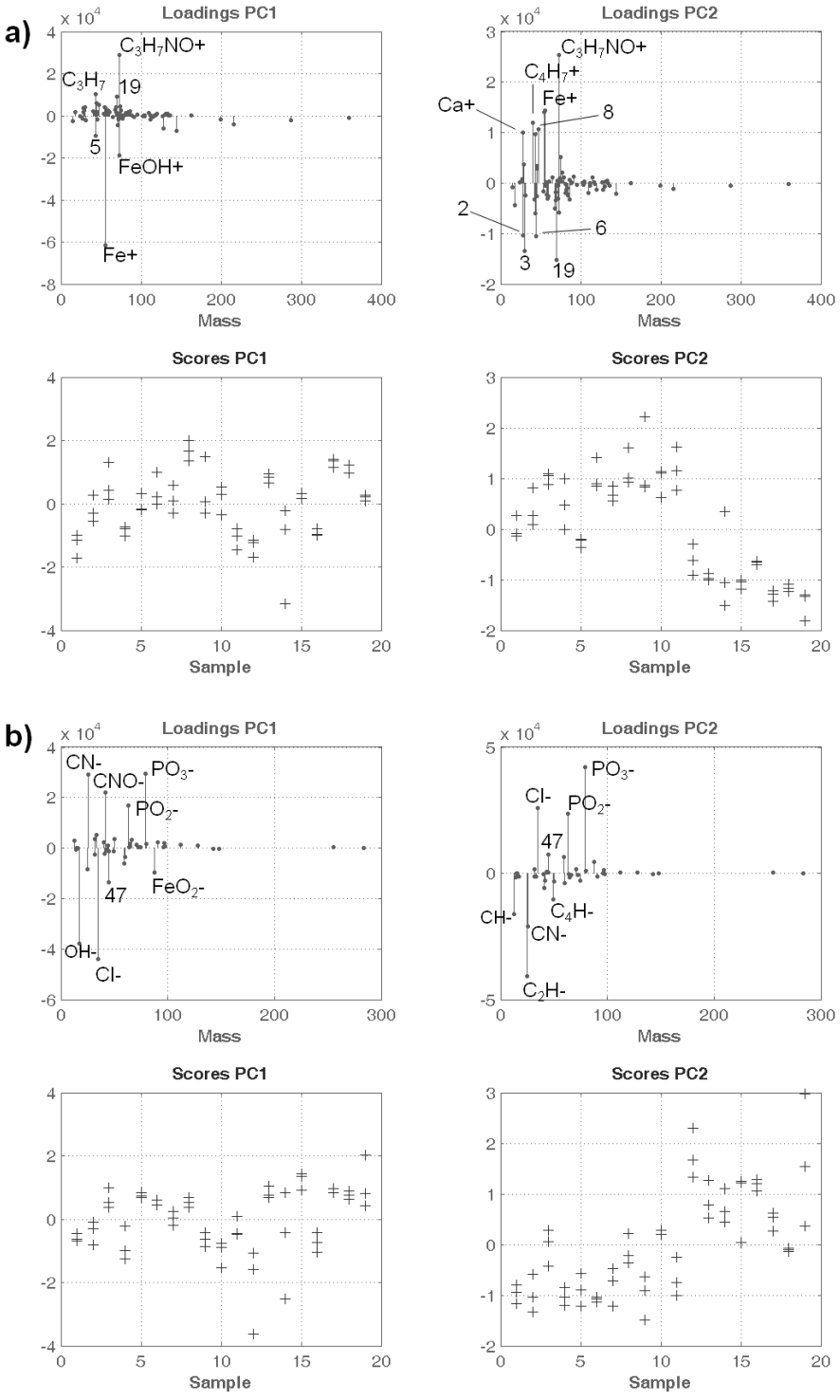

Figure 3.4: Loadings and Scores plotting from ToF-SIMS ions data. a) Positive spectra plotting and samples scores with the data normalized and mean-centered. b) Negative spectra plotting and sample scores with the data normalized and mean-centered. In loading plotting the numbers indicate the respective biomolecules listed in table 3.2. In score plotting the numbers indicate the respective sample ID listed in table 3.1.

3.3.2. ToF-SIMS chemical mapping and surface alteration

The chemical mapping of the main positive and negative ions of the samples unexposed to oxygen is shown in Fig. 3.5:

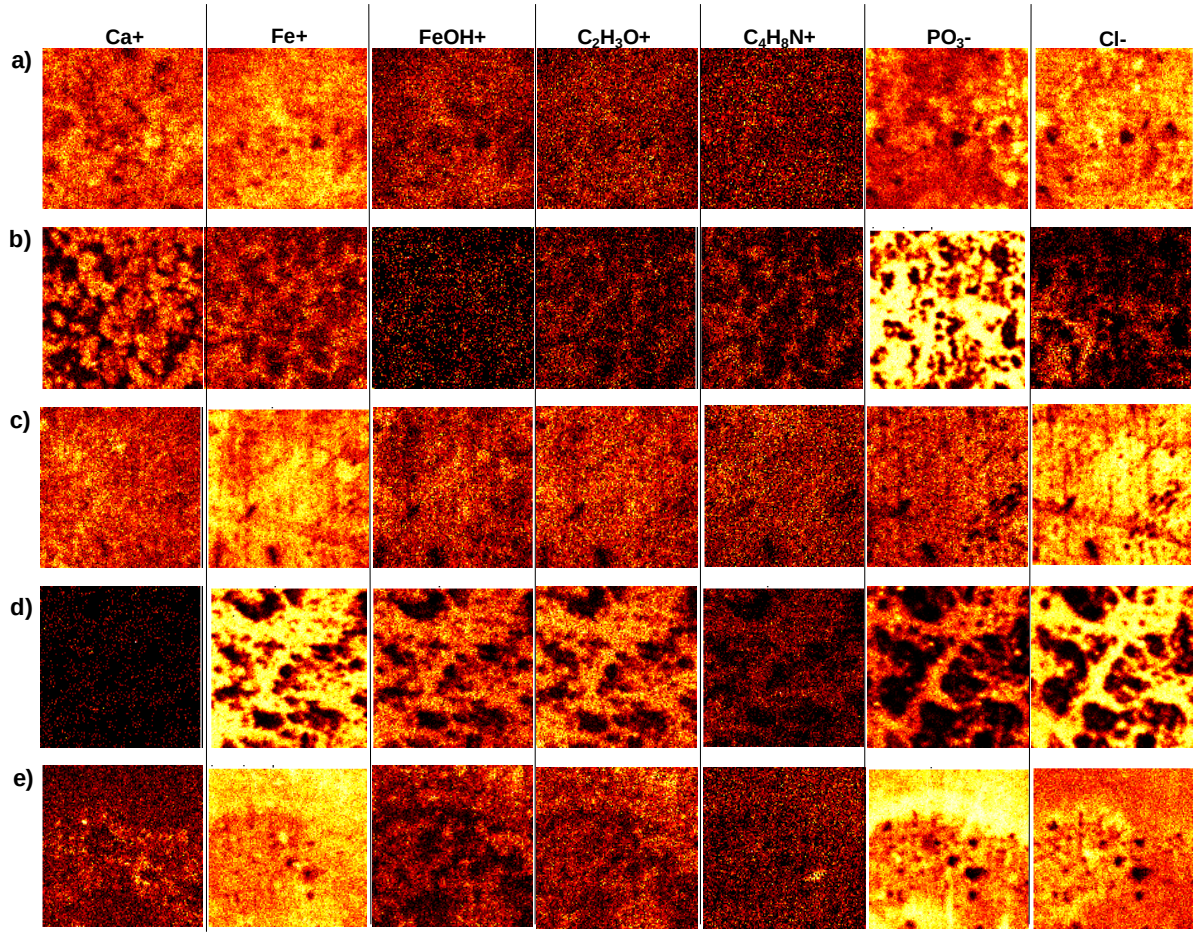

Figure 3.5: Chemical mapping from ToF-SIMS data of samples unexposed to oxygen. a) Main positive and negative ions from sample A30. b) Main positive and negative ions from sample B30. C) Main positive and negative ions from sample C30. d) Main positive and negative ions from sample D30. E) Main positive and negative ions from sample E30. All images are 500x500 μm^2. In all images the ion intensity is proportional to the brightness of the scale (the darker the weaker).

The analysis of figure 3.5 showed that there is a complementarity between the Ca^+ and the Fe^+ ions in the sulphate samples in all periods of incubation although in the case of the nitrate medium this was not observed. Some authors have shown that in the case of calcium ions, precipitation does not occur easily because of pairing with other organic compounds or sulphate [179]. However, the sulphate reduction with organic acid consumption, and consequent pH increase, can enhance the precipitation of carbonate minerals [180, 181] which are exactly the conditions created in the culture medium used during our tests.

When incubated with bacteria, the PO_x^- ions also seem to be more present in the zones were Fe^+ is not so high. This is also observed with HS^- ions (data not shown). This could be linked to the fact that at the pH of the bacteria culture, around 8.6-8.9, the Extracelullar

Polymeric Substances undergo a deprotonation of functional groups, mainly sulphate and phosphate groups which contributes to the negative charge of EPS [158]. This characteristic could be responsible for the observed increase of the iron uptake by the EPS and consequently corrosiveness from SRB's [7, 50]. This is also observed in the samples exposed to oxygen after incubation (Fig. 3.6).

In the nitrate incubations, Cl^- seems to be abundant, even though it does not exhibit the same behavior of complementarity to Fe^+ as in sulphate samples where there was a more localized corrosion evolution. Many studies have shown that chloride ions are highly aggressive to steel corrosion and that their abundance in the nitrate EPS could be responsible for the higher corrosion observed in the previous chapter comparing both respiratory substrates.

This result was observed also in the sulphate control without bacteria however not so strongly, demonstrating that the sulphide and EPS production enhance the precipitation of the inorganic ions and probably also the rate of localized corrosion.

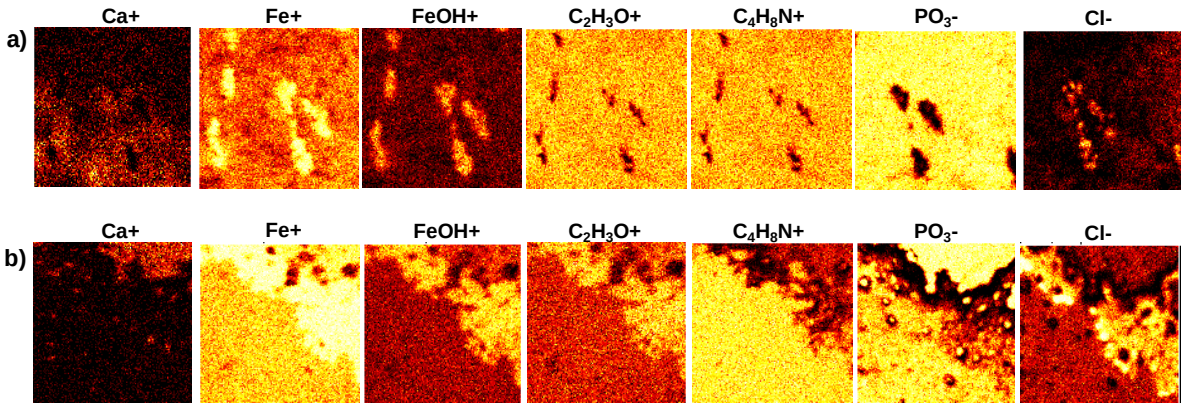

Figure 3.6: Chemical mapping from ToF-SIMS data from samples exposed to oxygen after incubation. a) Main positive and negative ions from sample BO30. b) Main positive and negative ions from sample DO30. All images are 500x500 μm^2. In all images the ion intensity is proportional to the brightness of the scale (the darker the weaker).

In the samples exposed to oxygen after incubation (Fig. 3.6), it appears that in sulphate incubation with bacteria pitting corrosion was taking place. On the other hands, in nitrate, in different areas it can be seen that they are rich in iron and poor in protein markers, which indicates the formation of rust that was detected by the XPS analysis. Also, as already shown in previous studies [8, 91], periods of oxygen exposure of surfaces already corroded anaerobically, increases the corrosion rate and pitting to levels much higher than in systems kept in anoxic conditions.

3.3.3. SEM-EDX and XPS: visual and chemical characterization of the metal/biofilm surface

The incubated metal coupons were also examined by scanning electron microscopy (SEM) and Energy-Dispersive X-ray Spectroscopy, for the ones unexposed to oxygen and SEM plus X-ray Photoelectron Spectroscopy, in the case of the samples exposed to oxygen after the incubation with SRB.

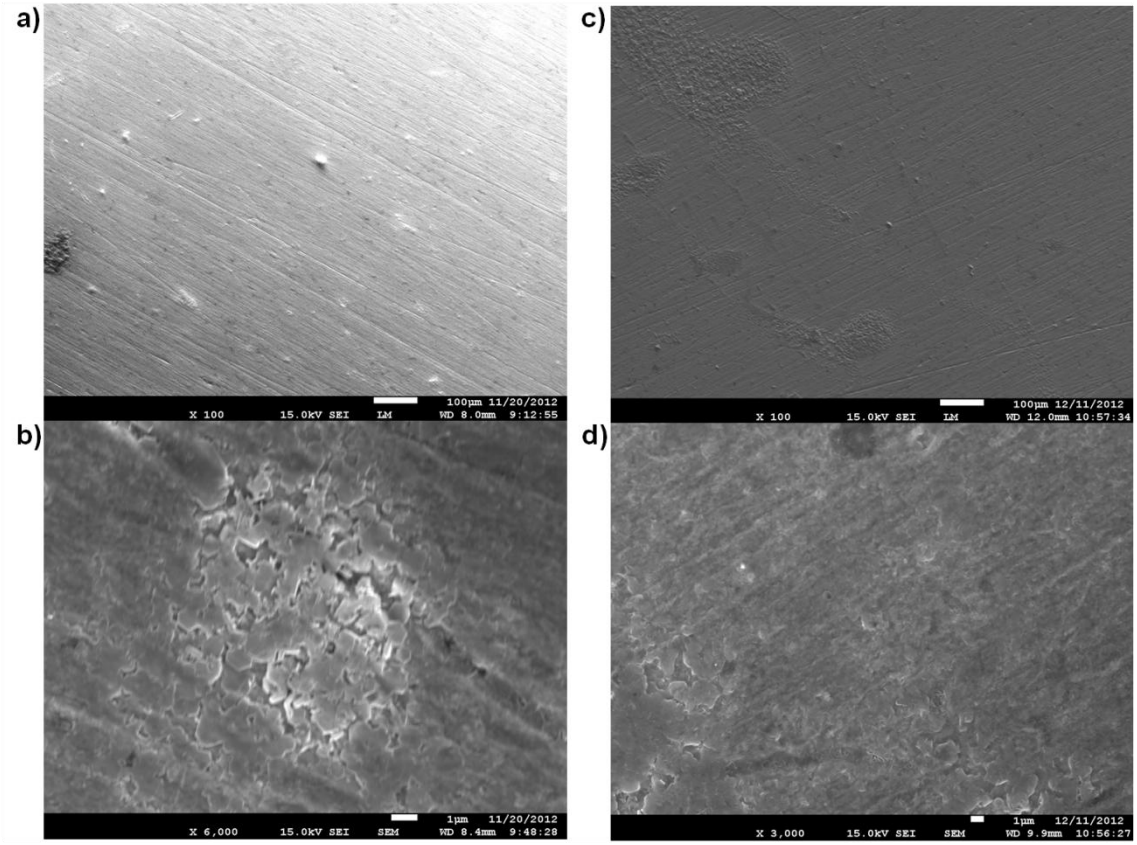

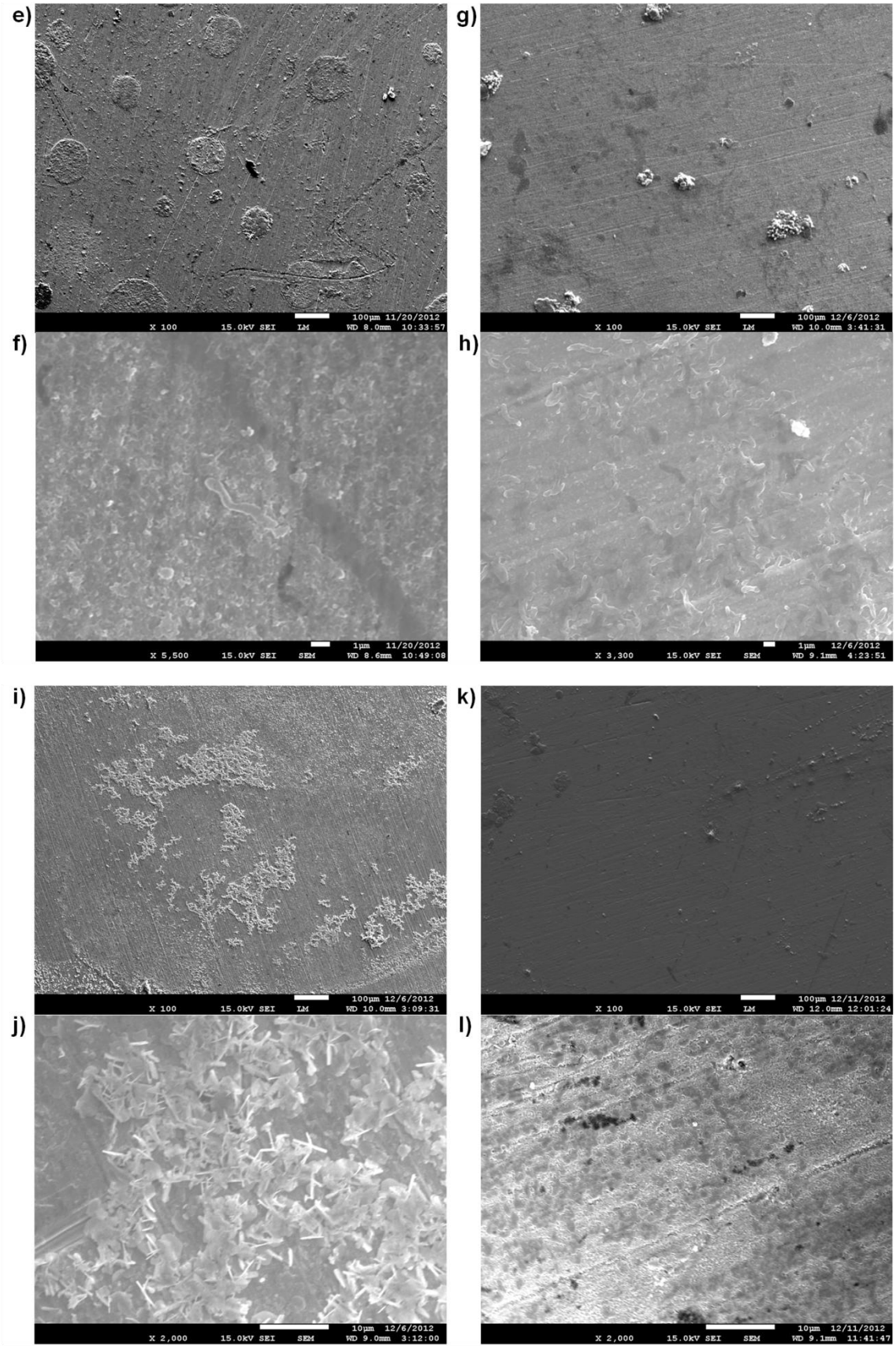

Figure 3.7: SEM micrographs of carbon steel samples after different incubation periods in VMN Sulphate medium. Sample Identification and correspondent magnification: a) A6, 100x; b) A6, 6000x; c) A30, 100x; d) A30, 3000x. e) B6, 100x; f) B6, 5500x; g) B30, 100x; h) B30, 3300x. i) E6, 100x; j) E6, 2000x; k) E30, 100x; l) E30, 2000x.

Fig. 3.6a-d shows the surface of the control samples without bacteria in sulphate medium. The surface at 6 days when observed at low magnification, exhibits polishing marks and almost no alteration. It is still possible to detect the polishing marks after 30 days, although a higher degree of deposits, mostly inorganic salts are present, as confirmed by EDX analysis (see table 3.3).

From Fig. 3.6e to 3.6h we can see the influence of the bacterial growth in the surface of the metal. Circles with high amount of sulphur can be spotted on the surface after 6 days, and with higher magnification a few cells could be identified in that area but not outside. By EDX, we could confirm that the areas around the cells were richer in sulphur content. After 30 days of incubation micro pits with the shape of bacterial cells can be seen spread in the surface indicating that the dissolution of iron occurs beneath the microorganism.

The control without microorganism and with 150 ppm of Na_2S can be seen in Fig. 3.6i to 3.6l. With 6 days a lot o calcium and phosphate precipitates can be observed at the surface. And after 30 days a few micro pits were detected. This behavior is different from the normal control where no corrosion was detected as the sulphide is probably responsible for the calcium and other salts precipitation and also the localized corrosion [94, 180]. Another interesting result, is that even with sulphide being added, the level of sulphur detected by EDX was lower than in the sample with biogenic sulphate reduction (see table 3.3). Therefore we were expecting to see more pits in the samples B6 and B30; however they could be hidden beneath the biofilm cover. The EDX chemical mappings of samples unexposed to oxygen are shown in figures 3.7 to 3.13.

In nitrate medium, the micrographs show a higher degree of inorganic salts precipitation in the case of the control. After 30 days, is clearly visible some deposits, mainly composed of nitrate salts. It appears that in the nitrate medium the precipitation of salts is more frequent and tends to increase and generate aggregates with time. In the incubation with bacteria (samples D6 and D30) we can recognize EPS covering the surface because the chemical map is rich in carbon, nitrogen and oxygen; nevertheless, fewer cells were spotted when compared to sulphate. The composition of the EPS has great influence in the corrosion rate and also the protein profile expressed can vary significantly accordingly to the respiratory substrate as already demonstrated by previous studies [24, 94, 150]. In the 30 days nitrate incubated samples, a rust layer was formed that during drying at the anaerobic glove box was partially detached, before the analysis could be performed. In all the surfaces analyzed remnants of silicon from the polishing were detected by EDX, however they seem to not have any impact in the corrosion evolution (see table 3.3). Finally, we could detect (only) after 30 days, what appears to be micropits below the cells in the nitrate incubated coupons. This could be a result of sulphate reduction taking place at the biofilm after nitrate

depletion as this was conducted as a batch experiment, and we known from the previous chapter that the nitrate consumption takes no more than 5 days in normal conditions.

The XPS results (see table 3.4) are similar to the ones from the EDX, even though in this case the samples were exposed to oxygen before the analysis. Nevertheless, the lower sensitivity, due to the impossibility of using the magnetic lenses with this type of sample, could have hidden some less concentrated elements. Another important restriction is the heterogeneity of the sample surface and the topography. Therefore, the results obtained have to be considered more as a trend of the overall composition. At this point the SEM-EDX has one big advantage, against XPS, of been able to select microscopically with great lateral resolution, the point of EDX analysis, even if it is semi-quantitative. Finally, in the case of corrosion studies both techniques are valuable and should be considered complementary.

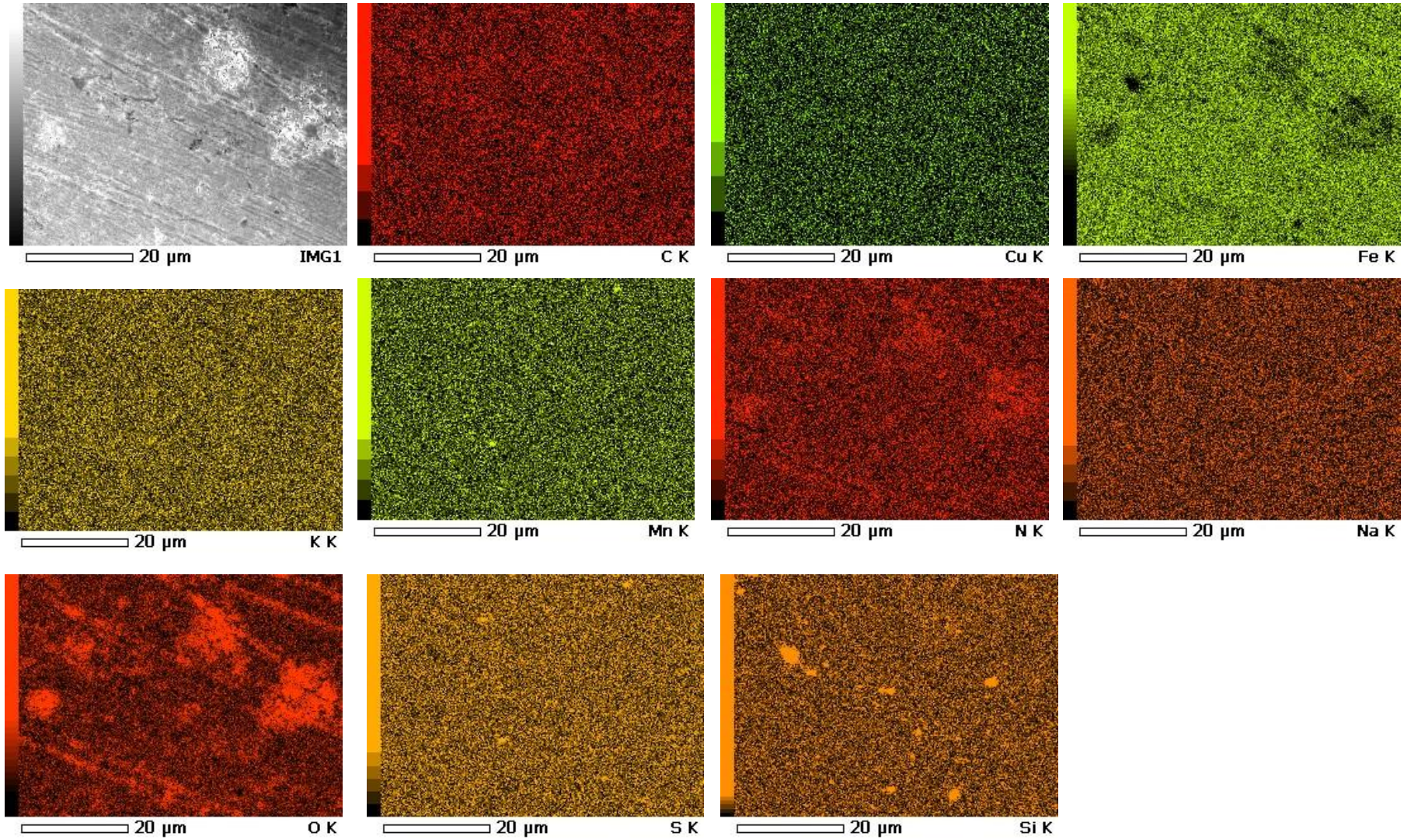

Figure 3.8: EDX chemical mapping of sample A6. In all images the element concentration is proportional to the brightness of the scale (the darker the weaker).

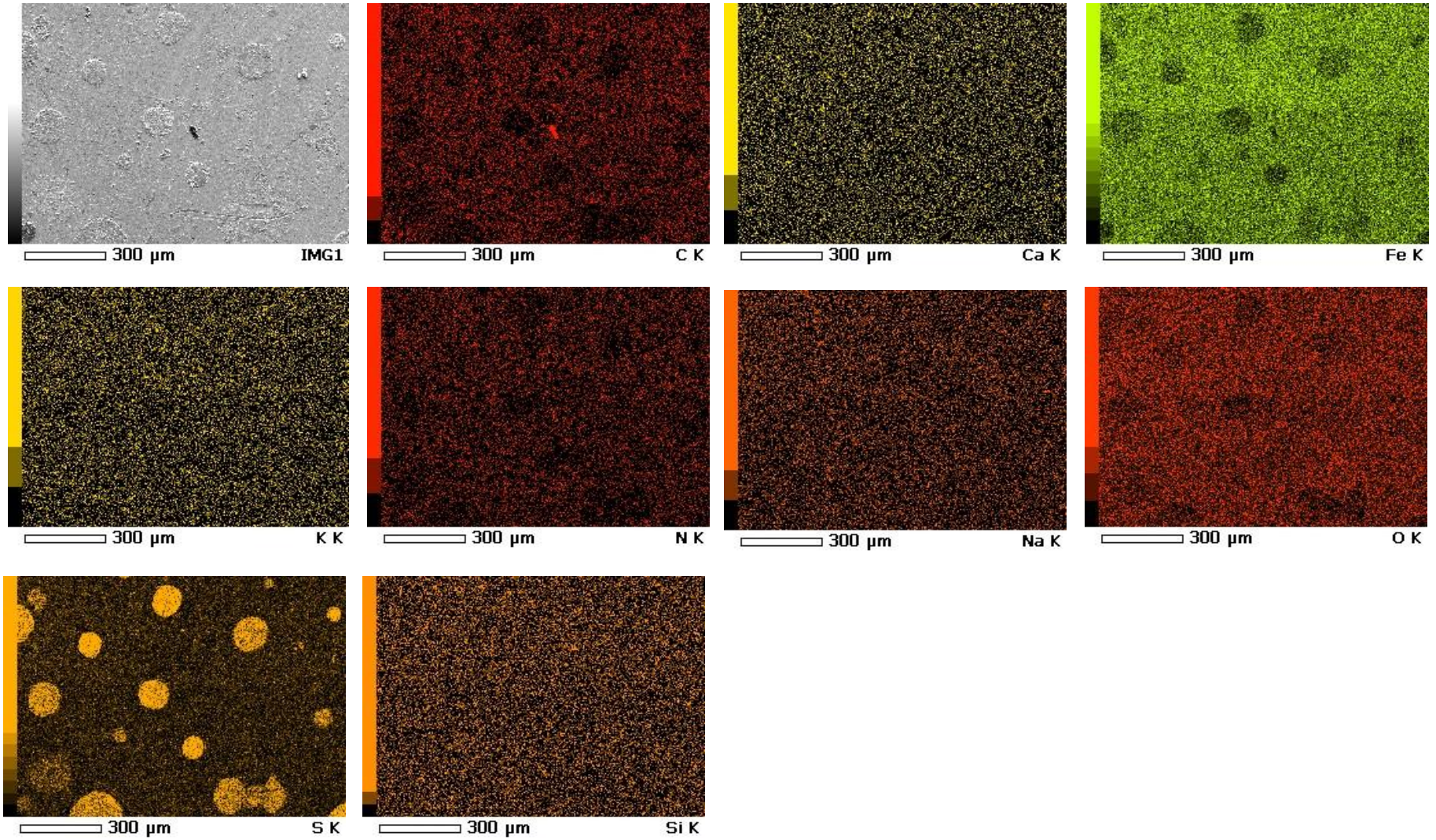

Figure 3.9: EDX chemical mapping of sample B6. In all images the element concentration is proportional to the brightness of the scale (the darker the weaker).

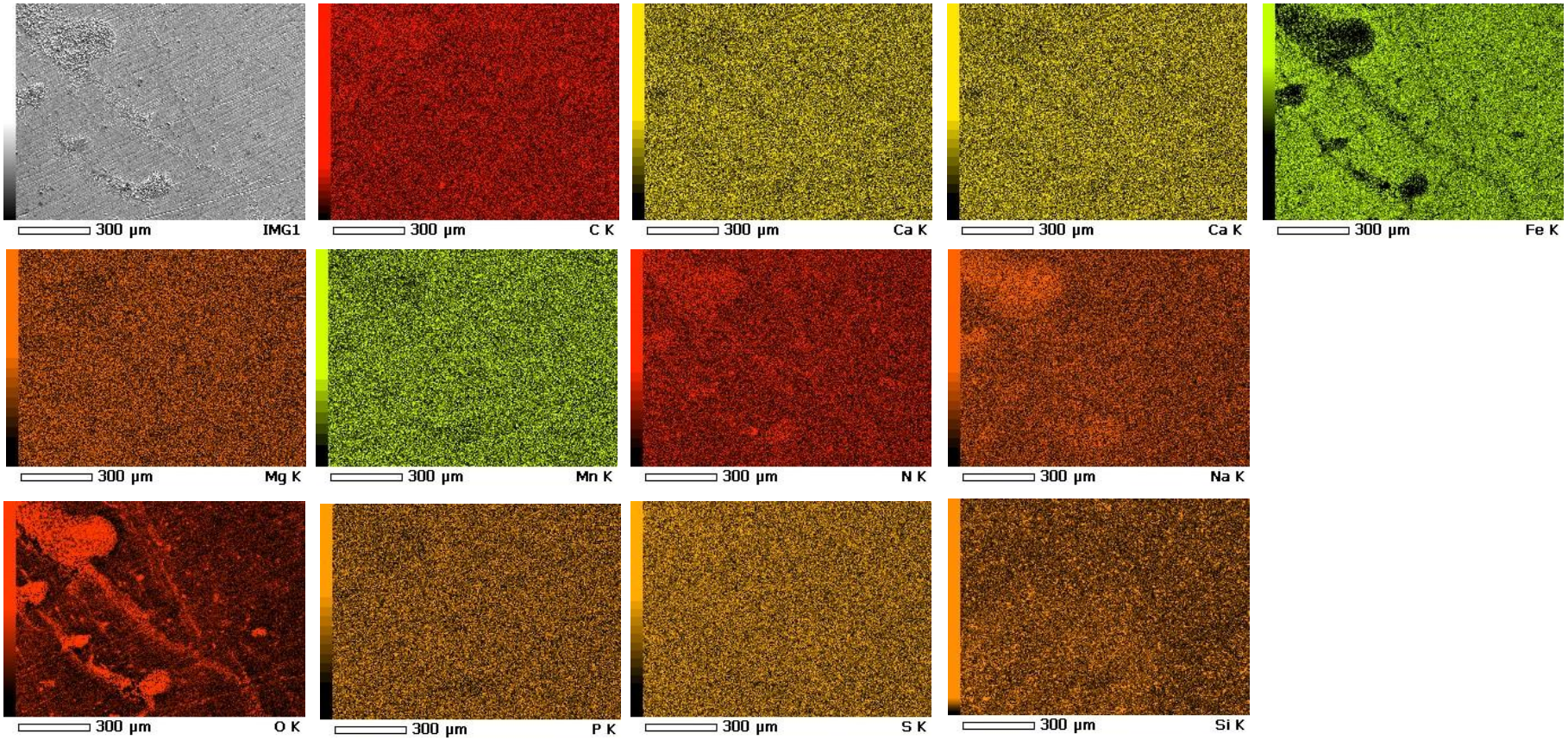

Figure 3.10: EDX chemical mapping of sample A30. In all images the element concentration is proportional to the brightness of the scale (the darker the weaker).

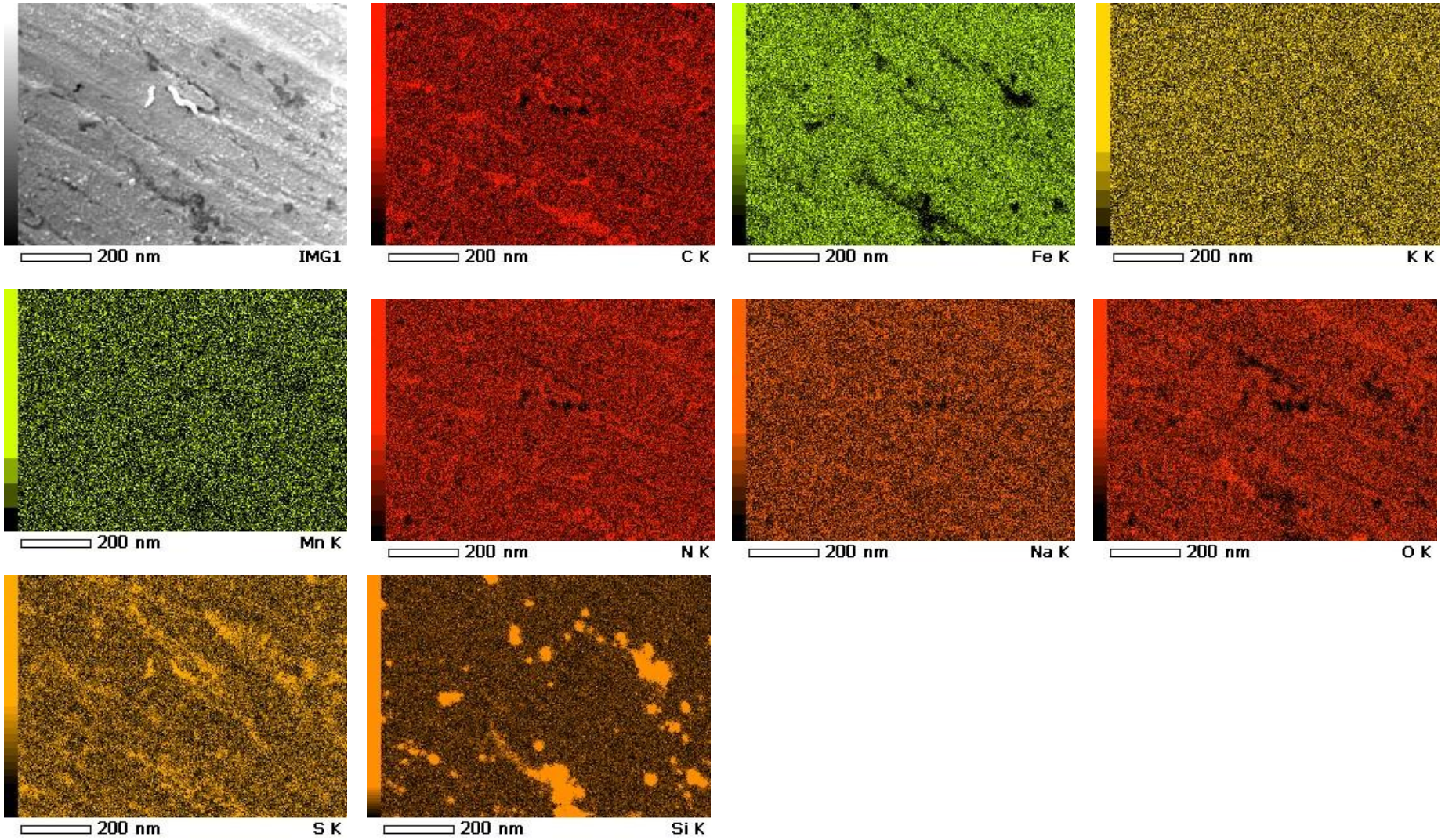

Figure 3.11: EDX chemical mapping of sample B30. In all images the element concentration is proportional to the brightness of the scale (the darker the weaker).

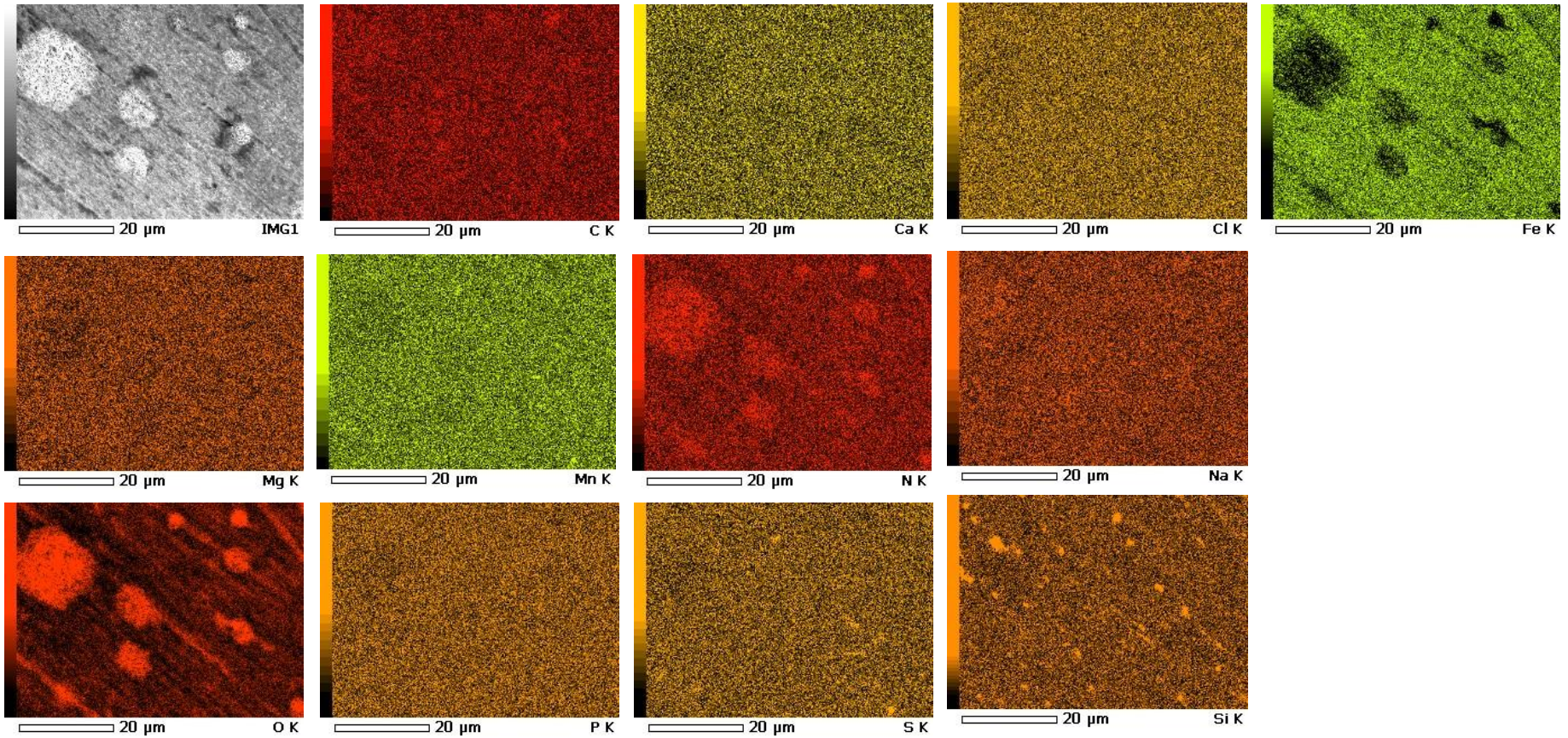

Figure 3.12: EDX chemical mapping of sample C30. In all images the element concentration is proportional to the brightness of the scale (the darker the weaker).

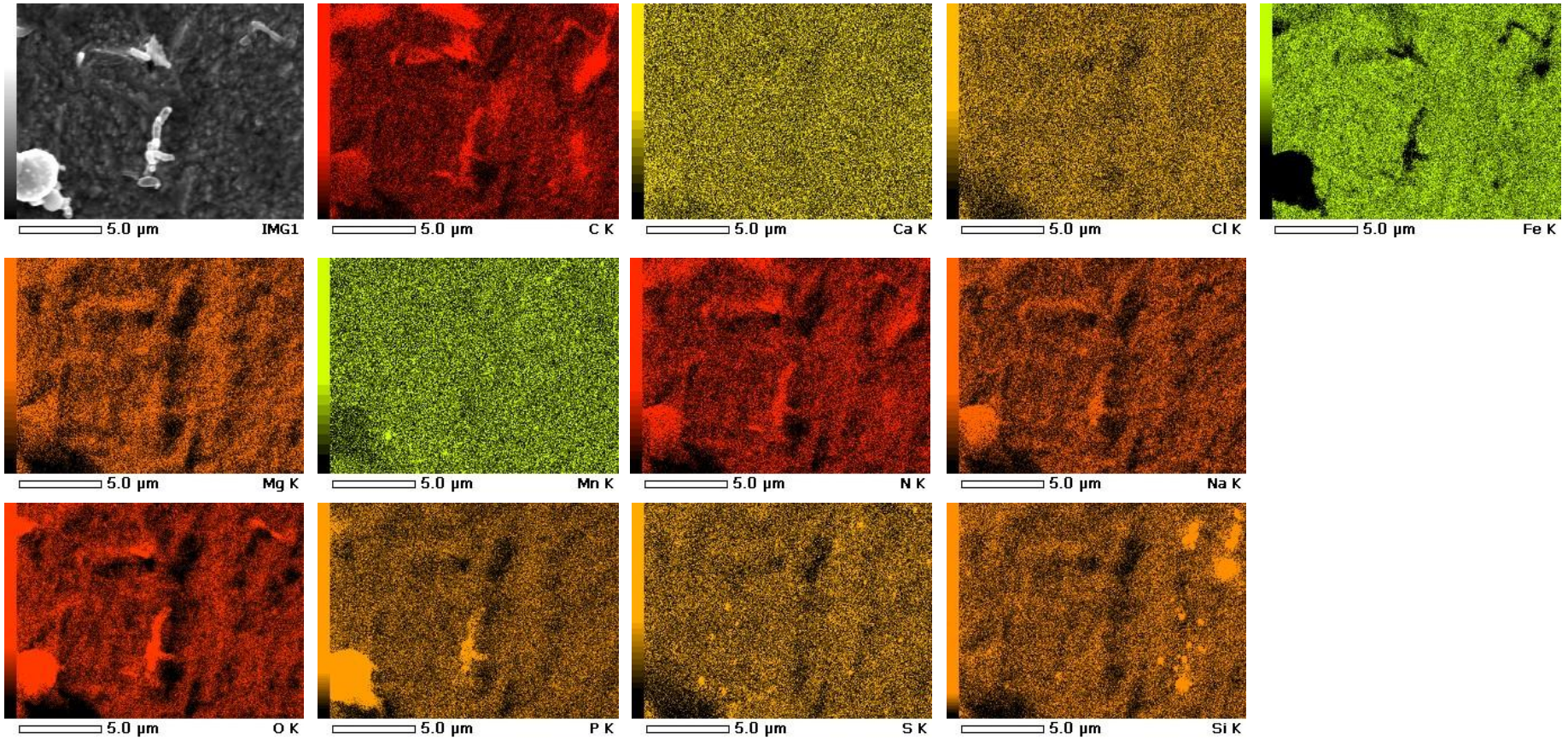

Figure 3.13: EDX chemical mapping of sample D30. In all images the element concentration is proportional to the brightness of the scale (the darker the weaker).

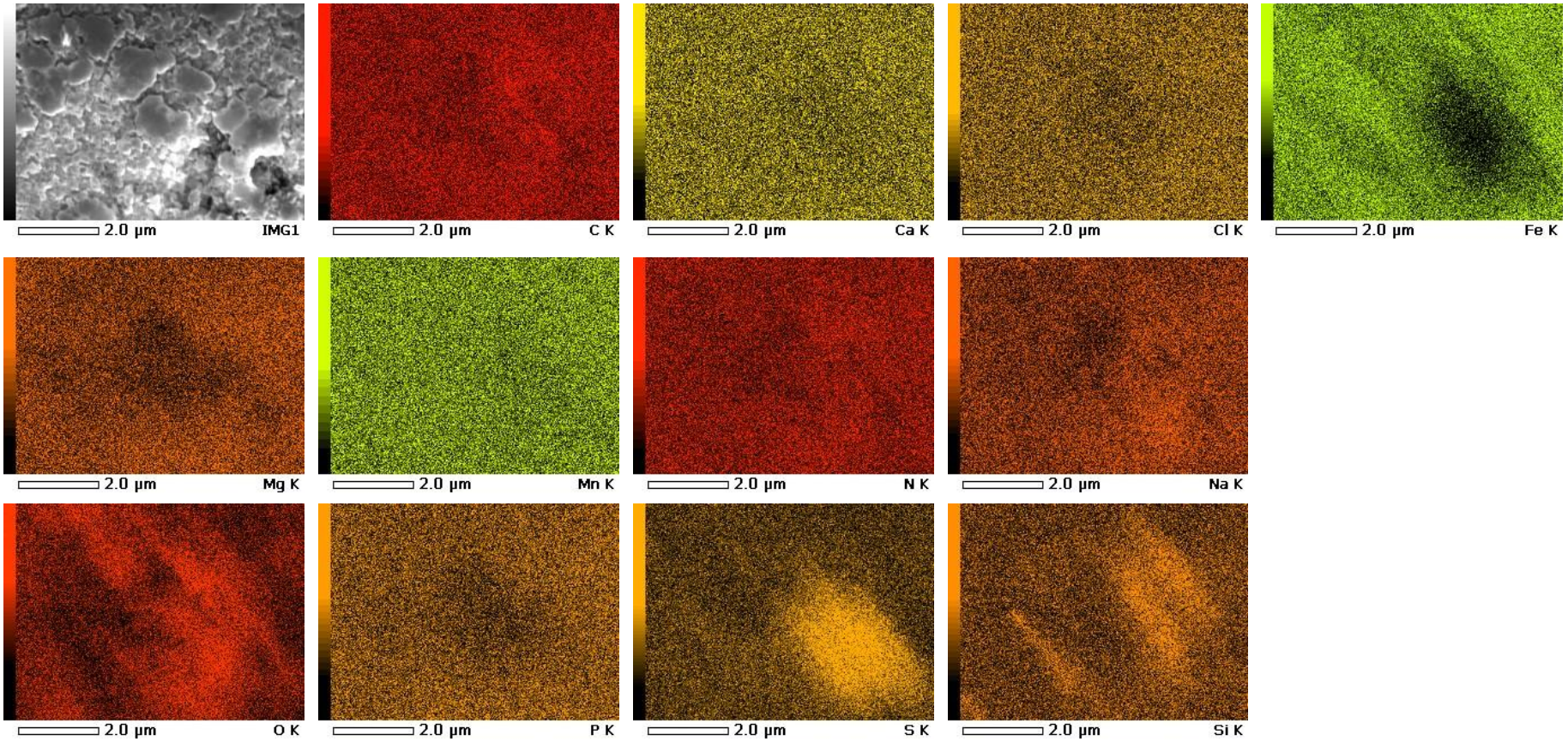

Figure 3.14: EDX chemical mapping of sample E30. In all images the element concentration is proportional to the brightness of the scale (the darker the weaker).

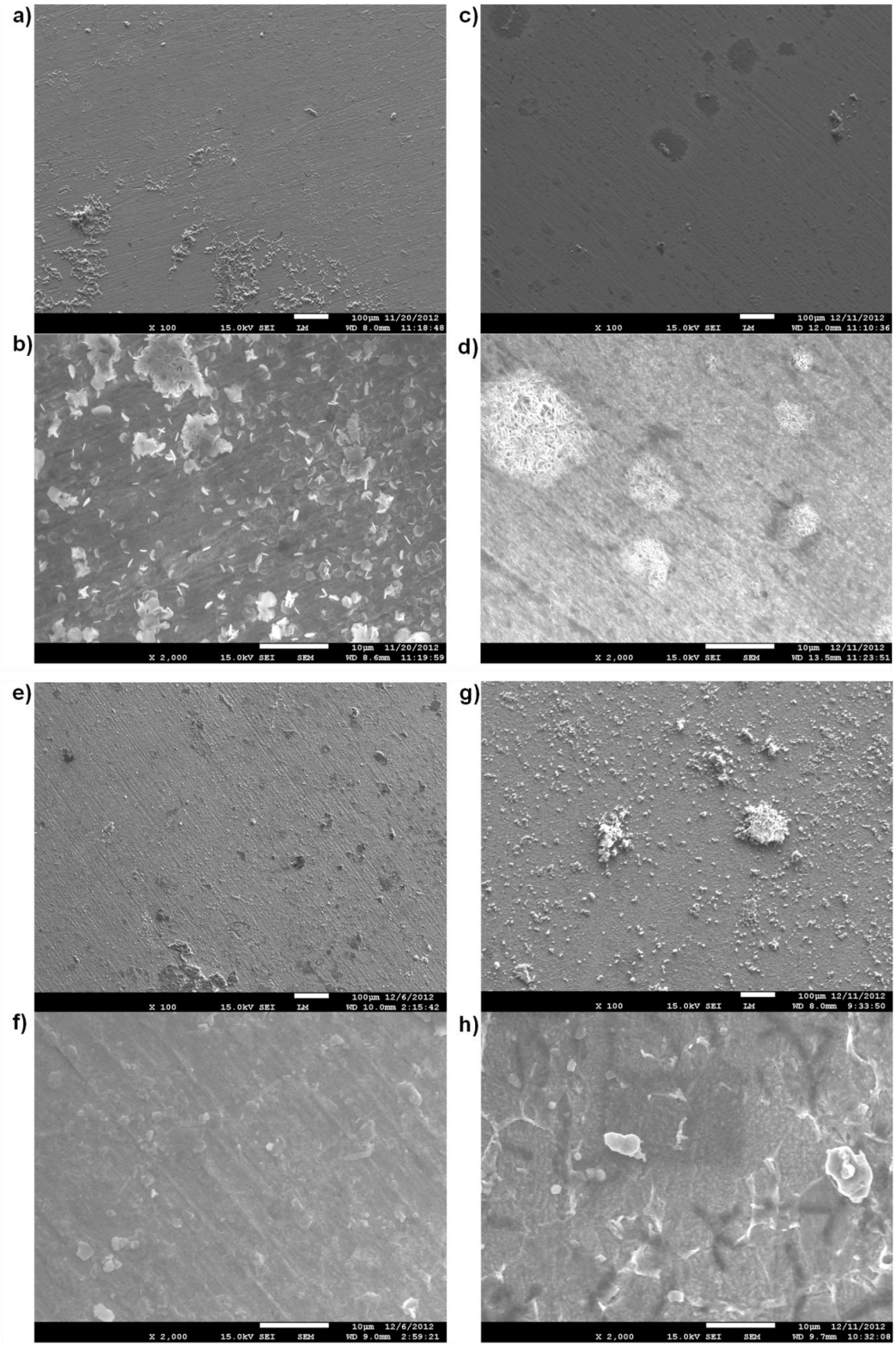

Figure 3.15: SEM micrographs of carbon steel samples after different exposure times in VMN Nitrate medium. Sample Identification and correspondent magnification: a) C6, 100x; b) C6, 2000x; c) C30, 100x; d) C30, 2000x. e) D6, 100x; f) D6, 2000x; g) D30, 200x; h) D30, 2000x.

Table 3.7: EDX semi-quantitative analysis of the general images presented from samples unexposed to oxygen.

	Sample	CS	A6	A30	B6	B30	C6	C30	D6	D30	E6	E30
Element	**Position (keV)**	**Mass%**	**Mass %**	**Mass %**	**Mass %**	**Mass %**	**Mass %**	**Mass %**	**Mass %**	**Mass %**	**Mass %**	**Mass %**
C	0.277	1.79 ± 0.34	4.10 ± 0.18	2.64 ± 0.34	11.56 ± 0.16	9.42 ± 0.42	5.58 ± 0.17	4.35 ± 0.24	4.48 ± 0.23	9.04 ± 0.19	6.54 ± 0.57	3.08 ± 0.37
O	0.525	0.63 ± 0.24	6.42 ± 0.14	6.49 ± 0.24	4.43 ± 0.14	7.06 ± 0.36	8.16 ± 0.13	10.41 ± 0.18	8.15 ± 0.17	8.05 ± 0.16	3.62 ± 0.44	5.59 ± 0.26
Na	1.041	BDL	0.19 ± 0.35	0.61± 0.62	1.23 ± 0.24	0.93 ± 0.73	1.17 ± 0.31	0.38 ± 0.43	BDL	0.07 ±0.35	0.68 ± 1.00	1.15 ± 0.64
Mg	1.253	BDL	BDL	0.16 ± 0.47	BDL	BDL	BDL	0.13 ± 0.33	BDL	BDL	BDL	0.20 ± 0.49
Si	1.739	0.22 ± 0.35	0.23 ± 0.19	0.56 ± 0.34	0.30 ± 0.14	0.20 ± 0.42	0.60 ± 0.18	0.59 ± 0.24	0.19 ± 0.23	0.70 ± 0.20	0.68 ± 0.56	0.79 ± 0.36
P	2.013	BDL	BDL	BDL	BDL	0.04 ± 0.36	BDL	BDL	0.01 ± 0.20	0.71 ± 0.17	0.05 ± 0.47	0.07 ± 0.30
S	2.307	0.04 ± 0.25	0.12 ± 0.14	0.02 ± 0.29	5.24 ±0.11	1.98 ± 0.31	0.15 ± 0.13	0.05 ± 0.21	0.25 ± 0.17	0.31 ±0.15	1.33 ± 0.41	1.43 ± 0.26
Cl	2.621	0.03 ± 0.28	BDL	0.23 ± 0.25	BDL	0.02 ± 0.36	0.23 ± 0.15	0.13 ± 0.18	BDL	0.14 ±0.17	0.03 ± 0.47	0.10 ± 0.30
K	3.312	0.01 ± 0.39	0.01 ± 0.22	BDL	0.04 ± 0.18	BDL	BDL	BDL	BDL	BDL	BDL	BDL
Ca	3.690	BDL	2.94 ± 0.68	0.04 ± 0.46	0.03 ± 0.21	BDL	0.12 ± 0.24	0.09 ± 0.20	BDL	BDL	BDL	0.01 ± 0.48
Mn	5.894	4.80 ± 1.21	BDL	5.56 ±1.24	BDL	2.46 ± 1.59	2.81 ± 0.65	3.82 ± 0.9	3.23 ± 0.85	3.49 ± 0.75	3.19 ± 2.04	5.92 ± 1.30
Fe	6.398	92.48 ± 1.34	85.75 ± 0.75	83.43 ±1.37	77.17 ± 0.60	77.88 ± 1.73	81.19 ± 0.72	80.05 ± 0.99	83.69 ± 0.94	77.48 ± 0.82	83.91 ± 2.23	81.67 ± 1.43

BDL: Below detection limit.

Table 3.8: XPS quantitative analysis of the samples exposed to oxygen.

Sample		**CS**	**AO30**	**BO30**	**CO30**	**DO30**
Element	**Aprox. Position**	**%Atomic Conc.**	**%Atomic Conc.**	**%Atomic Conc.**	**%Atomic Conc.**	**%Atomic Conc.**
C 1s	284	39.26	52.631	60.166	60.538	46.034
Fe 2p	710	20.308	8.822	3.39	4.635	6.378
O 1s	531	39.658	35.06	22.404	25.601	39.128
N 1s	399	0.566	1.915	9.008	6.229	3.36
Na 1s	1071	0.208	0.522	0.649	0.331	0.701
P	133	BDL	0.484	0.174	0.679	3.883
S	163	BDL	0.564	4.209	1.988	0.516

BDL: Below detection limit.

3.4. Conclusions

The use of high-throughput surface analysis techniques as ToF-SIMS and XPS allied with SEM-EDX can give new insights into the (bio)corrosion mechanism and evolution, and also some information on the interaction of the microorganisms with the metal surface. This information is important and must be compared in different conditions to build up a reliable comparison standard to differentiate normal corrosion from MIC. Because of the huge amount of data generated in this type of analysis it is of fundamental importance to use of bioinformatic tools to organize and prioritize the data. Alongside this, the implementation of multivariate statistical analysis should be better explored so it stops being used as a “black box”, as the data pre-treatment and peak selection can give big biases to the final result attained.

Our study demonstrated the influence of the respiratory substrate to *Desulfovibrio desulfuricans* EPS production and composition, surface interaction, and that it can be responsible for the precipitation of inorganic salts, like calcium and phosphates, and its relationship to the corrosion evolution and type. Our results can also be used as a model example for future comparison of corrosion cases to try to help determine the nature of field corrosion problems. Finally, we have shown that nitrate should not be considered a safe tool for preventing localized corrosion at the micro scale and must be considered more carefully as an option by the industry, as it can increases the presence of aggressive chloride ions at the metal surface and could, depending on the surface conditions, became nitrate depleted and sulphate reduction would start to occur.

Chapter 4

Biochemical characterization of EPS and iron uptake

Chapter 4 – Biochemical characterization of EPS and iron uptake

4.1. Introduction

Extracellular polymeric substances are a mixture of biopolymers produced by almost all prokaryotic and eukaryotic microorganisms (archaea, bacteria, algae and fungi). Initially, the studies in this field have focused their attention in the polysaccharides as it was believed they were the main constituent specially in biofilms [26]. However, many authors have since then demonstrated that this was a consequence of the extraction protocols used and that the EPS comprised, in addition, a diverse quantity of proteins (and glycoprotein's), lipids (plus glycolipids), eDNA, humic substances and ions [96, 182, 183]. More recently the EPS composition has been considered as "undefined" due to its variation with time, location and bacterial growing conditions, in a similar manner to what occurs with the protein expression profile [119].

The classification of the EPS is usually made considering its location relatively to the cell. If they are closely bound to the cell surface by non-covalent interactions they are called "capsular" or "tightly bond" EPS. On the other hand, if they are weakly associated to the cell surface, forming a type of colloid and so being easily detached to the surrounding environment, it is called "colloidal" or loosely bond" EPS [114]. It is noteworthy, that the EPS is produced both by planktonic and sessile microorganism, and is not only related to biofilm formation.

Beech and Cheung [7] have demonstrated the ability of colloidal EPS from planktonic SRB to complex Cr, Ni, and Mo from metal plates and that this effect was dependent on the metal type and the SRB isolate. The influence of the metal presence in the bacterial growth and EPS production has also been demonstrated in SRB and *Pseudomonas* [7, 184]. In addition, the ion chelating properties of the EPS have been investigated and proposed to be a key factor in the microbial influenced corrosion evolution [91, 104, 158].

Some authors have examined the possibility of using EPS for inhibit microbial influenced corrosion inhibition (MICI) [8]. Stadler and co-workers have demonstrated that the EPS extracted from *Desulfovibrio alaskensis* was able to inhibit corrosion by a process of oxygen removal from the biofilm, even though in *D. vulgaris* and *Pseudomonas* it increased the corrosion rate [185, 186]. Purified EPS was also used to prevent bacterial adhesion and therefore the formation of an "aggressive" biofilm at the metal surface [187]. Dong et al [158] reported that the concentration of EPS and the temperature plays a crucial role in corrosion inhibition properties, although the composition of the EPS layer is also very important as it could stimulate the anodic dissolution of iron through its chelating capacity.

The use of XPS to characterize bio-organic systems has become more common in recent years [172]. Aguié-Beghin has shown that polysaccharides and proteins were the

major components from champagne adsorbed layer [188]. In the study of Dupont-Gillain, XPS in combination with PCA have been used to analyze the adsorption of different proteins in different materials which allowed classifying them according to the nature of the substrate, to the adsorbed amount and the level of surface coverage [131]. Dufrêne et al validated the use of XPS to the analysis of whole cells and isolated cell walls of Gram-positive bacteria by comparing the results from biochemical methods [189]. Furthermore other studies with *Bacillus subtilis* have followed the deprotonation reactions at the cell wall surface as function of pH or the correlation between phosphate surface concentration and zeta potential [190, 191]. Boonaert et al [192] have validate the relationship between chemical composition and physicochemical properties of lactic acid bacteria by XPS. In the work of Pradier [193] the characterization of the external layer of marine bacterial strains was performed by FTIR, XPS and ToF-SIMS and correlated with the adhesion on stainless steel surfaces. All those results have proven the reliability of XPS for chemical characterization of microorganisms cells when supported by other biochemical and physical characterizations techniques [194]

In this context, this chapter describes an innovative approach for examining the influence of the respiratory substrate and metal presence on the chemical composition and iron uptake of EPS extracted from *Desulfovibrio desulfuricans* ATTCC 27774. The chemical analysis was conducted by depositing and evaporating EPS drops on gold surfaces in silicon wafers and examining the effects using high vacuum spectroscopy techniques, as ToF-SIMS and XPS. ICP was performed to quantify the Fe binding process to the exopolymers and SDS-PAGE was performed to complement the XPS data modeling and in this way fully characterize the proteins present in the EPS matrix.

4.2. Experimental

4.2.1. Incubation conditions for surface analysis techniques

The semi-defined culture media, VMN Sulphate and VMN Nitrate mentioned in the previous chapter were used. The dimensions of the metal plates used for the tests were of 10x10x2 mm. The mild steel plates nominal composition is the same as described in chapter 3, so was the polishing procedure. All coupons were hanged using a nylon thread at the rubber stopper and placed in an empty 100 mL glass anaerobic bottle, with 3 coupons per bottle. To sterilize the coupons the bottles were exposed for 1h to UV light (253.7 nm). Using argon positive pressure, previously autoclaved media were then transferred to the bottles. Negative controls of each media were prepared with a final concentration of 1µg/mL of Ampicillin and 5µg/mL of Kanamycin. When the pre-inoculums of *Desulfovibrio desulfuricans* ATCC 27774 reached 24h of growth, they were used as inoculums and incubated at 30ºC for 6 days in a total of four conditions per each respiratory substrate. A list with all the samples identification and conditions tested is given in Table 4.1. Aliquots of the EPS extracted from samples D and I were transferred into bottles with metal coupons as described for the other samples and purged with argon gas for 30 min and then incubated in the same conditions already described and are referred as samples E and J.

Table 4.1: Tested conditions and identification of samples.

Sample Number	ID	Respiratory substrate	Presence of bacteria	Presence of metal coupon
1.	**A**	Sulphate	No	No
2.	**B**	Sulphate	No	Yes
3.	**C**	Sulphate	Yes	Yes
4.	**D**	Sulphate	Yes	No
5.	**E**	Sulphate	No*	Yes
6.	**F**	Nitrate	No	No
7.	**G**	Nitrate	No	Yes
8.	**H**	Nitrate	Yes	Yes
9.	**I**	Nitrate	Yes	No
10.	**J**	Nitrate	No*	Yes

*Only sterile anoxic colloidal EPS extracted from samples D and I.

4.2.2. Colloidal EPS extraction and sterile media for chemical characterization by ToF-SIMS and XPS

After the incubation time the cultures were centrifuged at 10,000 x g for 15 min. The supernatant was collected and filtered close to a Bunsen burner with a 0.22 µm pore

cellulose membrane to remove contaminant cells. All samples were dialyzed at room temperature with a 3.5 kDa membrane against distilled water for 16h and then three times at 4ºC for 2h after changing the water. The samples were then concentrated by freeze-drying. Aliquots of 1 mL were used to confirm the presence of proteins by UV-Vis spectra (800-250 nm) using a Shimadzu® UV-VIS Spectrophotometer, model UV-1800. The samples were resuspended with deionized water to a final concentration of 10 mg ml^{-1}. Five aliquots of 10 µL were deposited in silicon wafers with gold surface and let to dry (EVAP). The gold coupons were analyzed by Time-of-Flight Secondary Ion Mass Spectrometry (ToF-SIMS) and X-ray photoelectron spectroscopy (XPS) in order to evaluate the general composition and the iron uptake by the EPS in each condition. The dialysed samples were also quantified by Inductively Coupled Plasma-Atomic Emission Spectrometry (ICP-AES), Ultima (Horiba Jobin-Yvon, France), in order to confirm the surface analysis results for iron content. The ToF-SIMS and XPS analysis were conducted in the same way as described in section 2 of chapter 3 for corroded surfaces.

4.2.3. EPS for biochemical composition analysis

For the biochemical composition determination, the bacteria were cultivated in 5 L anaerobic bottles with VMN Sulphate or VMN Nitrate for 3 days at 30ºC with magnetic stirring until they reached a minimum cell concentration of 10^8 cells per ml. The extraction of the colloidal and capsular EPS was made using a protocol modified from Aguilera et al [150]. Initially, the cultures were centrifuged at 10,000 x g for 15 min. The supernatant was collected and filtered with a 0.22 µm pore cellulose membrane to remove contaminant cells and already considered as colloidal EPS. The cells were then washed using the mineral VMN media and centrifuged at 10,000 x g for 15 min. The supernatant was collected and stored and the centrifuged cells were resuspended with Dowex® Marathon™C cation exchange resin, Na^+ form, 20–50 mesh size based on [122] with and ionic strength/conductivity similar to that of the sample/environment collected [113]. The Dowex® resin was resuspended using phosphate buffer saline (PBS) with the following composition: 2 mM $Na_2PO_4 \cdot 12H_2O$; 4 mM $NaH_2PO_4 \cdot H_2O$; 9 mM NaCl; 1 mM KCl, pH=7.4 (adjusted with KOH). The extraction step lasted for 2h at 4ºC with stirring and was followed by centrifugation at 10,000 x g for 15 min. The supernatant were collected and the procedure was repeated one more time. The supernatant samples were dialyzed as described in section 2.2 and stored at -20ºC.

Polysaccharide content in EPS was determined by the Dubois method [195], while uronic acids by the protocol from Filisetti – Cozzi and Carpita [196]. For the determination of extracellular protein concentration Bradford protocol [197] and DNA content Burton protocol

[198] were applied. Additionally cell lysis control was verified by determination of 2–keto–3–deoxyoctonate (KDO) that is a component of the cell wall [198].

4.2.4. Protein profile characterization

For the protein profile characterization the samples without metals were grown in 2 L anaerobic bottles with VMN Sulphate and VMN Nitrate for 3 days at 30ºC with magnetic stirring until they reached a minimum cell concentration of 10^8 cells/ml. The samples incubated with metal, were grown in 5L bioreactor, with 16 carbon steel plates of 100x50x2mm for 6 days at 30ºC with magnetic stirring. Nevertheless, for the extraction protocol only 2L of culture were used. The extraction of the colloidal and capsular EPS was made using the same procedure already mentioned in the previous section. All samples were concentrated and dialyzed against potassium phosphate buffer 100mM (KH_2PO_4/K_2HPO_4) using Vivacell 250/Vivacell 70 ultrafiltration concentrators (Sigma-Aldrich) and Amicon Ultra-15 centrifugal concentrators (Merck-Millipore) with a 5 kDa cutoff. Phenylmethylsulfonyl fluoride (PMSF) was added to a final concentration of 1mM as a protease inhibitor. The protein concentration was determined by UV spectroscopy (wavelenght of 595 nm) using a Shimadzu® UV-VIS Spectrophotometer model UV-1800 and the Protein Assay Dye Reagent from Bio-Rad following the manufacturer instructions.

4.2.5. Protein identification

For each sample, 5 µg of protein were used for the analysis by sodium dodecyl sulfate-polyacrylamide gel electrophoresis (SDS-PAGE) using a 10% acrylamide tris-glycine gel according to the method of Laemmli. Proteins were visualized by staining with colloidal Coomassie blue protocol described elsewhere [199].

Protein bands were excised from the gel and sent to the third part service at the REQUIMTE Associated Lab for MALDI-ToF analysis.

Protein identification was done using MASCOT Peptide mass fingerprint server (Matrix Science) using databases of Eubacteria at SwissProt and NCBInr. The following settings were used in the search: enzyme: Trypsin; peptide mass tolerance: ±150 ppm and maximum missed cleavages: one. The Carboxyamidomethylation of cysteine was set as fixed modification and as variable modification the oxidation of methionine.

4.3. Results and discussion

4.3.1. Chemical characterization by ToF-SIMS

The peak list used was based on the one used in the previous chapter, however it was slightly modified to be more focused on biomolecules such as proteins and gold as the substrate; the list had 54 positive ion peaks and 43 for negative ions. As we used the same protein markers, the ion/biomolecule identification can be done using the Table 3.2 from the previous chapter.

The data was normalized by the sum of all the selected peaks and mean-centered as already discussed in the analysis of the corroded metal surface results. In what respects the positive ions, the first principal component (PC1) collects 62.3%, the second (PC2) and the third (PC3), answer for 25.2% and 6.44% of the variance, respectively (see Fig. 4.1). The samples incubated with sulphate are all related to negative values in PC1 with exception of sample C and samples incubated in nitrate have positive values besides sample I. For PC2, the variant sample is sample E which has positive value instead of the rest of sulphate group and sample H that has negative values when the rest of the nitrate group all are in the positive zone. The observed intra-variation was high for some samples, although much less than compared to the corroded surfaces (from chapter 3), probably because of the more homogeneous composition and topography in the EPS group of samples.

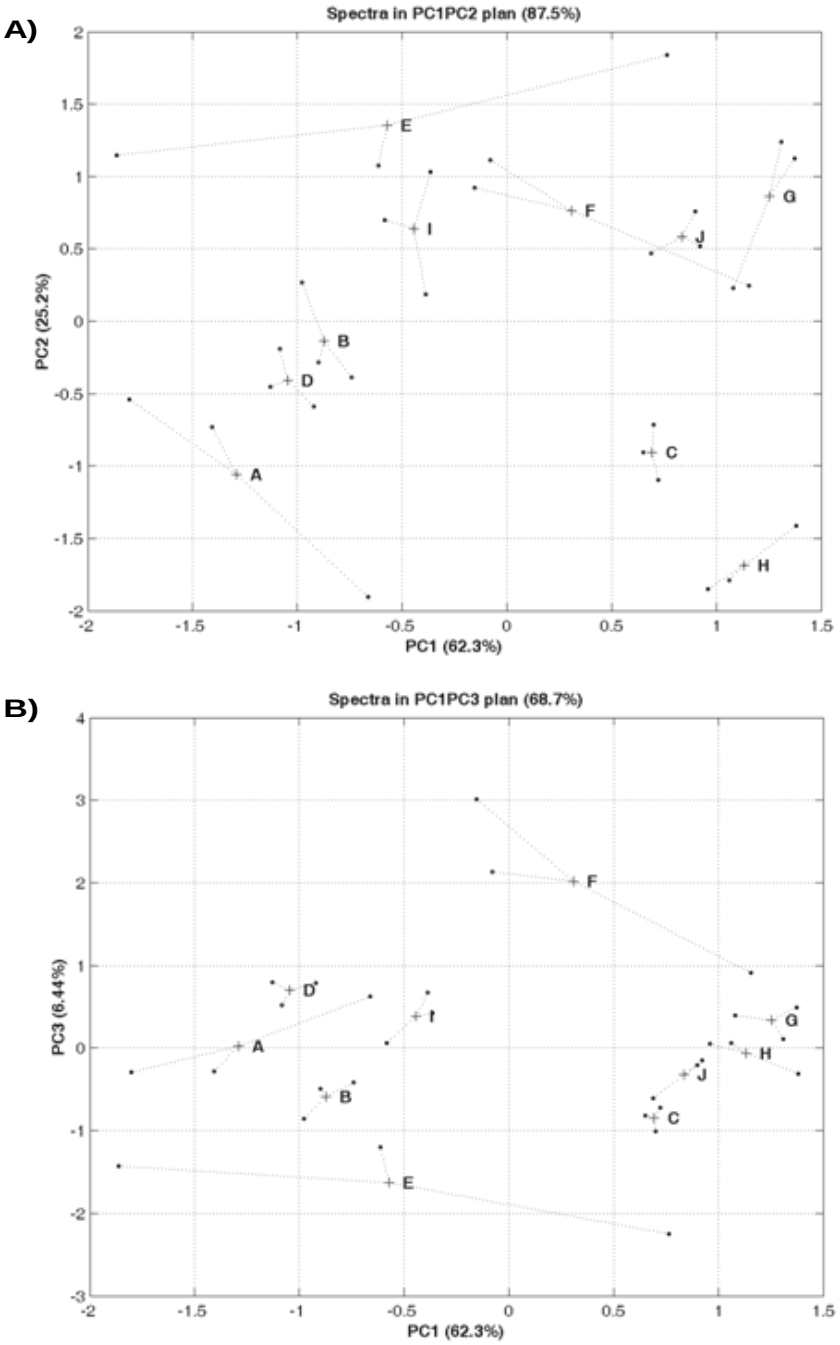

Figure 4.1: PCA results performed on ToF-SIMS positive spectra, significant PC's. a) PC1 *versus* PC2 positive spectra plotting; b) PC1 *versus* PC3 positive spectra plotting. The letters refer to the identification given in Table 4.1.

As shown in Fig. 4.2, it seems that the selected negative ion peaks represent a bigger challenge in the differentiation of the samples as PC1 collects only 46.7% of the total variance and PC2 and PC3, 17.7% and 16.4%, respectively. The combination of PC1 and PC2 can separate most of the sulphate from nitrate samples, having sulphate samples (excepts sample "E") a negative value for PC1 and a positive value for PC2. For nitrate,

samples “G” and “H” were positioned far apart from the rest of the group. The observed intra-variation is relatively low, except for sample “E”.

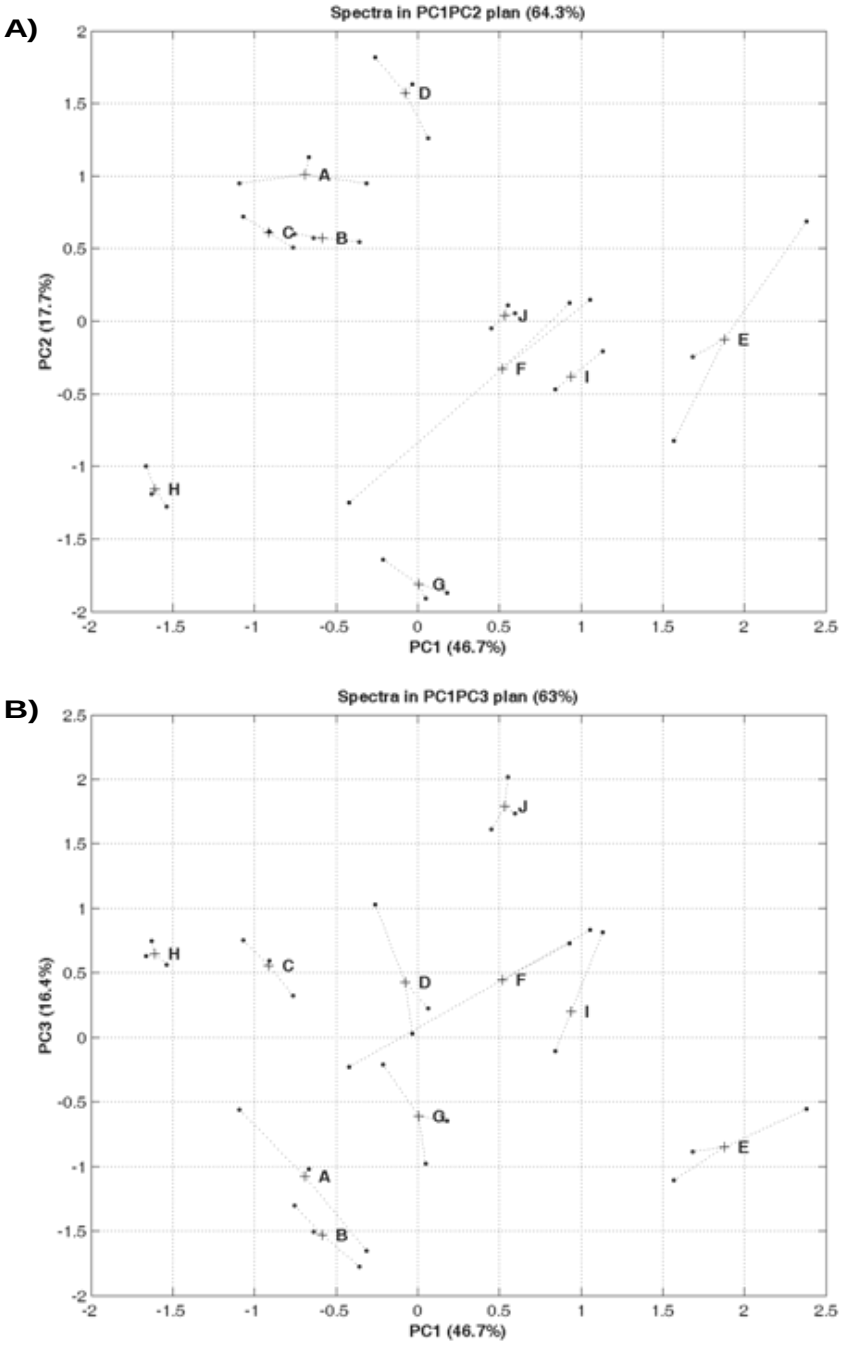

Figure 4.2: PCA results performed on ToF-SIMS negative spectra, significant PC’s. A) PC1 *versus* PC2 negative spectra plotting; B) PC1 *versus* PC3 negative spectra plotting. The letters refers to the identification given in Table 4.1.

Regarding the analysis of biological samples one of the main challenges is the complexity of the system which makes it impossible to assign properly all the peaks, even for EPS only. Nevertheless, it is possible to select a few markers that allow creating a useful

fingerprint for discriminating between the samples [132, 193]. Among the sulphate samples, in the positive ions, there is a prevalence of markers for non-polar or basic polar amino acids (See Fig.4.3 and Tables 4.2, 4.3, 4.4). Nitrate samples, on the other hand exhibit amino acid markers with all types of side chain polarity. This difference can be a consequence of the heterogeneity of protein profile expression between the two conditions as we will show in section 4.3.3 in more detail. However, it is difficult to precisely match the markers found with specific proteins as some of them can be generated by many different amino acid fragments and in both situations tested the expression profile is composed of many different proteins that probably cover all classes of amino acids.

It is also unfortunate that the configuration of the primary ion source used does not allow investigating ions with high masses that are characteristic of lipids. The only ion identified with lipids was phosphatidylcholine that can be found in the membrane and is present in about 10% of all bacteria, including in *Desulfovibrio* [200]. On the other hand, we were able to identify many polysaccharides markers as glycans and xylose, although some of them are ions shared with amino acids, which complicates the determination of the exact contribution of each molecule [161, 162, 178, 193].

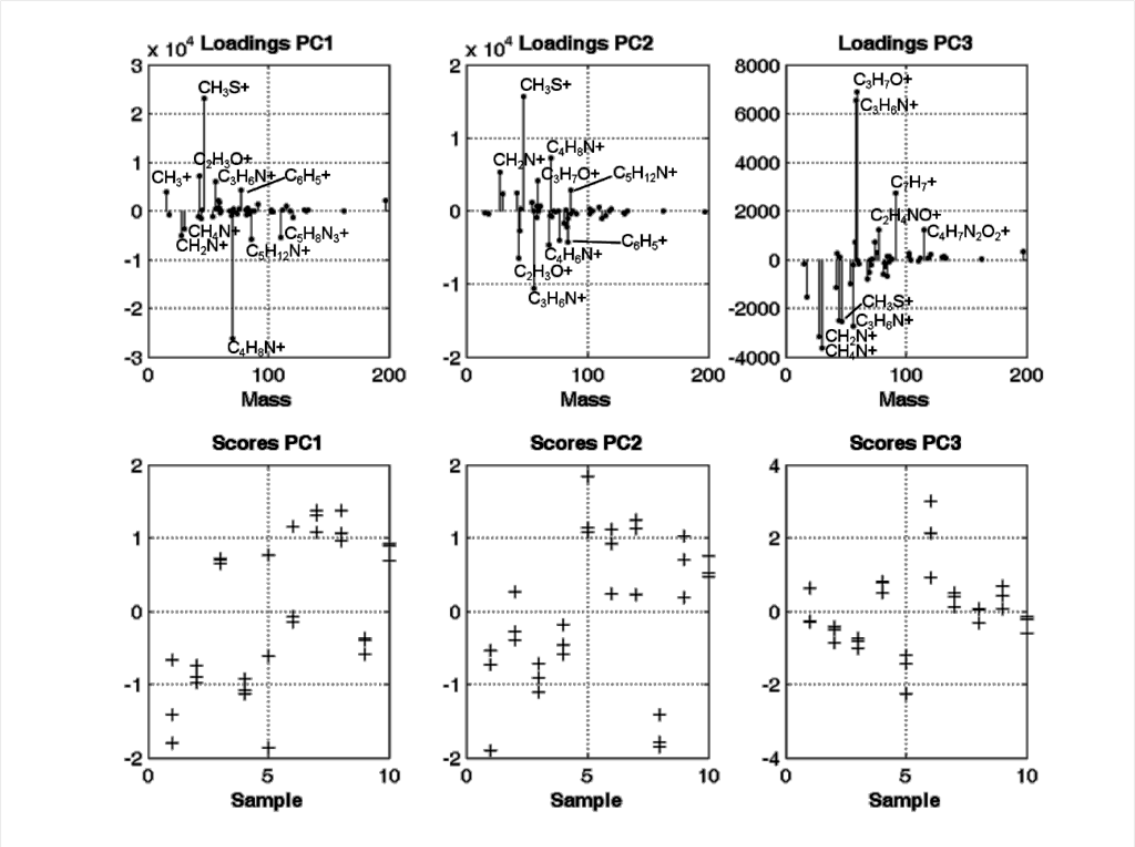

Figure 4.3: Loadings and Scores plotting from PC1, PC2 and PC3 ToF-SIMS positive ions data, respectively. In score plotting the numbers indicate the respective sample ID listed in Table 4.1.

Table 4.2: Top 10 positive and negative loading values for PC1 of positive ions.

N	Load	Mass	Ion	Biological molecule
# 9	23154.42737	46.99	CH_3S+	Cysteine
# 6	7140.77739	43.02	C_2H_3O+	Glutamic Acid
#12	5935.45026	56.05	C_3H_6N+	Lys, Met, Val, Glycan
#26	4271.52271	77.04	C_6H_5+	Phe, Tyr
# 1	3795.16568	15.02	CH_3+	
#48	2177.11776	197	Au+	
#14	2065.08414	58.07	C_3H_8N+	Glutamic acid
#16	1717.36839	59.05	C_3H_7O+	Glycan
#35	1405.26175	91.06	C_7H_7+	Tyr, Phe
#41	925.60352	115.05	$C_4H_7N_2O_2+$	Glycine, Xylose
#20	-1055.66583	69.04	C_4H_5O+	Threonine
#10	-1096.35116	54.04	C_3H_4N+	Histidine
# 5	-1262.01597	42.04	C_2H_4N+	Ala, Gly, His, Leu, ser
#43	-1368.30627	120.09	$C_8H_{10}N+$	Phenylalanine
# 7	-1608.2807	44.05	C_2H_6N+	Ala, Asn, Leu, Glycan
# 4	-3726.9031	30.04	CH_4N+	Gly, Arg, Asn, Glu, Leu, Lys, Ser, Glycan
# 3	-5056.64487	28.02	CH_2N+	Ala, Arg, Asn, Glu, Leu, Ser, Trp
#39	-5456.30948	110.08	$C_5H_8N_3+$	His, Arg
#33	-5863.7228	86.11	$C_5H_{12}N+$	Ile, Leu, Phosphatidycholine
#21	-26241.69223	70.07	C_4H_8N+	Pro, Val

Table 4.3: Top 10 positive and negative loading values for PC2 of positive ions.

N	Load	Mass	Ion	Biological molecule
# 9	15721.01506	46.99	CH_3S+	Cysteine
#21	7277.23708	70.07	C_4H_8N+	Pro, Val
# 3	5277.69557	28.02	CH_2N+	Ala, Arg, Asn, Glu, Leu, Ser, Trp
#16	4123.00356	59.05	C_3H_7O+	Glycan
#33	2806.00793	86.11	$C_5H_{12}N+$	Ile, Leu, Phosphatidycholine
# 5	2463.98343	42.04	C_2H_4N+	Ala, Gly, His, Leu, ser
# 4	2271.21215	30.04	CH_4N+	Gly, Arg, Asn, Glu, Leu, Lys, Ser, Glycan
#10	1115.97698	54.04	C_3H_4N+	Histidine
#18	623.22671	61.01	C_2H_5S+	Methionine
#15	620.54989	58.99	C_2H_3S+	Cysteine
#31	-978.11148	84.09	$C_5H_{10}N+$	Lys, Leu
#40	-990.5829	112.1	$C_6H_{10}NO+$	Arginine
#27	-1656.22352	81.04	$C_4H_5N_2+$	Histidine
#29	-2206.26389	83.06	C_5H_7O+	Valine

Table 4.3 (Cont.): Top 10 positive and negative loading values for PC2 of positive ions.

N	Load	Mass	Ion	Biological molecule
# 7	-2731.5204	44.05	C_2H_6N+	Ala, Asn, Leu, Glycan
#26	-3998.47938	77.04	C_6H_5+	Phe, Tyr
#30	-4252.60804	84.05	C_4H_6NO+	Gln, Glu
#19	-4674.72751	68.06	C_4H_6N+	Pro, Lys
# 6	-6432.75428	43.02	C_2H_3O+	Glutamic acid
#12	-10582.86747	56.05	C_3H_6N+	Lys, Met, Val, Glycan

Table 4.4: Top 10 positive and negative loading values for PC3 of positive ions.

N	Load	Mass	Ion	Biological molecule
#16	6885.54452	59.05	C_3H_7O+	Glycan
#14	6544.31479	58.07	C_3H_8N+	Glutamic acid
#35	2747.84586	91.06	C_7H_7+	Tyr, Phe
#26	1225.23291	77.04	C_6H_5+	Phe, Tyr
#41	1211.91427	115.05	$C_4H_7N_2O_2+$	Glycine, Xylose
#13	725.67901	58.04	C_2H_4NO+	Serine
#24	708.22464	74.07	C_3H_8NO+	Threonine
#48	341.25857	197	Au+	
#25	282.138	76.02	C_2H_6SN+	Cysteine
#37	249.95091	102.06	$C_4H_8NO_2+$	Glutamic acid
#30	-696.81271	84.05	C_4H_6NO+	Gln, Glu
#19	-787.74438	68.06	C_4H_6N+	Pro, Lys
#10	-996.35423	54.04	C_3H_4N+	Histidine
# 5	-1143.28445	42.04	C_2H_4N+	Ala, Gly, His, Leu, ser
# 2	-1547.078	18.04	NH_4+	Glycan
# 7	-2496.20739	44.05	C_2H_6N+	Ala, Asn, Leu, Glycan
# 9	-2529.52867	46.99	CH_3S+	Cysteine
#12	-2739.57576	56.05	C_3H_6N+	Lys, Met, Val, Glycan
# 3	-3158.53329	28.02	CH_2N+	Ala, Arg, Asn, Glu, Leu, Ser, Trp
# 4	-3644.6991	30.04	CH_4N+	Gly, Arg, Asn, Glu, Leu, Lys, Ser, Glycan

For the negative secondary ions, the most important peaks were related to fatty acid markers, oxygen and sulphur, for PC1 (See Fig. 4.4, table 4.5, 4.6 and 4.7). For PC2 there is also a contribution of phosphates, although it only collects 17% of the variation observed. For PC3 there is a mix of the previous two PC's. Accordingly to Braissant *et al.* [180] the EPS presents three main buffering abilities that can range from pK_a=3.0, from carboxylic acids, through sulphur containing groups with pK_a=7.0 until animo groups with pK_a=9.2. It is interesting to highlight that the sulphur groups (thiol, sulfonic acid and sulfinic acid) and phosphate groups present in the EPS may be related to calcium and iron precipitation and

binding, which have been discussed in the previous chapter in the light of corrosion behavior and will be analyzed further regarding the iron uptake. Another group of interest is the fatty acid (or carboxylic acid) marker as it has been detected also by XPS and can have some influence in the EPS interaction with metal surface and metal uptake [11, 96, 166, 179].

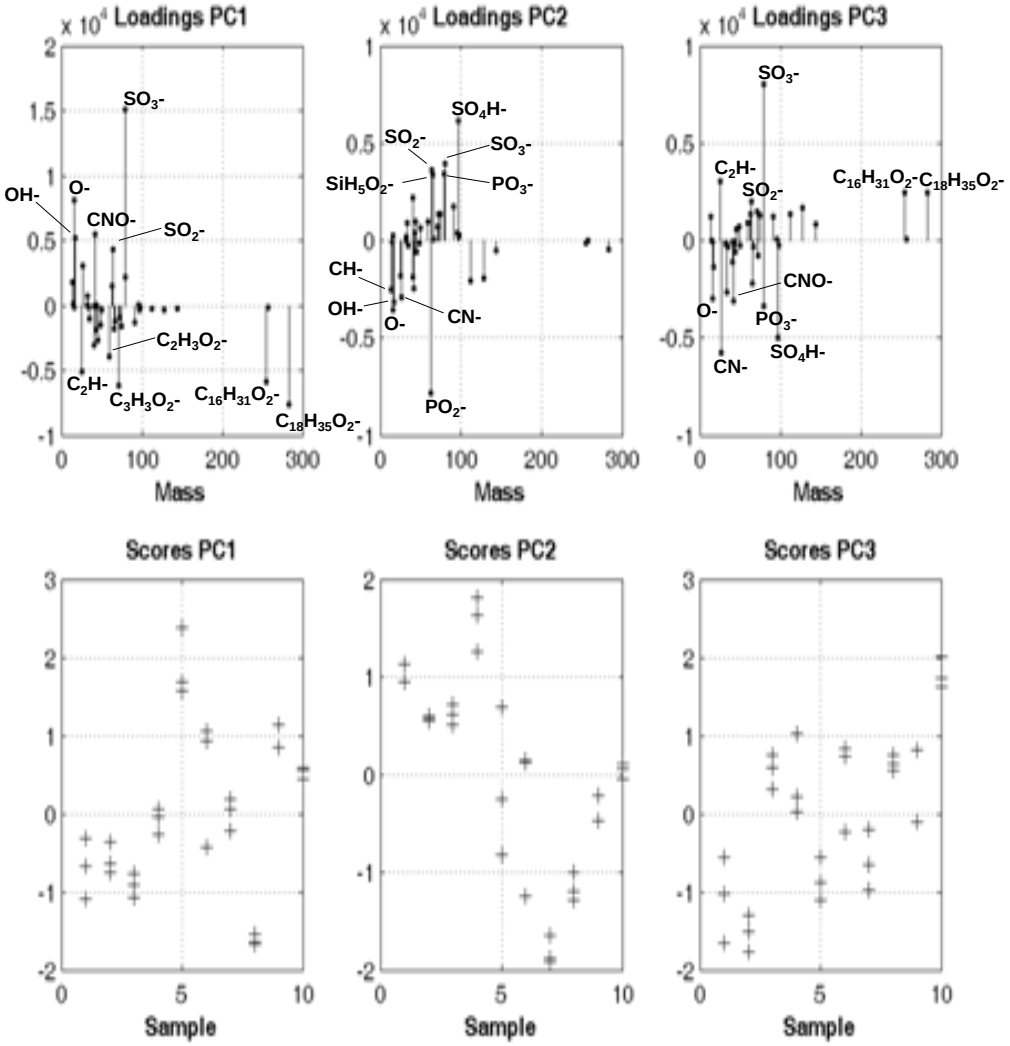

Figure 4.4: Loadings and Scores plotting from PC1, PC2 and PC3 ToF-SIMS negative ions data, respectively. In score plotting the numbers indicate the respective sample ID listed in Table 4.1.

Table 4.5: Top 10 positive and negative loading values for PC1 of negative ions.

N	Load	Mass	Ion	Biological molecule
#30	14921.8199	79.96	SO_3-	
# 3	8138.84029	16	O-	
#14	5893.06307	42	CNO-	
#23	4645.55239	63.96	SO_2-	
# 7	4126.07649	26	CN-	

Table 4.5 (Cont.): Top 10 positive and negative loading values for PC1 of negative ions.

N	Load	Mass	Ion	Biological molecule
#29	2101.80976	78.96	PO_3-	
# 5	1983.83768	17	OH-	
# 1	1831.35114	13.01	CH-	Hydrocarbon
#22	1679.75222	62.97	PO_2-	
# 8	728.32045	31.97	S-	
#19	-1505.10723	49.01	C_4H-	Hydrocarbon
#16	-2214.56707	43.02	C_2H_3O-	
#24	-2297.86459	65.01	SiH_5O_2-	
#18	-2536.24682	45	CHO_2-	Fatty acids
#13	-2694.65551	41.01	C_2HO-	
#21	-3902.99123	59.02	$C_2H_3O_2$-	Fatty acids
# 6	-4377.65956	25.01	C_2H-	Hydrocarbon
#38	-5778.82124	255.24	$C_{16}H_{31}O_2$-	Fatty acids
#26	-6071.60388	71.02	$C_3H_3O_2$-	Fatty acids
#40	-7456.34753	283.27	$C_{18}H_{35}O_2$-	Fatty acids

Table 4.6: Top 10 positive and negative loading values for PC2 of negative ions.

N	Load	Mass	Ion	Biological molecule
#33	6158.07667	96.97	SO_4H-	
#30	3939.08734	79.96	SO_3-	
#23	3637.03206	63.96	SO_2-	
#29	3416.26253	78.96	PO_3-	
#24	3378.87259	65.01	SiH_5O_2-	
#12	2194.05154	40.02	C_2H_2N-	
#31	1735.13475	90.99	$C_2H_4PO_2$-	
#27	1370.07556	72.01	$SiCH_4N_2$-	
#28	1331.74172	75	$CHNO_3$-	
#17	999.99331	44.02	CH_2NO-	
# 6	-1835.40014	25.01	C_2H-	Hydrocarbon
#13	-1889.66029	41.01	C_2HO-	
#36	-1952.97664	127.96	$Si_3H_2N_3$-	
#35	-2063.93692	111.96	SiC_3O_3-	
#14	-2462.19532	42	CNO-	
# 1	-2523.77859	13.01	CH-	Hydrocarbon
# 7	-2886.33128	26	CN-	
# 5	-3176.05963	17	OH-	
# 3	-3573.73722	16	O-	
#22	-7824.74524	62.97	PO_2-	

Table 4.7: Top 10 positive and negative loading values for PC3 of negative ions.

N	Load	Mass	Ion	Biological molecule
#30	8022.2594	79.96	SO_3-	
# 6	3056.4844	25.01	C_2H-	Hydrocarbon
#40	2447.0261	283.27	$C_{18}H_{35}O_2$-	Fatty acids
#38	2433.93058	255.24	$C_{16}H_{31}O_2$-	Fatty acids
#23	1995.43168	63.96	SO_2-	
#36	1698.83216	127.96	$Si_3H_2N_3$-	
#26	1481.42602	71.02	$C_3H_3O_2$-	Fatty acids
#22	1372.73898	62.97	PO_2-	
#35	1331.82641	111.96	SiC_3O_3-	
#28	1290.67857	75	$CHNO_3$-	
#27	-754.25183	72.01	$SiCH_4N_2$-	
#12	-1098.40141	40.02	C_2H_2N-	
# 5	-1348.2431	17	OH-	
#24	-2219.66609	65.01	SiH_5O_2-	
#10	-2667.53861	32.98	HS-	
# 3	-2981.04146	16	O-	
#14	-3138.14326	42	CNO-	
#29	-3364.13011	78.96	PO_3-	
#33	-4963.59871	96.97	SO_4H-	
# 7	-5734.93767	26	CN-	

4.3.2. Chemical composition analysis by XPS

A typical survey XPS spectrum of an EPS sample is shown in Fig. 4.5. The iron signal is very weak, which is why it does not appear in the survey. The sulphur signal was only detected in the samples incubated in sulphate medium.

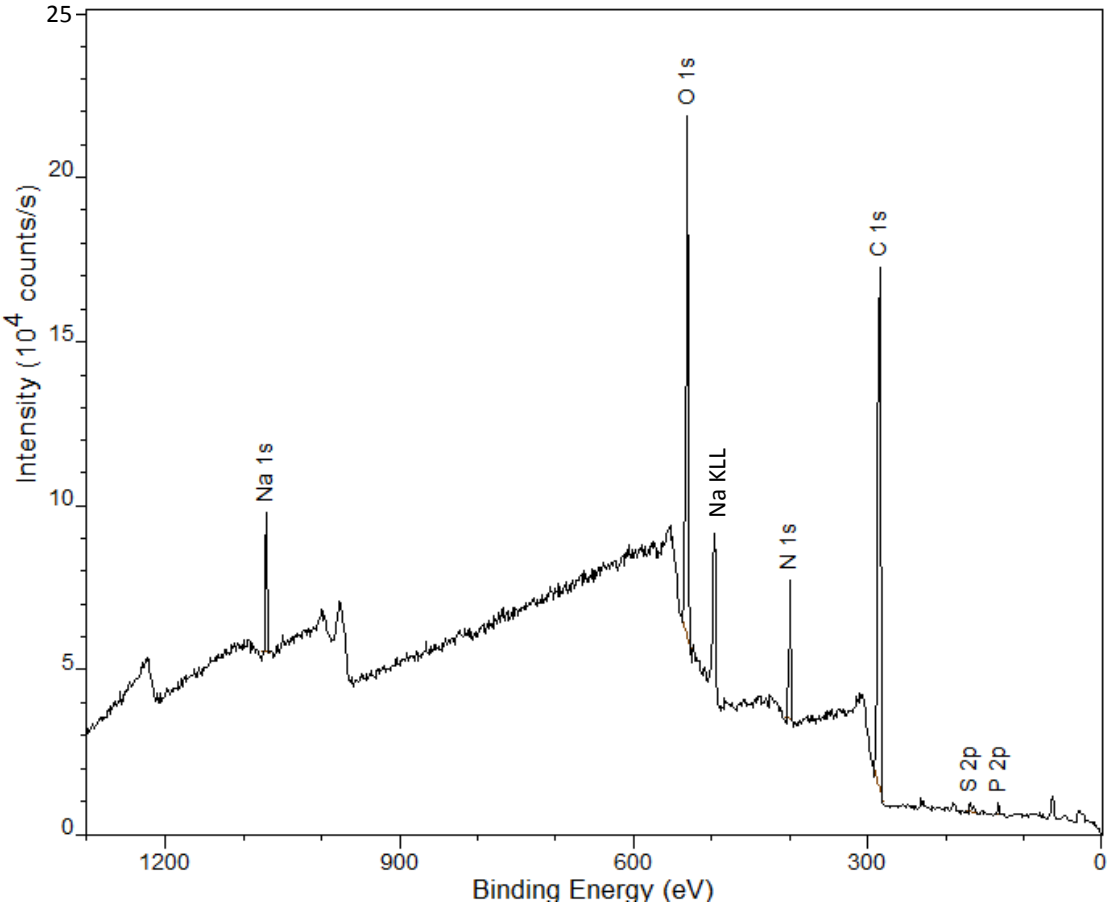

Figure 4.5: XPS spectrum of an EVAP EPS sample (representative survey).

The carbon, nitrogen and oxygen decomposition was very similar in all samples; a representative example can be seen in Fig. 4.6. All the peaks have been decomposed keeping a constant full width at half maximum (FWHM) to all components. The carbon peak was always decomposed into four components; nitrogen and oxygen peaks, in their turn, were decomposed in only two. Following the work of Rouxhet & Genet [172], the carbon components were assigned as follow: carbon bound to carbon or hydrogen (hydrocarbons) at 284.8 eV; carbon bound to oxygen or nitrogen, representative of amine, amide or alcohol at 286.1 eV; carbon doubly bound to oxygen or two single bonds to oxygen in aldehyde, carboxylate or amide functional groups at 287.9 eV; and carbon linked to carboxylic acid group at 288.8 eV. The nitrogen element spectrum was decomposed in two peaks related to nonprotonated nitrogen (amide, peptidic link) at 399.7 eV and protonated amine at 401.3 eV. The O 1s spectrum was fitted by two peaks: the first one is related to oxygen making a double bond to carbon or phosphorous in carboxylate, amide and phosphodiester at 531.2 eV; the second one is oxygen making one bond to carbon in alcohol at 532.6 eV. The complete summary of the chemical and biological functions are described in Table 4.8.

Table 4.8: Identification of the chemical function of biochemical compounds according to the binding energy position.

E_b (eV)	Function	Biochemical compound of reference
Carbon		
284.8	**C**-(C,H)	Hydrocarbon
286.1 ± 0.04	**C**-(O,N)	Amine; Amide, peptidic link; Alcohol[2]
287.9 ± 0.06	**C**=O, O-**C**-O; (**C**=O)-NH-C, O=**C**-O^-	Aldehyde, (hemi)acetal; Amide, peptidic link[1]; carboxylate
288.8 ± 0.3	(**C**=O)-OH	Carboxylic acid
Nitrogen		
399.7 ± 0.1	(C=O)-**N**H-C	Amide, peptidic link[1]
401.3 ± 0.2	C-**N**$H3^+$	Protonated amine
Oxygen		
531.2 ± 0.15	**O**=C-$\mathbf{O}^-$;(C=**O**)-NH-C; P=**O**, P-$\mathbf{O}^-$	Carboxylate; Amide, peptidic link[1]; Phosphodiester
532.6 ± 0.1	C-**O**H; C-**O**-C-**O**-C	Alcohol[2]; (hemi)acetal

[1], [2] related data, as relationship is expected between the outline components.

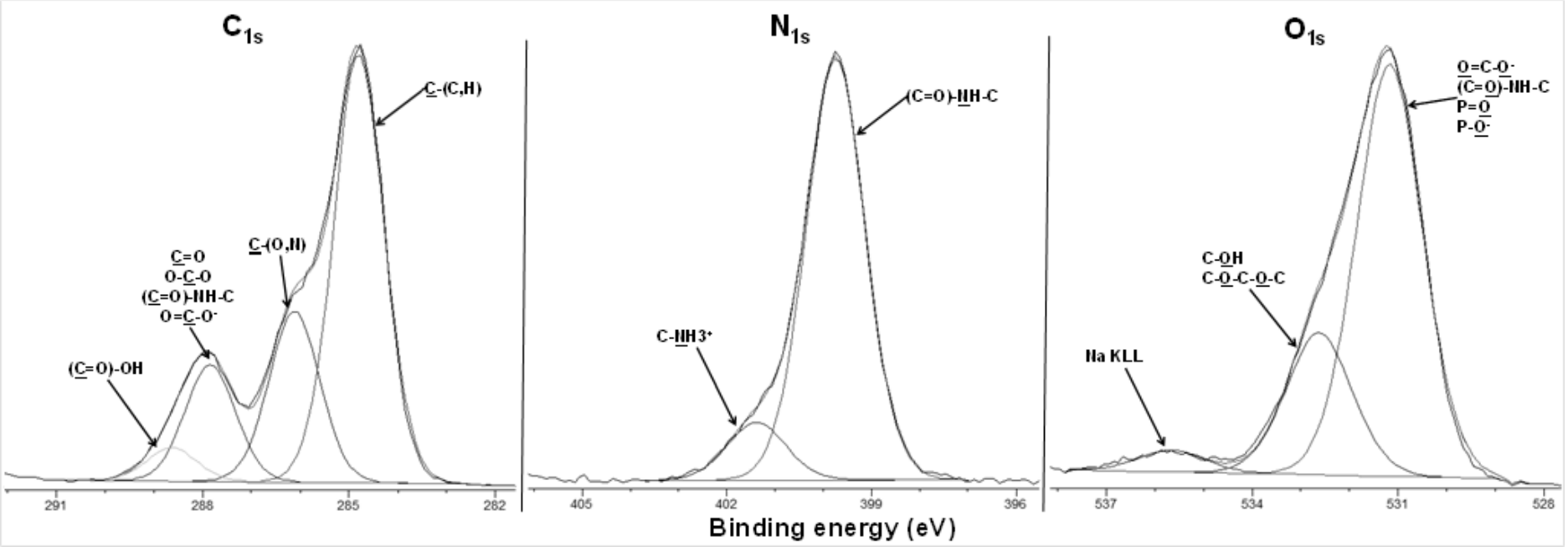

Figure 4.6: Representative carbon, nitrogen and oxygen XPS peaks of EVAP EPS sample with respective decomposition.

Accordingly to Leone *et al.* [191] the protonated amine is indicative of zwitter-ionic properties which have a positive charge that have to be balanced by negatively charged groups, that in EPS case, the candidates are carboxylates and/or phosphate groups which are also detected both by XPS and ToF-SIMS analysis. These negatively charged groups may also be responsible for the calcium/metal uptake properties observed in EPS of SRB as already discussed in the literature and the previous chapter [180]. The carboxylic groups, can also attract cations as calcium that can form bridges between alginate molecules helping to increase the mechanical stability of biofilms [96].

Ca, Fe, Na, P, S and Si were analyzed in narrow scans and although they were decomposed, the component identification was very difficult, because of the many possibilities of compounds that could be related to each binding energy in some case and as a result the quantification was conducted considering the whole region. The S 2p has some components indicative of sulphate/sulphite and organic sulphide (data not shown) in accordance with the studies of bacteria cell walls composition [189, 190, 192, 193].

Table 4.9 presents the major results from XPS measurements of all the EPS samples. The presence of Si was only detected in one sample and is probably a contamination during some step of the sample manipulation as it corresponds to the sterile nitrate medium that does not contain any silicon in its composition or has been in contact with the polished metal plates. Carbon is the main element in the table, being responsible for more than 60% of the total. As expected from a biological sample, oxygen and nitrogen are the next more important elements. Na is the fourth more common element, probably due to the presence of sodium sulphate and sodium nitrate in the media composition where the cultures were grown and it may have been “trapped” by the EPS. Phosphorous appears at 133.1 eV and is attributed to phosphate groups present in some salts from the media composition.

Table 4.9: Elemental composition and functional groups determined by XPS on EVAP EPS samples according to table 1 ID: molar ratios (%) and of species defined by the indicated binding energy (E_b, eV) of peak components.

	Si 2p[a]	P 2p[b]	S 2p[c]	C 1s				Ca 2p[d]	N 1s		O 1s		Fe $2p_{3/2}$[e]	Na 1s
E_b (eV)				284.8	286.1	287.9	288.8		399.7	401.3	531.2	532.6		1071
A	NM	0.813	0.896	33.729	16.485	12.949	1.767	NM	9.523	1.081	15.896	4.315	BDL	2.547
B	NM	1.055	1.036	34.392	15.311	11.887	2.071	0.084	8.354	1.097	16.666	4.614	0.292	3.141
C	NM	1.139	0.996	38.004	15.158	10.341	2.989	NM	7.596	1.044	14.787	5.155	BDL	2.791
D	NM	0.913	1.024	40.604	14.74	9.747	3.32	NM	7.784	1.014	14.286	4.232	BDL	2.337
E	NM	1.125	1.36	37.284	14.748	11.543	1.965	0.178	8.163	1.031	15.668	4.402	BDL	2.534
F	6.877	1.006	NM	37.632	13.623	9.828	2.421	0.262	6.733	0.873	12.759	6.222	BDL	1.766
G	NM	2.261	NM	34.293	14.76	11.637	1.955	NM	6.283	1.175	17.156	6.691	0.12	3.67
H	NM	1.418	NM	36.676	15.333	11.682	2.7	NM	8.426	0.722	15.359	4.777	0.135	2.773
I	NM	1.361	NM	36.869	15.749	12.411	1.647	0.148	8.383	1.023	15.065	4.933	BDL	2.411
J	NM	1.208	NM	36.396	16.156	13.351	0.906	NM	7.967	1.38	15.64	4.885	0.098	2.013

NM: Not measured; BDL: Below Detection Limit.
[a]: Si 2p in range of 98 to 106 eV.
[b]: P 2p in range of 131.5 to 135.5 eV.
[c]: S 2p in range of 162 to 172 eV
[d]: Ca 2p in range of 344 to 355 eV.
[e]: Fe $2p_{3/2}$ in range of 705 to 720 eV.

Table 4.10 summarizes the surface composition of EVAP EPS samples, in terms of atomic concentration ratios with respect to total carbon. The overall composition was very similar in all the samples with a few characteristic easily distinguishable: (i) the detection of sulphur only in sulphate medium samples indicates that it is related mainly to sulphate reduction and not to protein; (ii) a higher ratio of phosphorous in nitrate medium; (iii) the difference between sterile media and EPS was not remarkable and could not be distinguished by XPS analysis only.

Using the work of Ahimou [190] as reference, the **C**-(C,H) could be related to lipids or the side chains of amino acids. This second options seems to be more likely in our case as the hydrocarbon value was very high in all samples, being responsible for most of the carbon detected, and could be explained by the presence of peptides mixtures in the culture medium. The (hemi)acetal can be linked to polysaccharides and sugar moieties that are one the main constituents of EPS as also shown by colorimetric analysis (see Table 4.11). The proteins and uronic acids may be responsible for the carboxylates and carboxylic acids groups detected. And the protonated amine is likely to originate from the basic amino acids presents. Finally the source of ammonium is the medium composition, as it seems to stay constant in all samples.

Figure 4.7 presents a plot of the atomic concentration rationed to total carbon of carbon bound to oxygen or nitrogen (C_{ox}/C) in fuction of the sum of total oxygen and total nitrogen also rationed to carbon [(O+N)/C]. The dashed line indicates a 1:1 relationship that according to previous studies can be assigned to functional groups as alcohol, (hemi)acetal, amide, amine and ester. It was also demonstrated by the work of Dufrêne and co-workers [189, 201] that a small excess to the side of [(O+N)/C] in some samples indicates the presence of carboxylates and phosphates groups, which indicates that carbon is not bound to oxygen or nitrogen in 1:1 ratio.

Table 4.10: Atomic ratios of elements (Silicon, Phosphorous, Sulfur, Calcium, Nitrogen, Oxygen, Iron and Sodium) and functional groups *vs* total Carbon molar ratio.

	Si/C	**P/C**	**S/C**	**C 1s(/C)**				**Ca/C**	**N 1s(/C)**		**N_{tot}/C**	**O 1s(/C)**		**O_{tot}/C**	**Fe/C**	**Na/C**
E_b (eV)				284.8	286.1	287.9	288.8		399.7	401.3		531.2	532.6			
A	NM	0.013	0.014	0.519	0.254	0.199	0.027	NM	0.147	0.017	0.163	0.245	0.066	0.311	NM	0.039
B	NM	0.017	0.016	0.540	0.241	0.187	0.033	0.001	0.131	0.017	0.148	0.262	0.072	0.334	0.005	0.049
C	NM	0.017	0.015	0.572	0.228	0.156	0.045	NM	0.114	0.016	0.130	0.222	0.078	0.300	NM	0.042
D	NM	0.013	0.015	0.594	0.215	0.142	0.049	NM	0.114	0.015	0.129	0.209	0.062	0.271	NM	0.034
E	NM	0.017	0.021	0.569	0.236	0.176	0030	0.003	0.125	0.016	0.140	0.239	0.067	0.306	NM	0.039
F	0.108	0.016	NM	0.593	0.231	0.155	0.038	0.004	0.106	0.014	0.120	0.201	0.098	0.299	NM	0.028
G	NM	0.036	NM	0.547	0.236	0.186	0.031	NM	0.100	0.019	0.119	0.274	0.107	0.381	0.002	0.059
H	NM	0.021	NM	0.552	0.231	0.176	0.041	NM	0.127	0.011	0.138	0.231	0.072	0.303	0.002	0.042
I	NM	0.020	NM	0.553	0.236	0.186	0.025	0.002	0.126	0.015	0.141	0.226	0.074	0.300	NM	0.036
J	NM	0.018	NM	0.545	0.242	0.200	0.014	NM	0.119	0.021	0.140	0.234	0.073	0.307	0.001	0.030

NM: Not measured. E_b: Energy binding in electron Volt.

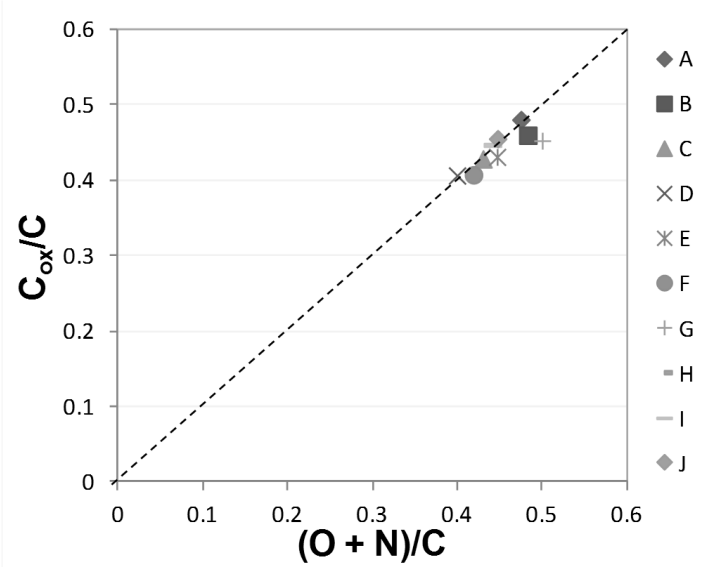

Figure 4.7: Plot of atomic concentration (rationed to total carbon) of carbon bond to oxygen or nitrogen (C_{ox}) in function of the sum of total Oxygen and total Nitrogen rationed to total carbon (O+N)/C for all samples (see Table 4.1 for identification). The dashed line represents a 1:1 relationship.

Figure 4.8 confirms the result presented in the previous figure as it shows an excess of oxygen making a double bond with carbon (**O**=C) or of carbon making double bond with oxygen or two single bonds (**C**=O). The data is farther from the 1:1 proportion presented in the other studies and that is expected for amide functions. The ratio is around 1.6 closer to a 2:1 proportion, and this indicates that the contribution of phosphates, carboxylates and (hemi)acetal is higher in our samples.

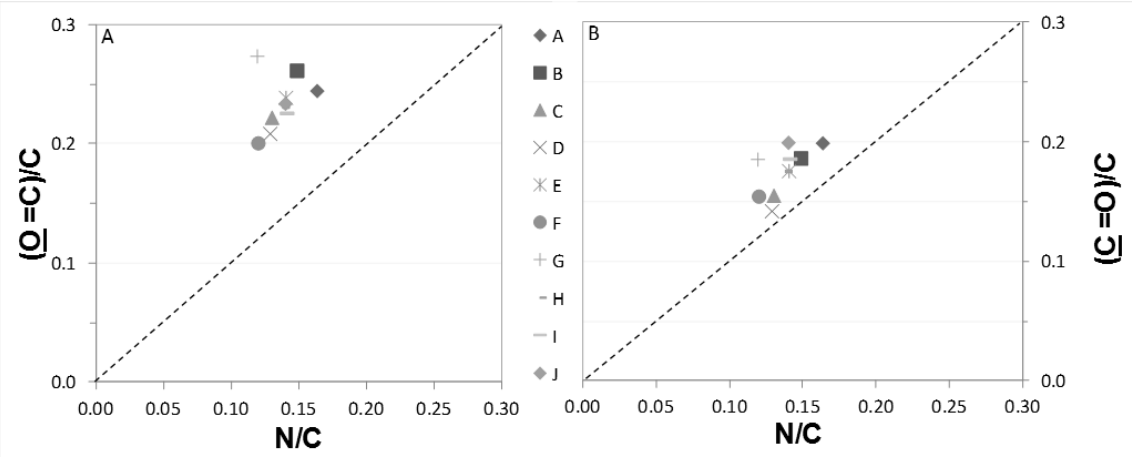

Figure 4.8: Plot of atomic concentration rationed to total carbon of A) oxygen doubly bond to carbon (**O**=C) and B) carbon making one double or two single bonds with oxygen (**C**=O/C). See Table 4.1 for identification. The dashed line represents a 1:1 relationship.

In Fig. 4.9 we try to assess the relation of the oxygen contributing to the component at 531.2 eV to phosphorous not counting with the oxygen related to amide. We observed an

excess to the side of the oxygen and according to Boonaert and Rouxhet [192] this could represent the phosphate containing compounds $Ca_2P_2O_7$, KH_2PO_4, $FePO_4$. This is in accordance to our findings about the EPS cations binding capabilities.

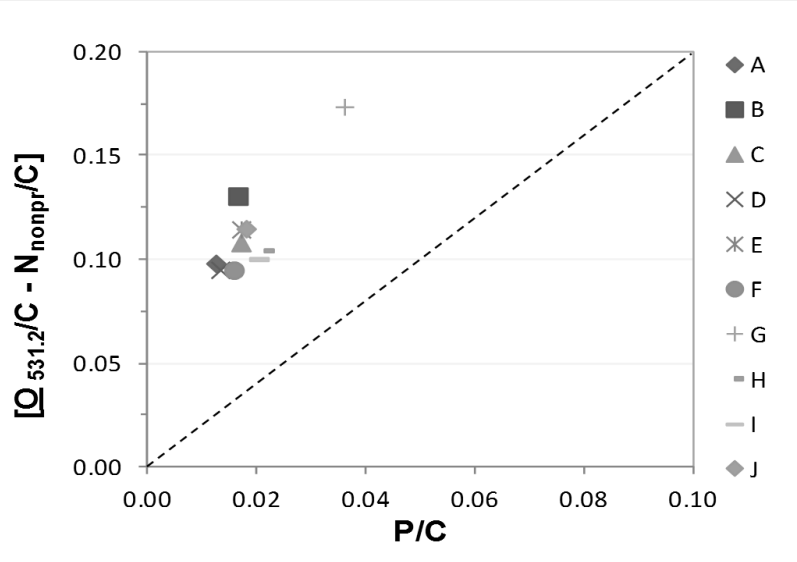

Figure 4.9: Plot of the difference between the molar concentration of oxygen peak 531.2 eV (rationed to total carbon) and nonprotonated nitrogen rationed to total carbon ($\underline{\mathbf{O}}_{531.2}$/C - $\underline{\mathbf{N}}_{nonpr}$/C) as function to molar ratio of phosphate to total carbon (P/C). See Table 4.1 for identification. The dashed line represents a 2:1 relationship.

Fig. 4.10A presents a plot of the molar concentration of carbon making one double bond or two single bonds to oxygen rationed to total carbon($\underline{\mathbf{C}}_{287.9}$/C) as a function of the ratio between nonprotonaed nitrogen and total carbon. There is a slight excess of the first ratio in comparison to the reference line, which indicates a higher contribution of amide and carboxylate functions [(O=$\underline{\mathbf{C}}$)-NH-C; O=$\underline{\mathbf{C}}$-O^-]. We can remove the contribution of acetal functions present in polysaccharides [(O-$\underline{\mathbf{C}}$-O)$_{AC}$/C] using the following equation:

$$(O\text{-}\underline{\mathbf{C}}\text{-}O)_{AC}/C = 0.2\ [\underline{\mathbf{C}}\text{-}(O,N)/C - N/C] \quad (4.1)$$

This equation assumes that there is one acetal per polysaccharide constituting unit and that the carbon from the component at 286.1 eV is due either to polysaccharides or amide. Fig. 4.10B shows that after the deduction of the acetal contribution from the $\underline{\mathbf{C}}_{287.9}$/C is above the dashed line indicating that most of the components are composed by carboxylate, which probably have origin in the lactate and derivatives that are in excess in the medium composition as shown in chapter 2. Figs 4.10C and 4.10D represent a plot of $\underline{\mathbf{O}}_{531.2}$/C and of [$\underline{\mathbf{O}}_{531.2}$/C – 2P/C] *versus* N_{nonpr}/C and they confirm that the oxygen peak component at 531.2 eV is mostly related to carboxylate, although some contribution from amide and phosphates groups could not be disregarded.

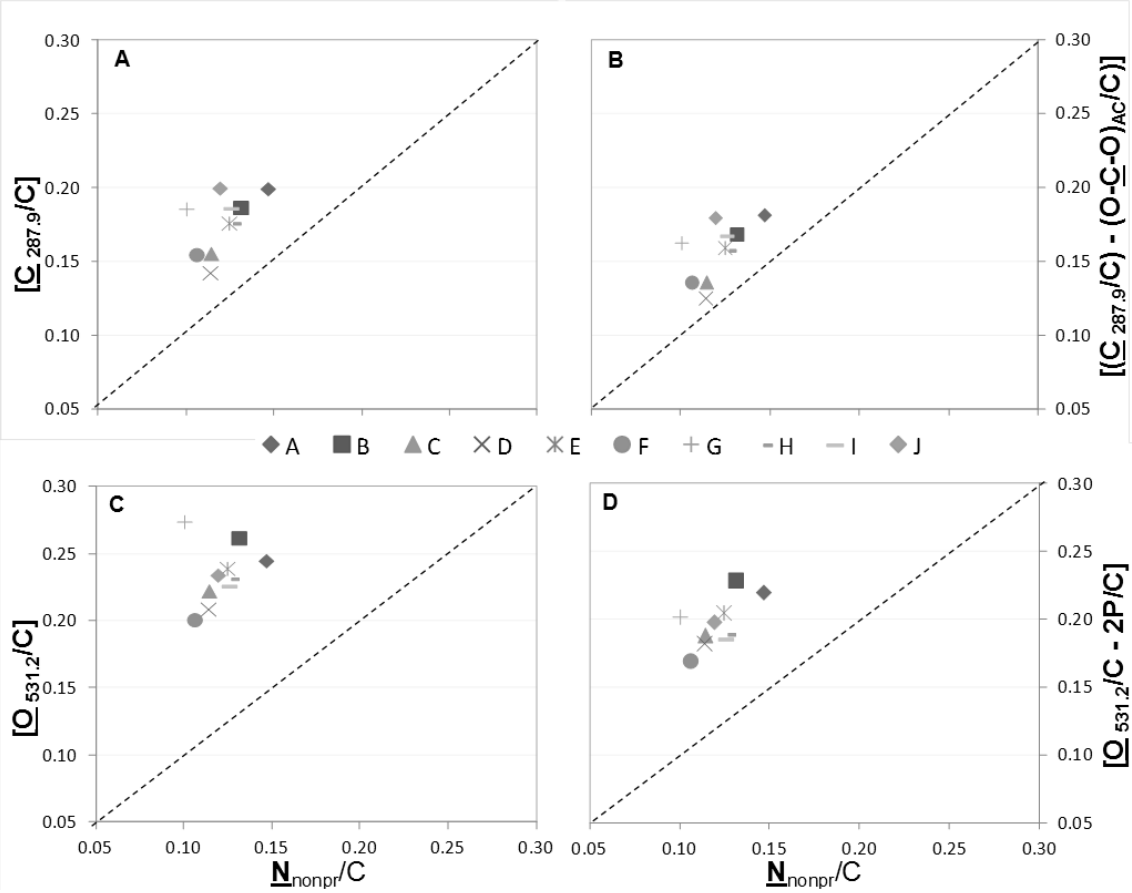

Figure 4.10: Molar concentrations (in ratio to total carbon), as function of the nitrogen nonprotonated rationed to total carbon ($\underline{\mathbf{N}}_{nonpr}$/C): A) Carbon making one double or two single bonds with oxygen (component 287.9 eV, $\underline{\mathbf{C}}$=O/C); B) the same after deduction of acetal contribution; C) Oxygen making double bond to carbon ($\underline{\mathbf{O}}$=C) related to the component 531.2 eV; D) the same after deduction of 2P rationed to total carbon. See Table 4.1 for identification. The dashed line represents the 1:1 relations expected for amide functions.

Fig. 4.11 is a plot of the $\underline{\mathbf{O}}_{532.6}$ eV rationed to total carbon as function of the difference between the carbon bound to oxygen or nitrogen and total nitrogen (in ratio to total carbon). The relation is in agreement with the findings of the previous study of Ahimou [190] where a relation close to 1:1 corroborates the attribution of the $\underline{\mathbf{O}}_{532.6}$ eV component mostly to (hemi)acetal and the $\underline{\mathbf{C}}_{286.1}$ eV to amide or peptidic link.

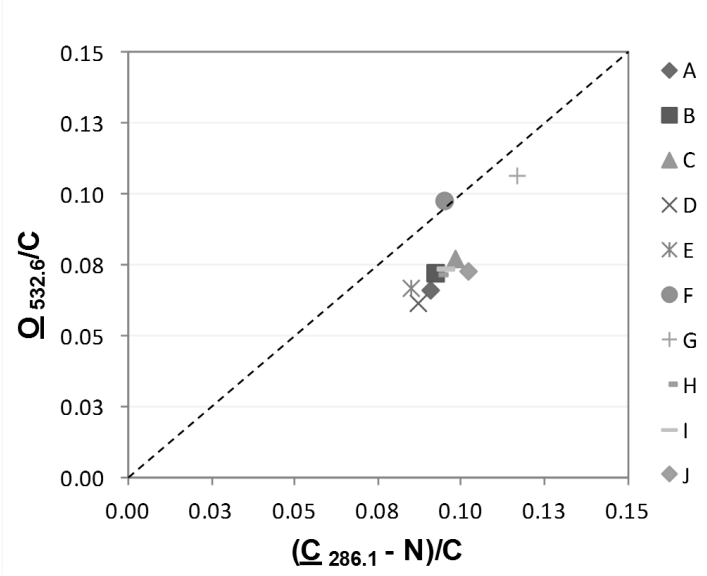

Figure 4.11: Molar concentration of oxygen peak 532.6 eV rationed to total carbon ($\underline{O}_{532.6}$/C) as function of the difference between carbon linked to oxygen or nitrogen (286.1 eV) and total nitrogen [($\underline{C}_{286.1}$ - N)/C], rationed to total carbon. See Table 4.1 for identification. The dashed line represents a 1:1 relationship.

We determined using traditional biochemical colorimetric assays, that the major constituents of the EPS are polysaccharides, proteins and lipids (see Table 4.11) [26, 96, 150, 158]. Therefore it is possible to model the surface composition of EVAP EPS samples considering these three classes of basic constituents according to the literature [172, 189, 201].

Table 4.11: Chemical composition of EPS samples from SRB incubated without metal determined by colorimetric assays.

Growth media	Concentration (µg/mL)			
	Polysaccharides	**Uronic Acids**	**DNA**	**Proteins**
Sulphate	1.67	0.21	BDL	0.34
Nitrate	5.38	0.11	BDL	2.31

BDL – Below detection limit

In order to perform this modeling it is necessary to solve three equations of the following elemental concentration ratios:

$$(N/C)_{obs} = 0.279\ (C_{PE}/C) \quad (4.2)$$

$$(O/C)_{obs} = 0.325\ (C_{PE}/C) + 0.833\ (C_{PS}/C) \quad (4.3)$$

$$(C/C)_{obs} = (C_{PE}/C) + (C_{PS}/C) + (C_{HC}/C) = 1 \quad (4.4)$$

Where PE is peptides, PS is polysaccharides and HC is hydrocarbon like compounds.

The solution of this system of equations will allow to assign the proportion of carbon associated with each molecular constituent and these proportions can be converted into

weight fractions using as reference the carbon concentration of each compound class provided by the work of Dufrêne and co-workers [189] (see table 4.12).

Table 4.12: Carbon concentration of the model constituents.

Constituent	Carbon concentration (mmol/g)
Polysaccharide	37.0
Peptides	43.5
Hydrocarbon	71.4

Fig. 4.12 presents the modeled molecular composition of the EVAP EPS samples calculated accordingly to the equation system outlined above. The high concentration of peptides (around 55%) observed that differs from the quantification done by colorimetric assays is probably a consequence of the fact that the XPS is unable to differentiate the peptides, that are also present in the media composition, from the proteins, that can be specifically quantified by the colorimetric methods. Nevertheless, this drawback does not invalidate the usefulness and accuracy of XPS to assess the chemical composition of biological systems.

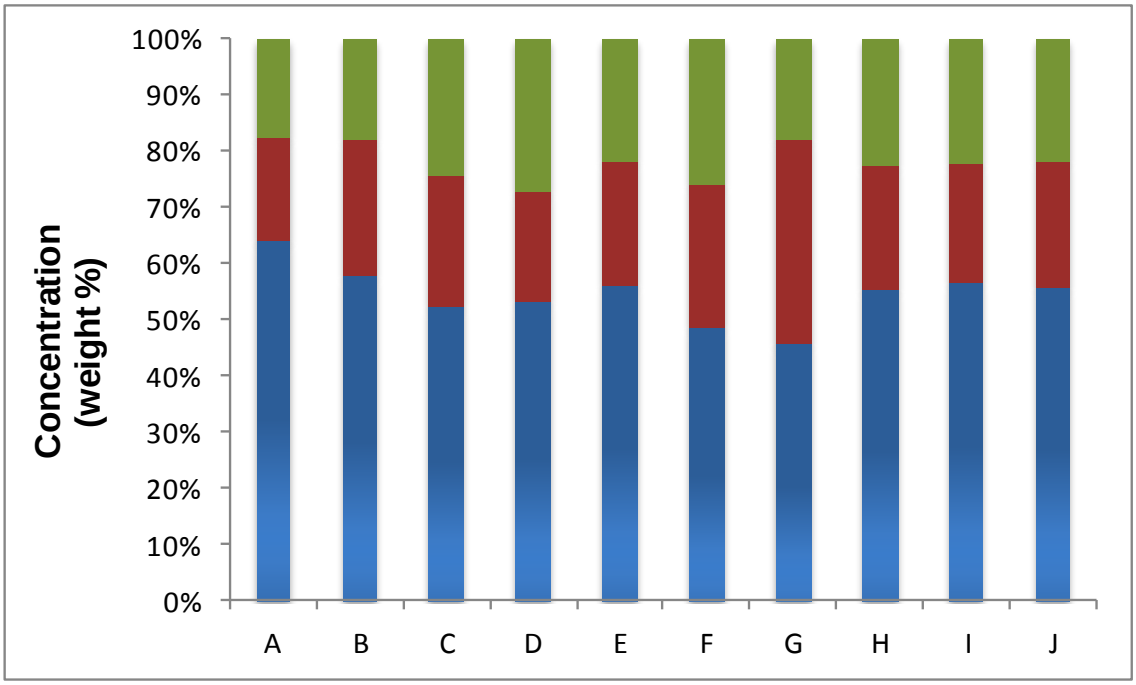

Figure 4.12: Modeled molecular composition (weight %) on EVAP EPS samples. Blue: Pepetides; Red: Polysaccharides; Green: Hydrocarbon. See Table 4.1 for identification.

A very interesting advantage is that XPS allowed quantifying the lipid content which often involves a series of laborious protocols and sample manipulation when done by

colorimetric assays and still represents one of the main limitations in the EPS analysis [96, 150].

4.3.3. Protein profile by SDS-PAGE

Even though the ToF-SIMS and XPS results could not differentiate the protein profile produced in the two culture media, it is well documented in the literature that the protein expression can vary significantly even for the same organism incubated in different conditions (for example temperature, respiratory substrate, and oxidative stress) [120, 202, 203]. Therefore a more specific approach to analyze the differential protein expression in EPS produced in different respiratory substrate and metal presence was needed. Considering the number of samples to analyze SDS-PAGE was selected as the best choice to do this characterization.

Fig. 4.13 presents the protein expression profile in EPS of *D. desulfuricans* in different conditions and the total proteome as controls.

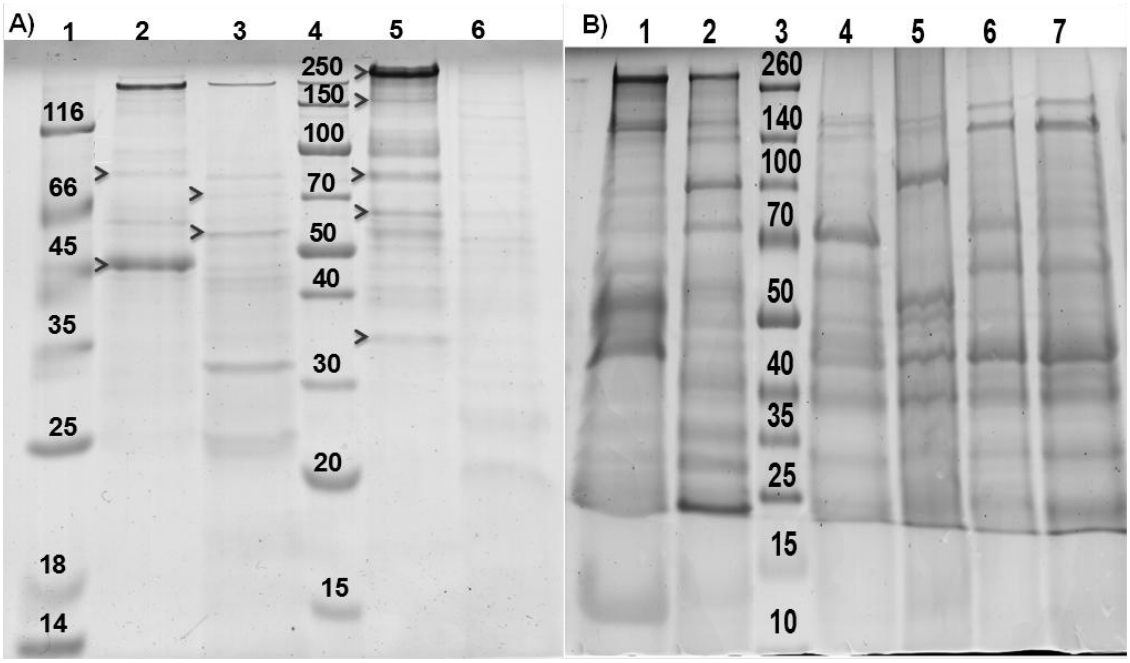

Figure 4.13: SDS-PAGE gel electrophoresis in a 10% polyacrylamide tris-glycine gel: A) Samples without metal plates incubation. A1-Molecular Weight Marker (kDa); A2- Colloidal EPS NO_3^-; A3- Capsular EPS NO_3^-; A4- Molecular Weight Marker (MWM); A5- Colloidal EPS $SO_4^=$; A6- Capsular EPS $SO_4^=$; B) Samples incubated in bioreactor with metal coupons and total proteomes: B1- Colloidal EPS Bioreactor $SO_4^=$; B2- Colloidal EPS Bioreactor NO_3^-; B3- Molecular Weight Marker (MWM); B4- Total Proteome Bioreactor $SO_4^=$; B5- Total Proteome Bioreactor NO_3^-; B6- Total Proteome without metal $SO_4^=$; B7- Total Proteome without metal NO_3^-; Red arrows indicate the protein successfully identified by MALDI-ToF.

The SDS-PAGE results demonstrate that the protein expression is different according to the respiratory substrate and to the presence/absence of metal plates. This confirms the results obtained by 2D Gel electrophoresis in the work of Silveira [204] where they have

shown important differences in protein content that were broader than the enzymes only involved in the nitrate and sulphate respective reduction pathways. This study has identified proteins from several functional categories protein biosynthesis, glucose, pyridoxal and phosphate metabolism, detoxification and transport, redox processes, translation, energy metabolism, stress response as well as putative proteins of unknown function, as being differentially expressed when the bacteria uses different respiratory substrates. Beech *et al*. [184] have demonstrated the influence of the growth conditions in *Pseudomonas* sp. NCIMB 2021 EPS protein profile.

From the analysis of the samples protein profile, we could observe that when the bacteria were grown without metal, the absence of low molecular weight proteins can be noted in the gel both in sulphate and nitrate condition. Some of the bands were cut considering it level of expression and processed by mass spectrometry to try to identify the metabolic process associated or if they were involved in electron transfer. The list of the successfully identified proteins is presented in Table 4.13. Unfortunately, we could not identify up to now any protein from the incubations with metal plates. It is worth mentioning that we only considered matches that had scores significant according to the definitions of the Mascot server, which varies for each protein.

Table 4.13: Sulphate and nitrate EPS protein identification by MALDI-ToF peptide mass fingerprint of bands from SDS-PAGE gels.

Sample	Protein weight (kDa)	Biological process	Cell location
Sulphate without metal			
Colloidal EPS			
Outer membrane adhesin-like protein [*Desulfovibrio desulfuricans* subsp. *desulfuricans* str. ATCC 27774]	321.7	Homophilic cell adhesion – Calcium biding	Membrane
Outer membrane adhesin-like protein [*Desulfovibrio desulfuricans* subsp. *desulfuricans* str. ATCC 27774]	292.8	Homophilic cell adhesion – Calcium biding	Membrane
Adenylylsulfate reductase subunit alpha [*Desulfovibrio desulfuricans* subsp. *desulfuricans* str. ATCC 27774]	75.2	Sulphate reduction	Cytoplasm
60 kDa chaperonin OS=*Desulfovibrio desulfuricans* (strain ATCC 27774 / DSM 6949)	58.6	Protein refolding	Cytoplasm
Hypothetical protein Ddes_0714 [*Desulfovibrio desulfuricans* subsp. *desulfuricans* str. ATCC 27774]	36.9	Undefined	Unknown
Nitrate without metal			
Colloidal EPS			
Immune inhibitor A metalloprotease [*Bacillus cereus* F65185]	87.9	Proteolysis	Unknown
Chitin-binding domain protein [*Bacillus cereus*]	49.9	Carbohydrate binding	Extracellular

Table 4.13 (Cont.): Sulphate and nitrate EPS protein identification by MALDI-ToF peptide mass fingerprint of bands from SDS-PAGE gels.

Sample	Protein weight (kDa)	Biological process	Cell location
Nitrate without metal Capsular EPS			
Nitrate reductase subunit alpha [*Anaeromyxobacter* sp. K]	66.5	Nitrate reduction	Cytoplasm
1-pyrroline-5-carboxylate dehydrogenase [*Bacillus cereus* ATCC 14579]	56.1	Proline and glutamate biosynthetic process;	Unknown

*Match according to Swissprot database instead of NCBInr.

One very interesting result is that some high molecular weight proteins, involved in cell adhesion and calcium binding where identified in sulphate growth samples, and this could be related to the calcium precipitation observed in the ToF-SIMS mapping of the corroded surfaces in chapter 3.

In both media, we could identify protein related to the reduction pathway of the respective respiratory substrate, although the controls for cell lyses (not shown) did not indicate significant disruption of cells during the EPS extraction procedure. This could mean that these proteins were released during the bacterial culture and remained in the EPS. Some studies have shown that some enzymes can stay active in biofilms even months after the cells have died [24].

In nitrate medium, we could also identify a protein involved in the metabolism of polysaccharides, which is expected as they are one of the main constituents of the EPS secreted and also represents a energy source for the cells.

4.3.4. Differential iron uptake by SRB Extracellular Polymeric Substance

ToF-SIMS analysis demonstrated that the iron detected in the EPS samples was released from the metal plates during its incubation in the VMN medium (see Fig. 4.14 and 4.15). The results also show that when the bacterium was incubated with sulphate, no Fe was detected in the EPS, although it could be detected in the sterile medium that was in contact with the coupons (data not shown). This data corroborate previous results presented in chapter 2 in the weight loss tests and with the study of Beech [104]. This phenomenon could be associated with the sulphide production that should leads the precipitation of the metal ions and could explain why there was no detection of iron bound to EPS although we could see iron sulphide precipitates in the bottle during the bacterial incubations. In the case of the sulphate sterile medium, there is no production of sulphides, so the released iron from the coupons could remain in suspension. Also Beech and Cheng [7] have demonstrated that biomolecules produced by SRB are capable of competing with sulphide for Fe binding during bacterial growth.

In both growth conditions the ToF-SIMS could not detect iron in the EPS when the bacteria was incubated without metal, therefore indicating that the iron from the media was used in the bacteria metabolism and did not bound to the EPS. This is in agreement with the findings of Beech and co-workers that have demonstrated the same trend with other species of *Desulfovibrio* [104].

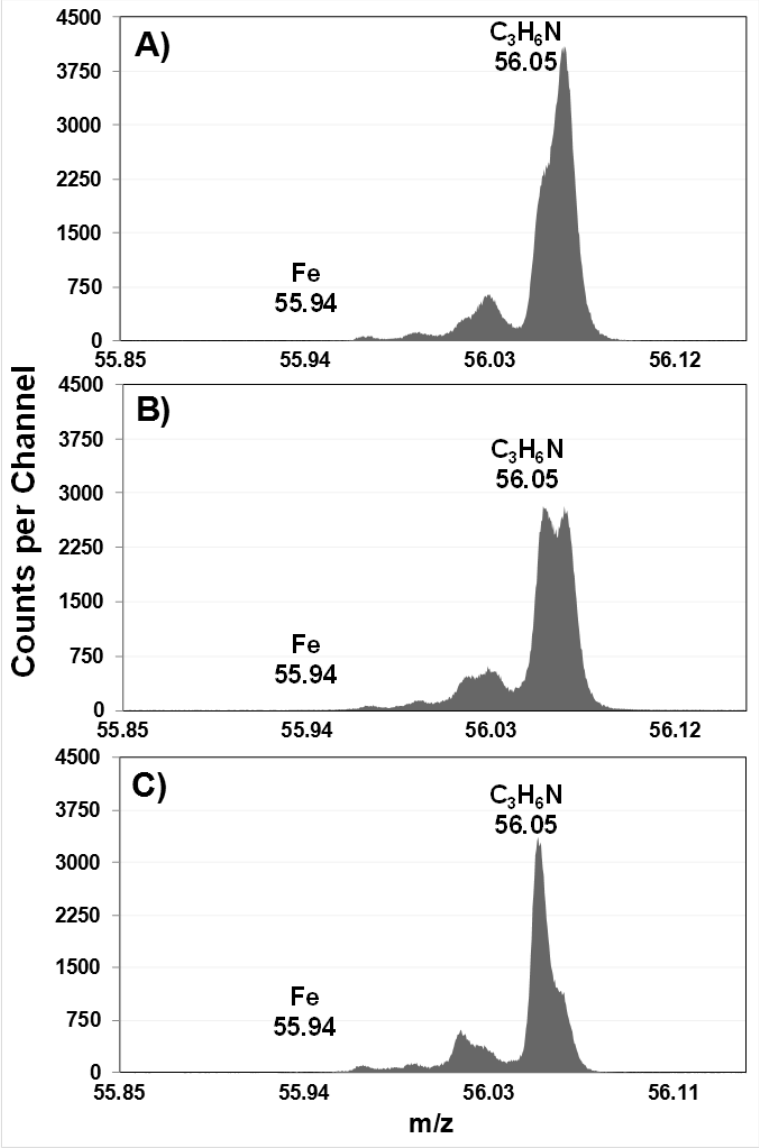

Figure 4.14: ToF-SIMS spectra of the colloidal EPS from SRB cultures in sulphate. A) Sample “C” (with metal); B) Sample “D” (without metal); Sample “E” (EPS from D incubated with metal).

The ToF-SIMS spectra also showed that the peak intensity and shape for the amino acid marker C_2H_6N (Lys, Met, Val) differed between all the samples indicating that the composition varied in some extent. However, the Fe intensity did not presented a significant variation as would be expected considering the results obtained by other techniques as

Weight loss and ICP measurements. This could be explained by variations in the ionization probabilities in ToF-SIMS which depend on the chemical matrix of the sample analyzed.

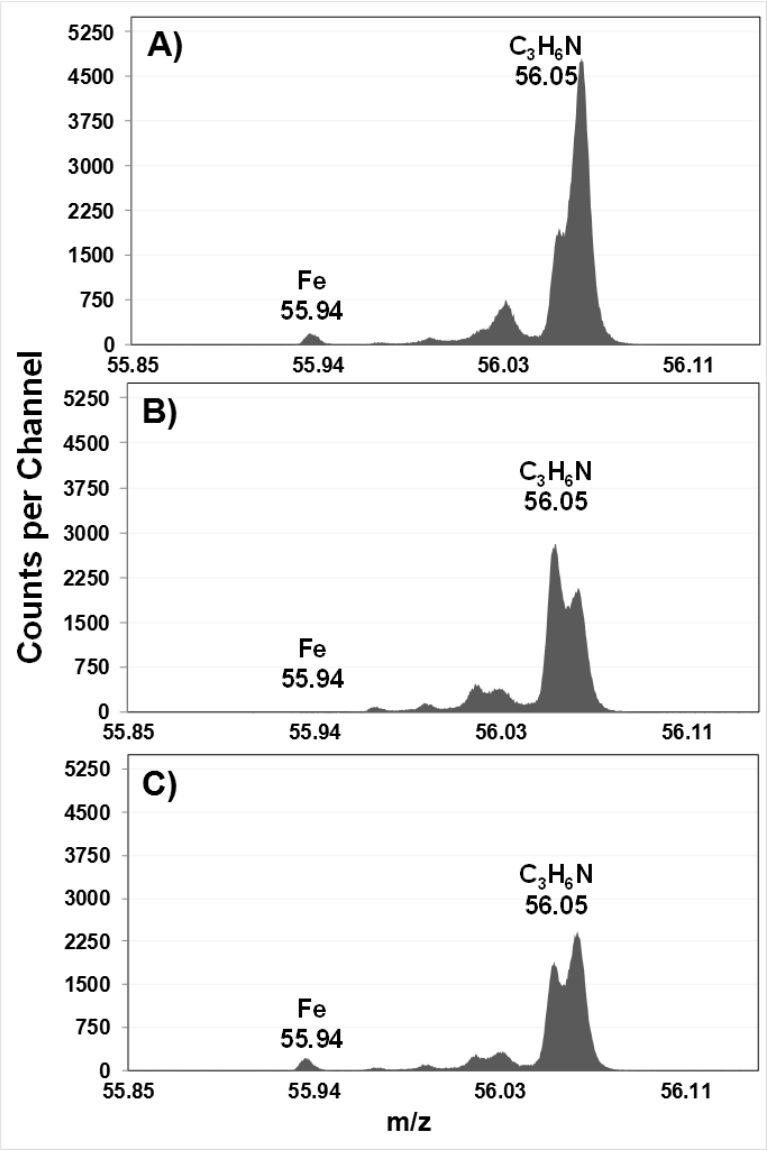

Figure 4.15: ToF-SIMS spectra of the colloidal EPS from SRB cultures in nitrate. A) Sample "H" (with metal); B) Sample "I" (without metal); Sample J (EPS from "I" incubated with metal).

ICP and XPS analysis were carried out to quantify the iron uptake by the EPS produced in different conditions as well as in the controls. The details of the data analysis were mentioned in section 4.3.2 as also in section 3.2. The Fe-chelating capability of the EPS and controls is listed in Table 4.14.

Table 4.14: Quantification by XPS and ICP of iron in colloidal EPS samples.

Sample	**A**	**B**	**C**	**D**	**E**	**F**	**G**	**H**	**I**	**J**
XPS										
%Conc	BDL	0.292	BDL	BDL	BDL	BDL	0.12	0.135	BDL	0.092
ICP										
mg/l	0.67	10.15	0.101	0.028	0.326	1.15	4.67	18.79	0.24	25.76
%Conc	*0.072*	*0.995*	*0.01*	*0.003*	*0.029*	*0.117*	*0.677*	*1.907*	*0.023*	*2.012*

XPS – X-ray spectsocropy; ICP- Inductively Coupled Plasma; BDL – Below Detection Limit.

It is clearly visible that the nitrate produced EPS has a higher iron bound concentration when compared to sulphate medium. This result demonstrates that the EPS produced by the same bacteria grown in similar medium but using different respiratory substrates have distinct capacities for iron uptake. According to Beech [104] the binding energy found in the peak components of Fe are indicative of a chelated iron in the Fe(III) form. Finally, the results from Table 4.14 also demonstrate the influence of biogenic sulphide in Fe precipitation and removal from the system as even in the samples incubated without metal more iron could be detected in nitrate produced EPS than in sulphate produced EPS.

4.4. Conclusions

The use of state-of-the-art techniques of surface science like ToF-SIMS and XPS supported by biochemical methods has proven to be valid methodology for the chemical characterization of extracellular polymeric substances. These techniques have the advantage of avoiding laborious extraction protocols, requiring low sample manipulation, small quantity of samples and having good accuracy.

When ToF-SIMS was allied with the multivariate statistical analysis, we were able to indentify some important ions related to the chelating properties of EPS and their influence in the biocorrosion process. Moreover, the samples could be grouped according to the respiratory substrate.

This was one of the first studies to characterize EPS using XPS. The result obtained supports the validity of using this tool for understanding the overall biochemical composition of the main classes of biomolecules on this type of sample. The XPS was able to demonstrate the importance of some chemical functions, as carboxylates and phosphates, having relation to calcium binding and iron uptake.

The SDS-PAGE results were complementary to the surface methodologies and provided new insights into the interconnection of the proteins present in the EPS and some of its corrosive properties, as Ca binding and iron chelation. The results also support that the EPS can be active even when the bacterial cells are dead, as it retain some enzymes in its scaffold.

Finally, the ICP, XPS and ToF-SIMS data confirmed the influence of the respiratory substrate in the iron chelating properties of the EPS produced by the same species of SRB. As presented in chapter 2, when growing in nitrate, *D. desulfuricans* exhibits a much higher iron uptake from metals. It was also shown that the metal is originating from the coupons and not from the medium composition itself.

Chapter 5

Electron transfer protein adsorption studies

Chapter 5 – Electron transfer proteins adsorption studies

5.1. Introduction

Protein adsorption at surfaces has important consequences to medical devices, technological applications and biocorrosion process. A deeper understanding of protein adsorption is fundamental to biosensors, immobilized enzymes for medical tests, cell culture, and biofilm development [205]. The protein behaviour at the surface is influenced by the properties of the material as hydrophobicity, charge polarity and free energy [206]. Also the protein concentration, charge and hardness are important variables to determine the amount of protein that can attach to the surface, its orientation, conformation, layer thickness and spatial distribution [207, 208]. Usually proteins can adsorb in hydrophobic surfaces despite the electrostatic conditions and cells, on the other way, attaches preferably to surfaces with hydrophilic or polar functional groups. For hydrophilic surfaces, hard proteins can only adsorb if they encounter favourable electrostatic conditions. Soft proteins are able to adsorb in adverse conditions, because of theirs ability to conformational changes at the surface [162].

Because of its complexity, no single technique can provide a full view of the protein films formed at the surface. A wide range of different techniques have been applied to study protein films, including ellipsometry, Fourier transform infrared spectroscopy (FTIR), surface Plasmon resonance (SPR), total internal reflection fluorescence, quartz crystal microbalance (QCM), time-of-flight secondary ions mass spectrometry (ToF-SIMS), scanning probe microscopy, scanning and transmission electron microscopy, X-ray photoelectron spectroscopy (XPS), atomic force microscopy and surface force measurements [206, 207, 209].

A quartz crystal microbalance (QCM) uses the phenomenon of piezoelectric effect that affects crystals to measure the adsorption of molecules to the surface of a crystal in a liquid flow. This is possible by measuring the shift in frequency of the crystal resonator due to the increase of its mass by the deposit of protein or other biomolecules, for example. Besides being able to measure the mass deposition at the surface of the crystal, the QCM is able to give information about the samples viscoelastic properties and can be couple to electrochemical techniques which allow to link fil formation at the surface of the electrode to electrochemical tests like cyclic voltammetry, for example [210].

Tetrahaem cytochrome c3 (Cyt c3) is an electron transfer protein that is located in the periplasmic space and is one of the most abundant protein in *Desulfovibrio* genera. Cytochromes c3 is a small protein with approximately 14 kDa and a globular shape. This protein is the biological couple of hydrogenase and plays a central role in the hydrogen cycling, metal reduction or oxygen detoxification. Because of its small size and good

electrochemical properties it has been extensively used for studies involving electron/proton linkage and electron transfer reactions [23, 71, 75, 80, 211-213].

Hydrogenases (Hase) are enzymes involved in the reversible conversion between H_2 and H^+. The operation of hydrogenase is coupled to redox complexes as ferredoxins or cytochromes, the last been it preferential physiological partner [63]. Hydrogenases are classified in three different classes based in the metal composition at the active site: (i) [NiFe], most common and sensitive to oxygen presence; (ii) [FeFe] usually more active and considered as on single superfamily with the first class; and (iii) [Fe]-only hydrogenase, that is found in some Achaea and have a different enzymatic mechanism and redox partners. The hydrogenase from Desulfovibrio gigas is a broadly used model and is a periplasmic enzyme with molecular weight of 89 kDa comprised of one bigger subunit (63 kDa) with the active site and a smaller subunit (26 kDa) that holds three iron-sulfur clusters that works as an “electron wire” to transfer electrons to the active site [29, 31, 51, 53, 214, 215]. Since the early work of von Wolzogen Kuhr & van der Flugt [28], many authors have demonstrated the importance of hydrogenase to the biocorrosion process through the hydrogen metabolism of SRB or as pure enzymes after the cell disruption at the biofilm [24, 30, 216, 217].

This chapter is focused in understanding the adsorption behaviour on gold of these two model proteins involved in the electron transfer process using QCM, XPS and ToF-SIMS.

.

5.2. Experimental

5.2.1. Proteins adsorption on gold

Cytochrome C_3 (cyt c_3) and Hydrogenase (Hase) obtained from *Desulfovibrio desulfuricans* ATCC 27774, purified at our lab, were used in all adsorption tests in a final concentration of 0.02 mg mL^{-1}. A degassed Tris-HCl buffer 20mM with 200mM of KNO_3 was used to dilute the protein stock solution. A total of five conditions were tested:

Table 5.1: Identification of samples and tested conditions

Sample ID	Conditions
1. AuNC	Control negative (CN; original surface)
2. AuTris	Only Tris-HCl buffer (overnight incubation at room temperature)
3. AuC3	Addition of cyt c_3 solely to the metal surface (overnight incubation at room temperature)
4. AuHase	Addition of only Hase to the metal surface (overnight incubation at room temperature)
5. AuC3Hase	Addition of cyt c_3 and incubation for 1h and then rinsing 5 times with deionized water followed by the addition of Hase (overnight incubation at room temperature)

After the incubation time, all samples were rinsed 3 times with deionized water to remove non-adsorbed proteins and dried with nitrogen, followed by characterization of gold coupon surfaces by XPS and ToF-SIMS as described in section 2 of chapter 3 and section 2 of chapter 4.

5.2.2. Quartz Microbalance with Dissipation (QCM-D)

QCM relies on a voltage being applied to a quartz crystal causing it to oscillate at a specific frequency. Changes in mass on the quartz surface are related to changes in frequency of the oscillating crystal through the Sauerbrey relationship reviewed elsewhere [218]. In summary, the shift of frequency (Δf) if proportional to the mass loaded on the surface of the crystal and the dissipation change (ΔD) is related to the viscoelastic properties of the molecule layer adsorbed in the surface.

The At-cut quartz crystals coated with gold, with a fundamental resonant frequency of 5MHz and a diameter of 14 mm where purchased from LOT ORIEL Europe. All measurements were done using a Q-sense E4 instrument (Q-sense, Gothenburg, Sweden) at 20ºC and flow rate of 50µL/min controlled by a peristaltic pump. Oscillations of the crystal at the resonant frequency (5 MHz) or at one of its overtones (15, 25, 35, 45, 55, 65 MHz) were obtained when applying AC voltage. A degassed Tris-HCl buffer 20mM with 200mM of

KNO_3, was used as the running solution in all experiments. Prior to the protein adsorption, the buffer was injected to establish the baseline.

5.3. Results and discussion

5.3.1. Adsorption of ET proteins on gold by QCM-D

Two types of proteins with different molecular weights (cyt c_3 and Hase) were used to study the adsorption on gold surface. The ΔD of cyt c_3 was lower than 1 x 10^{-6} (data not shown), then Δf was proportional to the amount of protein adsorbed on the surface, given by Sauerbrey equation [219]. Hase had a ΔD of 2.3 x 10^{-6} and the two combined of 1.66 x 10^{-6}, so the Sauerbrey equation cannot be applied.

In all cases an injection of buffer for 40 minutes took place to get a flat baseline. Then the adsorption of protein started. The proteins were monitored until they reached saturation and then were rinsed with buffer until the signal was stabilized.

These two proteins were chosen, because they are biological partners as cyt c_3 serves as an electron shutter for Hase in SRBs metabolism. Hase on the other hand has been implicated as an important player in corrosion process involving SRBs. We plan to perform some electrochemical tests with these proteins in gold and carbon steel, so was important to verify its adsorption prior.

Cyt c_3 is a very small and rigid protein and has a good adsorption on gold (Figure 5). Hase is 3 times bigger and much more flexible with 3,5x higher values of frequency shift. When we adsorb cyt c_3 first the Hase is able to displace the previous protein in some sites and adsorb directly in the metal, although it also adsorb in top of cyt c_3, creating a mix of hetero monolayer and hetero double layer as indicate by the lower frequency shift when compared to pure Hase and the results given from XPS shown below.

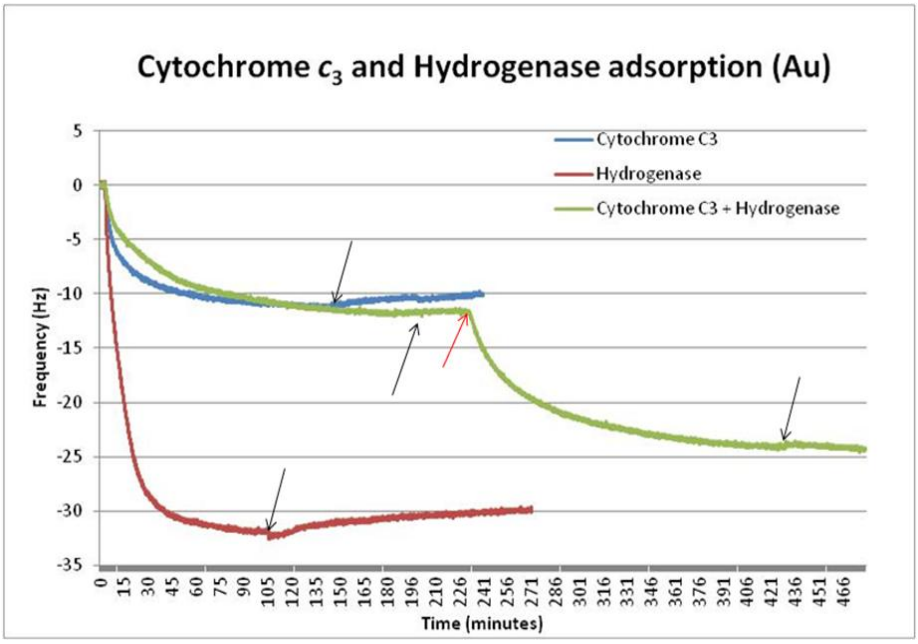

Figure 5.1: Δf *versus* time for different proteins adsorption on gold. Blue line Cytochrome C_3 (C3); Red line Hydrogenase (Hase); Green line C3 + Hase. Protein adsorption started at t=0, black arrows indicates buffer rinse after protein adsorption. Red arrow indicate when started Hase adsorption after rinsing C3.

5.3.2. Protein adsorption analysis by XPS

The carbon, nitrogen and oxygen decomposition was similar to all samples. All the peaks have been decomposed keeping a constant full width at half maximum (FWHM) constant to all components as described in chapter 4. The carbon peak was decomposed into four components for the controls and three components for the samples with protein; nitrogen was decomposed in three and oxygen was decomposed in only two. Following the work of Rouxhet and Genet [172], the carbon components were assigned as follow: at 284.8 eV hydrocarbons; carbon bound to oxygen or nitrogen, representative of amine, amide or alcohol at 286.2 eV; carbon doubly bound to oxygen or two single bonds to oxygen in aldehyde, carboxylate or amide functional groups at 287.9 eV; and carbon linked to carboxylic acid group at 289.2 eV. The nitrogen element spectrum was decomposed in three peaks related to nitrogen linke to carbon and hydrogen in amine at 397.9 eV; nonprotonated nitrogen (amide, peptidic link) at 399.9 eV and protonated amine at 401.7 eV. The O 1s spectrum was fit by two peaks: the first one is related to oxygen making a double bond to carbon or phosphorous in carboxylate, amide and phosphodiester at 531.6 eV; the second one is oxygen making one bond to carbon in (hemi)acetal, Ester, Carboxylic acid at 533.0 eV. The complete summary of the chemical and biological functions are described in Table 5.2.

Table 5.2: Identification of the chemical function of biochemical compounds according to the binding energy position.

E_b (eV)	Function	Biochemical compound of reference
Carbon		
284.8	**C**-(C,H)	Hydrocarbon
286.2 ±	**C**-(O,N)	Amine; Amide, peptidic link; Alcohol
287.9 ±	**C**=O, O-**C**-O; (**C**=O)-NH-C, O=**C**-O^-	Aldehyde, (hemi)acetal; Amide, peptidic link[1]; Carboxylate
289.2 ±	(**C**=O)-OH	Carboxylic acid
Nitrogen		
397.9 ±	C-**N**H2	Amine
399.9 ±	(C=O)-**N**H-C	Amide, peptidic link[1]
401.7 ±	C-**N**$H3^+$	Protonated amine

Table 5.2 (Cont.): Identification of the chemical function of biochemical compounds according to the binding energy position.

E_b (eV)	Function	Biochemical compound of reference
Oxygen		
531.6 ±	**O**=C-**O**$^-$;(C=**O**)-NH-C; P=**O**, P-**O**$^-$	Carboxylate; Amide, peptidic link[1]; Phosphodiester
533.0 ±	-**O**-C-**O**-, (C=O)-**O**-C, (C=O)-**O**H	(hemi)acetal, Ester, Carboxylic acid

[1] related data, as relationship is expected between the outline components.

Table 5.3 presents the major results from XPS measurements of all the adsorbed samples. It clearly shows a trend of decreasing of gold molar ratio from the controls to the hydrogenase or cytochrome c3 + hydrogenase. Also the presence of carboxylic acid was only detected in the abiotic controls samples. As expected, nitrogen was not detected in the controls, which indicated that there was almost no contamination by biomolecules in the gold surface.

In table 5.4 the atomic ratio of elements versus total carbon or gold is presented. From these results we can see that the ratio of oxidized carbon at the surface increases 4 to 5 times. Also, the nitrogen ratio both to carbon or gold increases around 200 times when compared to controls. The data also indicate that a higher surface coverage was achieved with the presence of hydrogenase when compared to only cytochrome c3.

According to the work of Ray and Shard [205], it is possible to calculate the thickness of the protein film using the atomic fraction of nitrogen in the substrate. In Fig. 5.3 the relation of atomic ratio of nitrogen and protein film thickness is presented. These results suggest along the QCM data, that the protein film when both proteins are adsorbed is a monolayer, as the higher nitrogen concentration is observed when only hydrogenase is adsorbed.

Table 5.3: Elemental composition and functional groups determined by XPS on adsorbed protein samples according to table 5.1 ID: molar ratios (%) and of species defined by the indicated binding energy (E_b, eV) of peak components.

	Au 4f	**C 1s**				**N 1s**			**O 1s**	
E_b (eV)		284.8	286.2	287.9	289.2	397.9	399.9	401.7	531.6	533.0
AuNC	68.954	18.936	3.387	1.205	0.84	BDL	BDL	BDL	4.644	2.033
AuTris	65.230	19.572	4.464	2.301	1.209	BDL	1.603	BDL	2.432	3.188
AuC3	44.564	20.990	10.145	7.673	BDL	0.49	6.386	0.292	7.207	2.252
AuHase	37.980	21.012	12.118	9.512	BDL	0.126	8.87	0.239	8.405	1.737
AuC3Hase	37.478	22.488	11.842	9.071	BDL	0.372	8.324	0.27	8.379	1.777

NM: Not measured; BDL: Below Detection Limit.
[a]: Au 4f in range of 82 to 92 eV.

Table 5.4: Atomic ratios of elements (Carbon, Nitrogen and Oxygen) and functional groups *vs* total Carbon or total Gold molar ratio.

	Au/C	**C 1s(/C)**				**C_{tot}/Au**	**C_{ox}/Au**	**N 1s(/C)**			**N_{tot}/C**	**N_{tot}/Au**	**O 1s(/C)**		**O_{tot}/C**	**O_{tot}/Au**
E_b (eV)		284.8	286.2	287.9	289.2			397.95	399.9	401.7			531.6	533.0		
AuNC	2.830	0.777	0.139	0.049	0.034	0.353	0.079	0.000	0.000	0.000	0.000	0.000	0.191	0.083	0.274	0.097
AuTris	2.368	0.711	0.162	0.084	0.044	0.422	0.122	0.000	0.058	0.000	0.058	0.025	0.088	0.116	0.204	0.086
AuC3	1.148	0.541	0.261	0.198	0.000	0.871	0.400	0.013	0.165	0.008	0.185	0.161	0.186	0.058	0.244	0.212
AuHase	0.891	0.493	0.284	0.223	0.000	1.123	0.570	0.003	0.208	0.006	0.217	0.243	0.197	0.041	0.238	0.267
AuC3Hase	0.864	0.518	0.273	0.209	0.000	1.158	0.558	0.009	0.192	0.006	0.207	0.239	0.193	0.041	0.234	0.271

E_b: Energy binding in electron Volt.
[a]: Au 4f in range of 82 to 92 eV.
C_{ox}: is comprised by all the carbon discounted the carbon bound to carbon or hydrogen (284.8 eV).

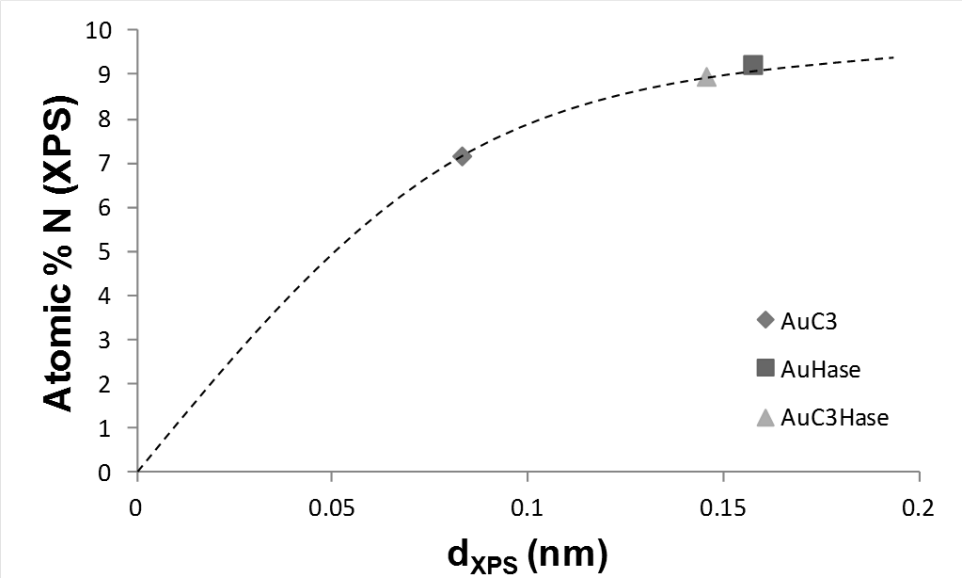

Fig. 5.2: Concentration of nitrogen compared to XPS thickness of protein showing nonlinear behaviour.

5.3.3. Chemical characterization of protein films by ToF-SIMS

The data was normalized by the sum of all the selected peaks and mean-centred as done with all data previously. A peak list was created with 42 peaks (for positive ions) which were used to treat ToF-SIMS data acquired on all samples.

Figure 5.3 presents the results of the PCA treatment applied to the positive with all samples (Fig. 5.3a) and the positive with only protein samples (Fig. 5.3b) spectra. The first PC (PC1) collects 61.2% and the second PC (PC2) answers for about 14.8% of the variance in the case of the positive ions. In Fig. 5.2a, PC1 was able to discriminate between the controls without proteins and the samples with adsorbed protein at the surface. Among the protein samples, they were separate by PC2, grouping the samples with Cyt c3 with more positive values against the sample with only hydrogenase that had negative loadings values in PC2.

When compared the samples without the presence of the controls, the PC1 collects 47% and the second PC (PC2) answers for about 28.3% of the variance in the case of the positive ions. Again, the sample with only hydrogenase adsorbed in the surface is place separated from the ones with the presence o cytochrome c3 which can suggest that the adsorbed layer with both proteins is mostly composed with cytochrome c3. The ToF-SIMS results corroborate the QCM and XPS data that the addition of hydrogenase increases the surface coverage and that a mix layer is attained in that case.

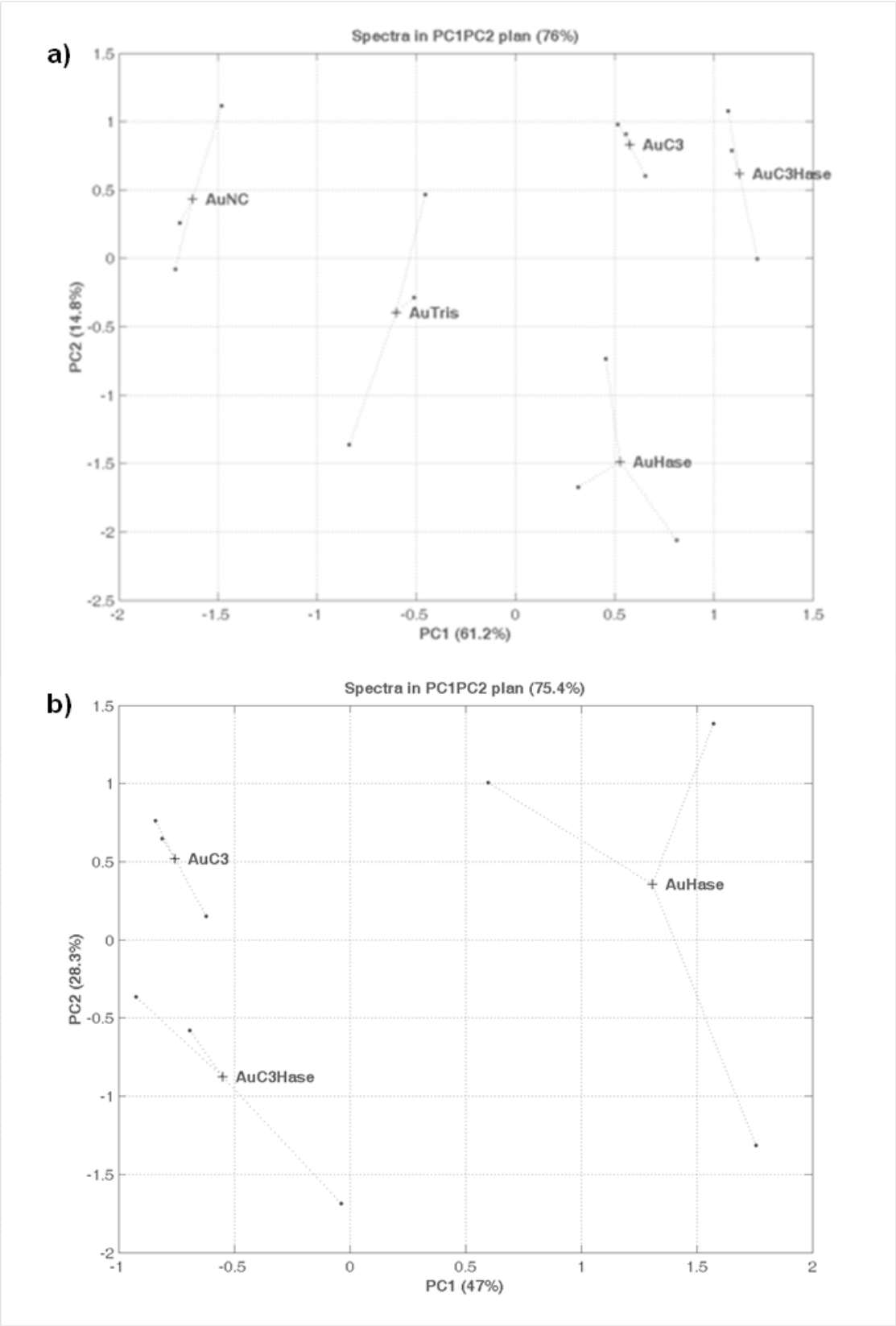

Figure 5.3: PCA results performed on ToF-SIMS positive spectra, significant PC's. a) PC1 *versus* PC2 positive ions spectra plotting with all samples; b) PC1 *versus* PC2 positive ions spectra plotting with only protein samples. AuNC: negative control; AuTris: negative control with tris-buffer; AuC3: Cytochrome c3 adsorbed; AuHase: Hydrogenase adsorbed; AuC3Hase: First Cyt. c3, then Hase adsorbed.

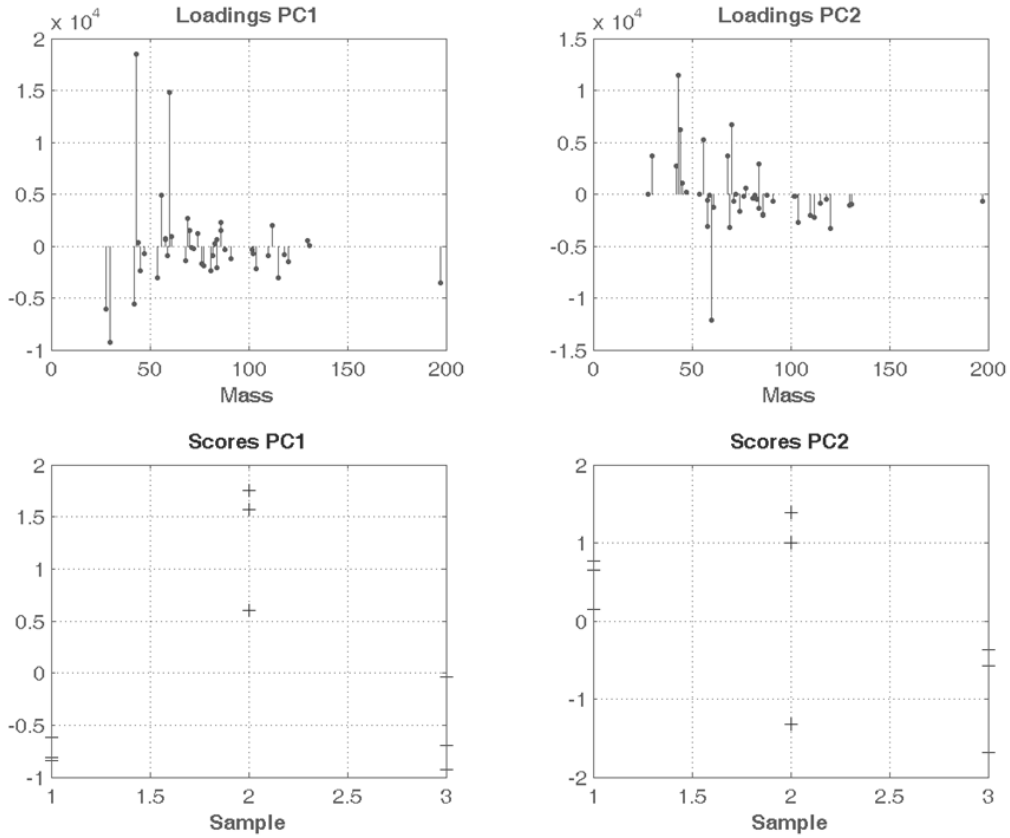

Figure 5.4: Loadings and scores plotting from ToF-SIMS positive ions data with proteins. In loadings plotting the 10 highest loadings values are listed in tables 5.4 to 5.5. Sample 1: AuC3; Sample 2: AuHase; Sample 3: AuC3Hase.

The data from Fig. 5.4, tables 5.5 and 5.6 indicates that for cytochrome c3 more nonpolar, neutral charge residues are exposed in the outer surface. For hydrogenase, a higher amount of polar residues (with mixed neutral or charged side chain) are detected at the extreme surface. ToF-SIMS analysis is performed in ultra high vacuum and in this condition a preferential exposure of nonpolar functions is expected according the literature [131]. The results obtained could be explained by the difference of surface coverage of both proteins. As cytochrome c3 is a small and hard protein, it possesses a lower ability to suffer rearrangements and seems to expose nonpolar side chains at the extreme surface. Hydrogenase, on the contrary, is a bigger and softer protein and thus can go through rearrangements to increase it interactions between proteins and the substrate leading to a more pronounced exposure of polar side chains at the outer surface [63].

Table 5.5: Top 10 positive and negative loading values for PC1 of positive ions.

N	Load	Mass	Ion	Biological molecule
# 4	18520.26329	43.02	C_2H_3O+	Glu
#13	14781.69201	60.05	C_2H_6NO+	Ala, Asn, Leu
# 9	4929.37385	56.05	C_3H_6N+	Lys, Met, Val
#16	2631.69223	69.04	C_4H_5O+	Thr
#29	2281.97709	86.11	$C_5H_{12}N+$	lle, Leu
#36	1959.71413	112.09	$C_6H_{10}NO+$	Arg
#28	1475.14943	86.03	$C_3H_4NO_2+$	Asp
#17	1457.50634	70.07	C_4H_8N+	Pro, Val
#20	1230.75411	74.07	C_3H_8NO+	Thr
#14	950.17586	61.02	C_2H_5S+	Met
#27	-2087.87727	84.09	$C_5H_{10}N+$	Lys, Leu
#34	-2184.6559	104.06	$C_4H_{10}SN+$	Met
#23	-2333.28576	81.05	$C_4H_5N_2+$	
# 6	-2403.68448	44.98	CHS+	Cys
# 8	-3056.2212	54.04	C_3H_4N+	His
#37	-3075.20153	115.06	$C_4H_7N_2O_2+$	Gly
#42	-3520.06488	196.99	Au+	
# 3	-5581.77902	42.04	C_2H_4N+	Ala, Gly, His, Leu, ser
# 1	-6063.2568	28.02	CH_2N+	Ala, Arg, Asn, Glu, Leu, Ser, Trp
# 2	-9316.00115	30.04	CH_4N+	Many amino acids

Table 5.6: Top 10 positive and negative loading values for PC2 of positive ions.

N	Load	Mass	Ion	Biological molecule
# 4	11487.58639	43.02	C_2H_3O+	Glu
#17	6678.47523	70.07	C_4H_8N+	Pro, Val
# 5	6251.49102	44.05	C_2H_6N+	Ala, Asn, Leu
# 9	5274.7772	56.05	C_3H_6N+	Lys, Met, Val
#15	3721.0068	68.06	C_4H_6N+	Pro, Lys
# 2	3644.14738	30.04	CH_4N+	Many amino acids
#27	2892.42031	84.09	$C_5H_{10}N+$	Lys, Leu
# 3	2711.82962	42.04	C_2H_4N+	Ala, Gly, His, Leu, ser
# 6	1104.40594	44.98	CHS+	Cys
#22	554.16437	77.04	C_6H_5+	Phe, Tyr
#20	-1679.45018	74.07	C_3H_8NO+	Thr
#29	-1969.7566	86.11	$C_5H_{12}N+$	lle, Leu
#35	-2032.79408	110.08	$C_5H_8N_3+$	His, Arg
#28	-2045.43278	86.03	$C_3H_4NO_2+$	Asp
#36	-2230.30772	112.09	$C_6H_{10}NO+$	Arg
#34	-2750.7345	104.06	$C_4H_{10}SN+$	Met
#10	-3125.64249	58.03	C_2H_4NO+	Ser
#16	-3204.52799	69.04	C_4H_5O+	Thr
#39	-3283.34401	120.09	$C_8H_{10}N+$	Phe
#13	-12139.06937	60.05	C_2H_6NO+	Ser

5.4. Conclusions

We have used QCM, XPS and ToF-SIMS to qualitatively and quantitatively characterize protein films adsorbed in gold surface. These results have given new insights into the electron transfer protein behaviour in this model substrate. The correlation of the data is not perfect as one technique is not performed under high vacuum and the proteins remains hydrated. Even though, the results can be discussed as trends shows consistency between all methods. The method presented in the literature to estimate protein thickness has demonstrated to be very useful and widely applicable.

Chapter 6

Conclusions and future perspectives

Chapter 6 – Conclusions and future perspectives

6.1. Conclusions

The interaction of the microorganisms with the environment and the metal surfaces leading to MIC is far too complex to be tackled by just one scientific field. The influence of the respiratory substrate reflects perfectly the importance which small variations in the environmental conditions can have on the corrosion evolution. The present study demonstrated that the integration of electrochemical, surface analysis and biochemical techniques allowed obtaining complementary information and therefore to improve our knowledge of the mechanisms involved in the complex biocorrosion processes.

The kinetics studies of the *D. desulfuricans* ATCC 27774 planktonic and sessile cells with carbon steel coupons enable a better understanding of the metabolism shift due to the introduction of nitrate in SRB communities. This strain has shown that it can grow faster in nitrate presence depleting the respiratory substrate much quicker when compared to sulphate. This can have important consequences to the nitrate strategy used so far by the Oil and Gas industries. The OCP showed an increase of around 200mV in sulphate (LFR) and 90mV in nitrate and a decrease about -80mV in sulphate (HFR). These results indicate that the equilibrium of sulphide in the solution/gas phases is a key factor to determine the evolution of the corrosion process. Our electrochemistry results allied with the weight loss test have shown that short time experiments can overestimate the corrosion rate, although the tendency observed are worth to many industrial applications and corrosion monitoring. Nitrate prevents pitting corrosion but, on the other hand, promotes uniform corrosion and also increases the corrosion potential and iron dissolution 40 times when compared to sulphate. The electrochemistry results have shown that the Extracellular Polymeric Substances (EPS) produced in the two conditions maintain the characteristic observed during bacterial growth regarding the corrosion behaviour. The cyclic voltammetry (CV) done with the EPS samples indicate the ability of EPS produced in sulphate to promote pitting as observed in the biofilm samples. Nitrate EPS, on the other hand, seems to be less aggressive by CV but this was not confirmed by the weight loss tests.

Time of Flight-Secondary Ions Mass Spectrometry, Scanning Electron Microscopy-Electron Dispersive X-ray Spectroscopy and X-ray Photoelectron Spectroscopy were used to characterize the surface alteration of metal plates surface incubated with *Desulfovibrio desulfuricans* ATCC 27774 in different growth media. Our results demonstrated that the respiratory substrate has important consequences to the EPS composition, surface interaction and ultimately with the biofilm configuration and corrosion process. The use of Principal Component Analysis with this kind of data has allowed us to differentiate between the groups of samples and also to identify the most important ion peaks for the variance

observed. PCA proved to be a useful tool for analyzing the results of high-throughput surface analysis techniques; however caution is necessary for the selection of the correct data pre-treatment. The sulphate reduction is one of the main factors responsible for the precipitation of inorganic salts, like calcium and phosphates, and may be related to the corrosion behaviour exhibited by the EPS and ultimately by the biofilm. Our study also demonstrated that nitrate rich medium can increase the precipitation of chloride ions at the surface and increase the general corrosion rate.

Surface science techniques like ToF-SIMS and XPS have been used for a long time by the microchip and electronic industry; in recent years its development allowed it to be used in more complex samples systems. These high-throughput techniques, supported by biochemical methods, were proven to delivery accurate data on the chemical composition of complex samples as EPS. Our study was one of the few to use XPS to chemically characterize EPS using small volumes/quantity and avoiding extraction procedures that can introduce bias to the results. Both ToF-SIMS, allied to PCA, and XPS have confirmed the importance of the inorganic ions, like sulphite and calcium, in the EPS composition and so this could be related to the results obtained in the surface analysis chapter (3). The ions studied by the PCA analysis could be used as markers to identify corrosion cases related to microorganisms. The data suggests that carboxylates and phosphates functions are present in large quantities in EPS and could be related to calcium precipitation observed by the ToF-SIMS surface analysis. The relation of calcium precipitation sites and iron dissolution was also suggested by the results obtained. The only limitation of the XPS analysis is the inability to differentiate proteins from peptides in complex samples. Nevertheless, this could be overcome by the SDS-PAGE results that provided the confirmation of the heterogeneity of the protein profile in EPS produced in different growth media. We were able to identify some Ca binding proteins and some enzymes that could be responsible to the corrosive features of the EPS. Finally, we confirmed that the iron present in the EPS is originating from the metal plates and not from the media and that the higher iron uptake observed in nitrate samples could be explained by the higher concentration of ammonia ions present in this medium.

This work gives news insights into the mechanisms involved in the biocorrosion process related to sulphate reducing bacteria and on the importance of the respiratory substrate in the corrosive aggressiveness of the microorganisms.

6.2. Future work/Perspectives

Regarding the results presented in this work some further research topics could be looked at to improve our knowledge of the biocorrosion mechanisms:

- Longer period of OCP monitoring (at least 180 days) should be performed in order to reproduce the field conditions. This would prevent the overestimation observed in electrochemical results providing more reliable results similar to the field observed data.
- Use of mixed microbial communities instead of pure cultures can also have important consequences to the biofilm development, composition and therefore its behavior.
- Comparison of XPS data analysis of EPS from different species to validate the results attained with our sample.
- Validation of the ToF-SIMS markers identified in our study in corroded metal surfaces from the field.
- A 2D-Gel electrophoresis and proteomic analysis of the protein profile expressed in the presence and absence of metal plates could give important hints in the bacterial adhesion to the surface and biofilm formation and ultimately corrosion process.
- Finally the identification of chelating or electron transfer proteins as well as proteins important for biofilm development that could be used as targets to prevent biocorrosion occurrence.

References

References

[1] E. Mattsson, Basic corrosion technology for scientists and engineers, Ellis Horwood Publishers, West Sussex, England, 1989.
[2] J.R. Davis, Corrosion: Understanding the Basics, A S M International, 2000.
[3] H.A. Videla, Manual of Biocorrosion, Lewis Publishers, 1996.
[4] X. Shi, R. Avci, M. Geiser, Z. Lewandowski, Comparative study in chemistry of microbially and electrochemically induced pitting of 316L stainless steel, Corrosion Science, 45 (2003) 2577-2595.
[5] B.J. Little, J.S. Lee, Microbiologically influenced corrosion, Wiley-Interscience, Hoboken, N.J., 2007.
[6] J.H. Garrett, The Action of Water on Lead, London, 1891.
[7] I.B. Beech, C.W.S. Cheung, Interactions of exopolymers produced by sulphate-reducing bacteria with metal ions, International Biodeterioration & Biodegradation, 35 (1995) 59-72.
[8] H.A. Videla, L.K. Herrera, Microbiologically influenced corrosion: looking to the future, International microbiology : the official journal of the Spanish Society for Microbiology, 8 (2005) 169-180.
[9] D. Enning, H. Venzlaff, J. Garrelfs, H.T. Dinh, V. Meyer, K. Mayrhofer, A.W. Hassel, M. Stratmann, F. Widdel, Marine sulfate-reducing bacteria cause serious corrosion of iron under electroconductive biogenic mineral crust, Environmental microbiology, 14 (2012) 1772-1787.
[10] M.J. Feio, V. Zinkevich, I. Beech, E. Llobet-Brossa, P. Eaton, J. Schmitt, J. Guezennec, Desulfovibrio alaskensis sp. nov., a sulphate-reducing bacterium from a soured oil reservoir, Int J Syst Evol Microbiol., 54 (2004) 5.
[11] W. Lee, W.G. Characklis, Corrosion of Mild-Steel under Anaerobic Biofilm, Corrosion, 49 (1993) 186-199.
[12] H.Y. Ma, X.L. Cheng, G.Q. Li, S.H. Chen, Z.L. Quan, S.Y. Zhao, L. Niu, The influence of hydrogen sulfide on corrosion of iron under different conditions, Corrosion Science, 42 (2000) 1669-1683.
[13] G. Bodtker, T. Thorstenson, B.L. Lillebo, B.E. Thorbjornsen, R.H. Ulvoen, E. Sunde, T. Torsvik, The effect of long-term nitrate treatment on SRB activity, corrosion rate and bacterial community composition in offshore water injection systems, Journal of industrial microbiology & biotechnology, 35 (2008) 1625-1636.
[14] H. Dahle, F. Garshol, M. Madsen, N.K. Birkeland, Microbial community structure analysis of produced water from a high-temperature North Sea oil-field, Antonie van Leeuwenhoek, 93 (2008) 37-49.
[15] I.A. Davidova, K.E. Duncan, B.M. Perez-Ibarra, J.M. Suflita, Involvement of thermophilic archaea in the biocorrosion of oil pipelines, Environmental microbiology, 14 (2012) 1762-1771.
[16] K.E. Duncan, L.M. Gieg, V.A. Parisi, R.S. Tanner, S.G. Tringe, J. Bristow, J.M. Suflita, Biocorrosive thermophilic microbial communities in Alaskan North Slope oil facilities, Environmental science & technology, 43 (2009) 7977-7984.
[17] D. Li, D.J. Midgley, J.P. Ross, Y. Oytam, G.C. Abell, H. Volk, W.A. Daud, P. Hendry, Microbial biodiversity in a Malaysian oil field and a systematic comparison with oil reservoirs worldwide, Archives of microbiology, 194 (2012) 513-523.
[18] B. Little, R. Ray, A review of fungal influenced corrosion, Corros Rev, 19 (2001) 401-417.
[19] C.M. Xu, Y.H. Zhang, G.X. Cheng, W.S. Zhu, Localized corrosion behavior of 316L stainless steel in the presence of sulfate-reducing and iron-oxidizing bacteria, Mat Sci Eng a-Struct, 443 (2007) 235-241.
[20] W.A. Hamilton, Sulphate-reducing bacteria and anaerobic corrosion, Annu Rev Microbiol, 39 (1985) 195-217.
[21] F.A. Lopes, P. Morin, R. Oliveira, L.F. Melo, Interaction of Desulfovibrio desulfuricans biofilms with stainless steel surface and its impact on bacterial metabolism, Journal of applied microbiology, 101 (2006) 1087-1095.
[22] W. Buckel, R.K. Thauer, Energy conservation via electron bifurcating ferredoxin reduction and proton/Na(+) translocating ferredoxin oxidation, Biochimica et biophysica acta, 1827 (2013) 94-113.
[23] C. Correia, E. Monzani, I. Moura, J. Lampreia, J.J.G. Moura, Cross-linking between cytochrome c(3) and flavodoxin from Desulfovibrio gigas, Biochem Bioph Res Co, 256 (1999) 367-371.
[24] S. Da Silva, R. Basseguy, A. Bergel, The role of hydrogenases in the anaerobic microbiologically influenced corrosion of steels, Bioelectrochemistry, 56 (2002) 77-79.
[25] V.B. Paixao, H. Vis, D.L. Turner, Redox linked conformational changes in cytochrome c3 from Desulfovibrio desulfuricans ATCC 27774, Biochemistry, 49 (2010) 9620-9629.
[26] H.C. Flemming, T.R. Neu, D.J. Wozniak, The EPS matrix: the "house of biofilm cells", J Bacteriol, 189 (2007) 7945-7947.
[27] B.J. Little, J.S. Lee, R.I. Ray, The influence of marine biofilms on corrosion: A concise review, Electrochimica Acta, 54 (2008) 2-7.
[28] C.A.H. von Wolzogen Kuhr, L.S. van der Flugt, De grafiteering van gietijzer als electrobiochemisch proces in anaerobe gronden, Water (den Haad), 18 (1934) 147-165.
[29] C.M. Cordas, I. Moura, J.J. Moura, Direct electrochemical study of the multiple redox centers of hydrogenase from Desulfovibrio gigas, Bioelectrochemistry, 74 (2008) 83-89.

[30] S. Da Silva, R. Basseguy, A. Bergel, Electron transfer between hydrogenase and 316L stainless steel: identification of a hydrogenase-catalyzed cathodic reaction in anaerobic MIC, Journal of Electroanalytical Chemistry, 561 (2004) 9.
[31] M.J. Marshall, A.E. Plymale, D.W. Kennedy, L. Shi, Z. Wang, S.B. Reed, A.C. Dohnalkova, C.J. Simonson, C. Liu, D.A. Saffarini, M.F. Romine, J.M. Zachara, A.S. Beliaev, J.K. Fredrickson, Hydrogenase- and outer membrane c-type cytochrome-facilitated reduction of technetium(VII) by Shewanella oneidensis MR-1, Environmental microbiology, 10 (2008) 125-136.
[32] W.A. Hamilton, Microbially influenced corrosion as a model system for the study of metal microbe interactions: a unifying electron transfer hypothesis, Biofouling, 19 (2003) 65-76.
[33] T. Gu, New Understandings of Biocorrosion Mechanisms and their Classifications, Journal of Microbial & Biochemical Technology, 4 (2012) 3-6.
[34] L.L. Barton, G.D. Fauque, Biochemistry, physiology and biotechnology of sulfate-reducing bacteria, Advances in applied microbiology, 68 (2009) 41-98.
[35] A. Marietou, L. Griffiths, J. Cole, Preferential reduction of the thermodynamically less favorable electron acceptor, sulfate, by a nitrate-reducing strain of the sulfate-reducing bacterium Desulfovibrio desulfuricans 27774, J Bacteriol, 191 (2009) 882-889.
[36] I. Moura, S. Bursakov, C. Costa, J.J. Moura, Nitrate and nitrite utilization in sulfate-reducing bacteria, Anaerobe, 3 (1997) 279-290.
[37] J.J.G. Moura, P. Gonzalez, I. Moura, G. Fauque, Dissimilatory nitrate and nitrite ammonification by sulphate-reducing eubacteria, in: L.L. Barton, W.A. Hamilton (Eds.) Sulphate-Reducing Bacteria: Environmental and Engineered Systems, Cambridge University Press, 2007.
[38] G. Muyzer, A.J. Stams, The ecology and biotechnology of sulphate-reducing bacteria, Nat Rev Microbiol, 6 (2008) 441-454.
[39] H.D. Peck, Jr., J. LeGall, Inorganic Microbial Sulfur Metabolism, Academic Press, 1994.
[40] K. Tang, V. Baskaran, M. Nemati, Bacteria of the sulphur cycle: An overview of microbiology, biokinetics and their role in petroleum and mining industries, Biochemical Engineering Journal, 44 (2009) 73-94.
[41] J. Zhou, Q. He, C.L. Hemme, A. Mukhopadhyay, K. Hillesland, A. Zhou, Z. He, J.D. Van Nostrand, T.C. Hazen, D.A. Stahl, J.D. Wall, A.P. Arkin, How sulphate-reducing microorganisms cope with stress: lessons from systems biology, Nature reviews. Microbiology, 9 (2011) 452-466.
[42] L. Barton, Sulfate-Reducing Bacteria, Springer, 1995.
[43] J.J.R.F. da Silva, R.J.P. Williams, The Biological Chemistry of the Elements: The Inorganic Chemistry of Life, OUP Oxford, 2001.
[44] R. Javaherdashti, Impact of sulphate-reducing bacteria on the performance of engineering materials, Appl Microbiol Biotechnol, 91 (2011) 1507-1517.
[45] J. LeGall, G. Fauque, Dissimilatory reduction of sulfur compounds, in: A.J.B. Zehnder (Ed.) Biology of anaerobic microorganisms, Wiley, 1988.
[46] F. Widdel, Microbiology and ecology of sulfate- and sulfur-reducing bacteria, in: A.J.B. Zehnder (Ed.) Biology of anaerobic microorganisms, Wiley, 1988.
[47] A.S. Bradley, W.D. Leavitt, D.T. Johnston, Revisiting the dissimilatory sulfate reduction pathway, Geobiology, 9 (2011) 446-457.
[48] G.M. Gadd, Metals, minerals and microbes: geomicrobiology and bioremediation, Microbiology, 156 (2010) 609-643.
[49] T. Dalsgaard, F. Bak, Nitrate Reduction in a Sulfate-Reducing Bacterium, Desulfovibrio desulfuricans, Isolated from Rice Paddy Soil: Sulfide Inhibition, Kinetics, and Regulation, Appl Environ Microbiol, 60 (1994) 291-297.
[50] I.T.E. Fonseca, M.J. Feio, A.R. Lino, M.A. Reis, V.L. Rainha, The influence of the media on the corrosion of mild steel by Desulfovibrio desulfuricans bacteria: an electrochemical study, Electrochimica Acta, 43 (1998) 213-222.
[51] K.L. Keller, J.D. Wall, Genetics and molecular biology of the electron flow for sulfate respiration in desulfovibrio, Frontiers in microbiology, 2 (2011) 135.
[52] L.l. Barton, J. LeGall, J.M. Odom, H.D. Peck, Jr., Energy coupling to nitrite respiration in the sulfate-reducing bacterium Desulfovibrio gigas, (1983).
[53] M. Carepo, J.F. Baptista, A. Pamplona, G. Fauque, J.J. Moura, M.A. Reis, Hydrogen metabolism in Desulfovibrio desulfuricans strain New Jersey (NCIMB 8313)--comparative study with D. vulgaris and D. gigas species, Anaerobe, 8 (2002) 325-332.
[54] I. Moura, P. Tavares, J.J. Moura, N. Ravi, B.H. Huynh, M.Y. Liu, J. LeGall, Direct spectroscopic evidence for the presence of a 6Fe cluster in an iron-sulfur protein isolated from Desulfovibrio desulfuricans (ATCC 27774), The Journal of biological chemistry, 267 (1992) 4489-4496.
[55] D.R. Bond, D.R. Lovley, Evidence for involvement of an electron shuttle in electricity generation by Geothrix fermentans, Appl Environ Microbiol, 71 (2005) 2186-2189.

[56] E.D. Brutinel, J.A. Gralnick, Shuttling happens: soluble flavin mediators of extracellular electron transfer in Shewanella, Appl Microbiol Biotechnol, 93 (2012) 41-48.
[57] J. Liu, Z. Wang, S.M. Belchik, M.J. Edwards, C. Liu, D.W. Kennedy, E.D. Merkley, M.S. Lipton, J.N. Butt, D.J. Richardson, J.M. Zachara, J.K. Fredrickson, K.M. Rosso, L. Shi, Identification and Characterization of MtoA: A Decaheme c-Type Cytochrome of the Neutrophilic Fe(II)-Oxidizing Bacterium Sideroxydans lithotrophicus ES-1, Frontiers in microbiology, 3 (2012) 37.
[58] Y. Liu, D.R. Bond, Long-distance electron transfer by G. sulfurreducens biofilms results in accumulation of reduced c-type cytochromes, ChemSusChem, 5 (2012) 1047-1053.
[59] R. Cammack, M. Frey, R. Robson, Hydrogen as a Fuel: Learning from Nature, Taylor & Francis, 2002.
[60] K. Rabaey, N. Boon, M. Hofte, W. Verstraete, Microbial phenazine production enhances electron transfer in biofuel cells, Environmental science & technology, 39 (2005) 3401-3408.
[61] R.M. Almeida, C.F.G.C. Geraldes, S.R. Pauleta, J.J.G. Moura, Gd(III) Chelates as NMR Probes of Protein-Protein Interactions. Case Study: Rubredoxin and Cytochrome c(3), Inorg Chem, 50 (2011) 10600-10607.
[62] L. Krippahl, J.J. Moura, P.N. Palma, Modeling protein complexes with BiGGER, Proteins, 52 (2003) 19-23.
[63] X. Morelli, M. Czjzek, C.E. Hatchikian, O. Bornet, J.C. Fontecilla-Camps, N.P. Palma, J.J.G. Moura, F. Guerlesquin, Structural model of the Fe-hydrogenase/cytochrome c(553) complex combining transverse relaxation-optimized spectroscopy experiments and soft docking calculations, J Biol Chem, 275 (2000) 23204-23210.
[64] X. Morelli, A. Dolla, M. Czjzek, P.N. Palma, F. Blasco, L. Krippahl, J.J.G. Moura, F. Guerlesquin, Heteronuclear NMR and soft docking: An experimental approach for a structural model of the cytochrome c(553)-ferredoxin complex, Biochemistry, 39 (2000) 2530-2537.
[65] P.N. Palma, I. Moura, J. Legall, J. Vanbeeumen, J.E. Wampler, J.J.G. Moura, Evidence for a Ternary Complex Formed between Flavodoxin and Cytochrome C(3) - H-1-Nmr and Molecular Modeling Studies, Biochemistry, 33 (1994) 6394-6407.
[66] L.T. Dall'Agnol, C.M. Cordas, J.J.G. Moura, Influence of respiratory substrate in carbon steel corrosion by a SRP model organism, Bioelectrochemistry, XX (2013).
[67] T.A. Hansen, Metabolism of sulfate-reducing prokaryotes, Antonie van Leeuwenhoek, 66 (1994) 165-185.
[68] J.M. Dias, S. Bursakov, C. Carneiro, J.J. Moura, I. Moura, M.J. Romao, Crystallization and preliminary x-ray analysis of a nitrate reductase from Desulfovibrio desulfuricans ATCC 27774, Acta crystallographica. Section D, Biological crystallography, 55 (1999) 877-879.
[69] J.M. Dias, M.E. Than, A. Humm, R. Huber, G.P. Bourenkov, H.D. Bartunik, S. Bursakov, J. Calvete, J. Caldeira, C. Carneiro, J.J. Moura, I. Moura, M.J. Romao, Crystal structure of the first dissimilatory nitrate reductase at 1.9 A solved by MAD methods, Structure, 7 (1999) 65-79.
[70] J.J. Moura, C.D. Brondino, J. Trincao, M.J. Romao, Mo and W bis-MGD enzymes: nitrate reductases and formate dehydrogenases, Journal of biological inorganic chemistry : JBIC : a publication of the Society of Biological Inorganic Chemistry, 9 (2004) 791-799.
[71] C.A. Cunha, S. Macieira, J.M. Dias, G. Almeida, L.L. Goncalves, C. Costa, J. Lampreia, R. Huber, J.J. Moura, I. Moura, M.J. Romao, Cytochrome c nitrite reductase from Desulfovibrio desulfuricans ATCC 27774. The relevance of the two calcium sites in the structure of the catalytic subunit (NrfA), The Journal of biological chemistry, 278 (2003) 17455-17465.
[72] O. Einsle, P. Stach, A. Messerschmidt, J. Simon, A. Kroger, R. Huber, P.M. Kroneck, Cytochrome c nitrite reductase from Wolinella succinogenes. Structure at 1.6 A resolution, inhibitor binding, and heme-packing motifs, The Journal of biological chemistry, 275 (2000) 39608-39616.
[73] I.A. Pereira, J. LeGall, A.V. Xavier, M. Teixeira, Characterization of a heme c nitrite reductase from a non-ammonifying microorganism, Desulfovibrio vulgaris Hildenborough, Biochimica et biophysica acta, 1481 (2000) 119-130.
[74] I.C. Pereira, I.A. Abreu, A.V. Xavier, J. LeGall, M. Teixeira, Nitrite reductase from Desulfovibrio desulfuricans (ATCC 27774)--a heterooligomer heme protein with sulfite reductase activity, Biochem Bioph Res Co, 224 (1996) 611-618.
[75] P. Tavares, A.S. Pereira, J.J. Moura, I. Moura, Metalloenzymes of the denitrification pathway, Journal of inorganic biochemistry, 100 (2006) 2087-2100.
[76] J. Qu, B. Fan, S. Liu, P. Lei, H. Liu, Autotrophic denitrification of groundwater by electrochemical process, Huan jing ke xue= Huanjing kexue / [bian ji, Zhongguo ke xue yuan huan jing ke xue wei yuan hui "Huan jing ke xue" bian ji wei yuan hui.], 22 (2001) 49-52.
[77] H. Toda, Y. Uemura, T. Okino, T. Kawanishi, H. Kawashima, Use of nitrogen stable isotope ratio of periphyton for monitoring nitrogen sources in a river system, Water science and technology : a journal of the International Association on Water Pollution Research, 46 (2002) 431-435.
[78] S.B. Joye, A. Boetius, B.N. Orcutt, J.P. Montoya, H.N. Schulz, M.J. Erickson, S.K. Lugo, The anaerobic oxidation of methane and sulfate reduction in sediments from Gulf of Mexico cold seeps, Chemical Geology, 205 (2004) 219-238.

[79] J. Kallmeyer, A. Boetius, Effects of temperature and pressure on sulfate reduction and anaerobic oxidation of methane in hydrothermal sediments of Guaymas Basin, Appl Environ Microbiol, 70 (2004) 1231-1233.
[80] C. Costa, J.J. Moura, I. Moura, Y. Wang, B.H. Huynh, Redox properties of cytochrome c nitrite reductase from Desulfovibrio desulfuricans ATCC 27774, The Journal of biological chemistry, 271 (1996) 23191-23196.
[81] O.Y. Gavel, A.V. Kladova, S.A. Bursakov, J.M. Dias, S. Texeira, V.L. Shnyrov, J.J. Moura, I. Moura, M.J. Romao, J. Trincao, Purification, crystallization and preliminary X-ray diffraction analysis of adenosine triphosphate sulfurylase (ATPS) from the sulfate-reducing bacterium Desulfovibrio desulfuricans ATCC 27774, Acta crystallographica. Section F, Structural biology and crystallization communications, 64 (2008) 593-595.
[82] A.V. Kladova, O.Y. Gavel, A. Mukhopaadhyay, D.R. Boer, S. Teixeira, V.L. Shnyrov, I. Moura, J.J. Moura, M.J. Romao, J. Trincao, S.A. Bursakov, Cobalt-, zinc- and iron-bound forms of adenylate kinase (AK) from the sulfate-reducing bacterium Desulfovibrio gigas: purification, crystallization and preliminary X-ray diffraction analysis, Acta crystallographica. Section F, Structural biology and crystallization communications, 65 (2009) 926-929.
[83] J. Lampreia, G. Fauque, N. Speich, C. Dahl, I. Moura, H.G. Truper, J.J. Moura, Spectroscopic studies on APS reductase isolated from the hyperthermophilic sulfate-reducing archaebacterium Archaeglobus fulgidus, Biochem Bioph Res Co, 181 (1991) 342-347.
[84] A. Mukhopadhyay, A.V. Kladova, S.A. Bursakov, O.Y. Gavel, J.J. Calvete, V.L. Shnyrov, I. Moura, J.J. Moura, M.J. Romao, J. Trincao, Crystal structure of the zinc-, cobalt-, and iron-containing adenylate kinase from Desulfovibrio gigas: a novel metal-containing adenylate kinase from Gram-negative bacteria, Journal of biological inorganic chemistry : JBIC : a publication of the Society of Biological Inorganic Chemistry, 16 (2011) 51-61.
[85] B. Ollivier, J.-L. Cayol, G. Fauque, Sulphate-reducing bacteria from oil fields environments and deep-sea hydrothermal vents, in: L.L. Barton, W.A. Hamilton (Eds.) Sulphate-Reducing Bacteria: Environmental and Engineered Systems, Cambridge University Press, 2007.
[86] N.M. Cerqueira, P.J. Gonzalez, C.D. Brondino, M.J. Romao, C.C. Romao, I. Moura, J.J. Moura, The effect of the sixth sulfur ligand in the catalytic mechanism of periplasmic nitrate reductase, Journal of computational chemistry, 30 (2009) 2466-2484.
[87] S. Dell'Acqua, S.R. Pauleta, I. Moura, J.J. Moura, The tetranuclear copper active site of nitrous oxide reductase: the CuZ center, Journal of biological inorganic chemistry : JBIC : a publication of the Society of Biological Inorganic Chemistry, 16 (2011) 183-194.
[88] M.G. Rivas, P.J. Gonzalez, C.D. Brondino, J.J. Moura, I. Moura, EPR characterization of the molybdenum(V) forms of formate dehydrogenase from Desulfovibrio desulfuricans ATCC 27774 upon formate reduction, Journal of inorganic biochemistry, 101 (2007) 1617-1622.
[89] P.M. Matias, I.A. Pereira, C.M. Soares, M.A. Carrondo, Sulphate respiration from hydrogen in Desulfovibrio bacteria: a structural biology overview, Progress in biophysics and molecular biology, 89 (2005) 292-329.
[90] B.A. Barata, J. LeGall, J.J. Moura, Aldehyde oxidoreductase activity in Desulfovibrio gigas: in vitro reconstitution of an electron-transfer chain from aldehydes to the production of molecular hydrogen, Biochemistry, 32 (1993) 11559-11568.
[91] I.B. Beech, J. Sunner, Biocorrosion: towards understanding interactions between biofilms and metals, Curr Opin Biotechnol, 15 (2004) 181-186.
[92] I.B. Beech, J.A. Sunner, K. Hiraoka, Microbe-surface interactions in biofouling and biocorrosion processes, International microbiology : the official journal of the Spanish Society for Microbiology, 8 (2005) 157-168.
[93] K. Sauer, The genomics and proteomics of biofilm formation, Genome biology, 4 (2003) 219.
[94] I.B. Beech, C.C. Gaylarde, Recent advances in the study of biocorrosion: an overview, Revista de Microbiologia, 30 (1999) 117-190.
[95] H.C. Flemming, J. Wingender, Relevance of microbial extracellular polymeric substances (EPSs)--Part I: Structural and ecological aspects, Water Sci Technol., 43 (2001) 1-8.
[96] H.C. Flemming, J. Wingender, The biofilm matrix, Nat Rev Microbiol, 8 (2010) 623-633.
[97] B. Little, J. Lee, R. Ray, A review of 'green' strategies to prevent or mitigate microbiologically influenced corrosion, Biofouling, 23 (2007) 87-97.
[98] C.M. Cordas, L.T. Guerra, C. Xavier, J.J.G. Moura, Electroactive biofilms of sulphate reducing bacteria, Electrochimica Acta, 54 (2008) 29-34.
[99] B.C. Kim, C. Leang, Y.H. Ding, R.H. Glaven, M.V. Coppi, D.R. Lovley, OmcF, a putative c-Type monoheme outer membrane cytochrome required for the expression of other outer membrane cytochromes in Geobacter sulfurreducens, J Bacteriol, 187 (2005) 4505-4513.
[100] M.Y. El-Naggar, G. Wanger, K.M. Leung, T.D. Yuzvinsky, G. Southam, J. Yang, W.M. Lau, K.H. Nealson, Y.A. Gorby, Electrical transport along bacterial nanowires from Shewanella oneidensis MR-1, Proceedings of the National Academy of Sciences of the United States of America, 107 (2010) 18127-18131.

[101] Y.A. Gorby, S. Yanina, J.S. McLean, K.M. Rosso, D. Moyles, A. Dohnalkova, T.J. Beveridge, I.S. Chang, B.H. Kim, K.S. Kim, D.E. Culley, S.B. Reed, M.F. Romine, D.A. Saffarini, E.A. Hill, L. Shi, D.A. Elias, D.W. Kennedy, G. Pinchuk, K. Watanabe, S. Ishii, B. Logan, K.H. Nealson, J.K. Fredrickson, Electrically conductive bacterial nanowires produced by Shewanella oneidensis strain MR-1 and other microorganisms, Proceedings of the National Academy of Sciences of the United States of America, 103 (2006) 11358-11363.
[102] G. Reguera, K.D. McCarthy, T. Mehta, J.S. Nicoll, M.T. Tuominen, D.R. Lovley, Extracellular electron transfer via microbial nanowires, Nature, 435 (2005) 1098-1101.
[103] G. Reguera, K.P. Nevin, J.S. Nicoll, S.F. Covalla, T.L. Woodard, D.R. Lovley, Biofilm and nanowire production leads to increased current in Geobacter sulfurreducens fuel cells, Appl Environ Microbiol, 72 (2006) 7345-7348.
[104] I.B. Beech, V. Zinkevich, R. Tapper, R. Gubner, R. Avci, Study of the interaction of sulphate-reducing bacteria exopolymers with iron using X-ray photoelectron spectroscopy and time-of-flight secondary ionisation mass spectrometry, J Microbiol Methods, 36 (1999) 3-10.
[105] C.M. Lacerda, K.F. Reardon, Environmental proteomics: applications of proteome profiling in environmental microbiology and biotechnology, Briefings in functional genomics & proteomics, 8 (2009) 75-87.
[106] M.A. Patrauchan, S.A. Sarkisova, M.J. Franklin, Strain-specific proteome responses of Pseudomonas aeruginosa to biofilm-associated growth and to calcium, Microbiology, 153 (2007) 3838-3851.
[107] S.P. Diggle, R.E. Stacey, C. Dodd, M. Camara, P. Williams, K. Winzer, The galactophilic lectin, LecA, contributes to biofilm development in Pseudomonas aeruginosa, Environmental microbiology, 8 (2006) 1095-1104.
[108] D.J. Lynch, T.L. Fountain, J.E. Mazurkiewicz, J.A. Banas, Glucan-binding proteins are essential for shaping Streptococcus mutans biofilm architecture, FEMS microbiology letters, 268 (2007) 158-165.
[109] I. Lasa, J.R. Penadés, Bap: A family of surface proteins involved in biofilm formation, Research in Microbiology, 157 (2006) 99-107.
[110] P. Larsen, J.L. Nielsen, M.S. Dueholm, R. Wetzel, D. Otzen, P.H. Nielsen, Amyloid adhesins are abundant in natural biofilms, Environmental microbiology, 9 (2007) 3077-3090.
[111] G. Reguera, R.B. Pollina, J.S. Nicoll, D.R. Lovley, Possible nonconductive role of Geobacter sulfurreducens pilus nanowires in biofilm formation, J Bacteriol, 189 (2007) 2125-2127.
[112] C. Mayer, R. Moritz, C. Kirschner, W. Borchard, R. Maibaum, J. Wingender, H.C. Flemming, The role of intermolecular interactions: studies on model systems for bacterial biofilms, International Journal of Biological Macromolecules, 26 (1999) 3-16.
[113] J. Wingender, T.R. Neu, H.C. Flemming, Microbial Extracellular Polymeric Substances: Characterization, Structure, and Function, Springer-Verlag GmbH, 1999.
[114] J. Wingender, T.R. Neu, H.C. Flemming, What are Bacterial Extracellular Polymeric Substances?, in: J. Wingender, T. Neu, H.-C. Flemming (Eds.) Microbial Extracellular Polymeric Substances, Springer Berlin Heidelberg, 1999, pp. 1-19.
[115] E. Karatan, P. Watnick, Signals, Regulatory Networks, and Materials That Build and Break Bacterial Biofilms, Microbiology and Molecular Biology Reviews, 73 (2009) 310-347.
[116] X. Zhang, P.L. Bishop, Biodegradability of biofilm extracellular polymeric substances, Chemosphere, 50 (2003) 63-69.
[117] I.W. Sutherland, The biofilm matrix – an immobilized but dynamic microbial environment, Trends in Microbiology, 9 (2001) 222-227.
[118] E.D. van Hullebusch, M.H. Zandvoort, P.N.L. Lens, Metal immobilisation by biofilms: Mechanisms and analytical tools, Re/Views in Environmental Science and Bio/Technology, 2 (2003) 9-33.
[119] M. Marvasi, P.T. Visscher, L. Casillas Martinez, Exopolymeric substances (EPS) from Bacillus subtilis : polymers and genes encoding their synthesis, FEMS Microbiology Letters, 313 (2010) 1-9.
[120] W. Zhang, D.E. Culley, L. Nie, J.C.M. Scholten, Comparative transcriptome analysis of Desulfovibrio vulgaris grown in planktonic culture and mature biofilm on a steel surface, Appl Microbiol Biotechnol, 76 (2007) 447-457.
[121] J.B. Xavier, K.R. Foster, Cooperation and conflict in microbial biofilms, Proceedings of the National Academy of Sciences, 104 (2007) 876-881.
[122] B. Frølund, R. Palmgren, K. Keiding, P.H. Nielsen, Extraction of extracellular polymers from activated sludge using a cation exchange resin, Water Research, 30 (1996) 1749-1758.
[123] S. Molin, T. Tolker-Nielsen, Gene transfer occurs with enhanced efficiency in biofilms and induces enhanced stabilisation of the biofilm structure, Curr Opin Biotechnol, 14 (2003) 255-261.
[124] L. Yang, K.B. Barken, M.E. Skindersoe, A.B. Christensen, M. Givskov, T. Tolker-Nielsen, Effects of iron on DNA release and biofilm development by Pseudomonas aeruginosa, Microbiology, 153 (2007) 1318-1328.
[125] H. Mulcahy, L. Charron-Mazenod, S. Lewenza, Extracellular DNA chelates cations and induces antibiotic resistance in Pseudomonas aeruginosa biofilms, PLoS pathogens, 4 (2008) e1000213.

[126] W. Sand, T. Gehrke, Extracellular polymeric substances mediate bioleaching/biocorrosion via interfacial processes involving iron(III) ions and acidophilic bacteria, Research in Microbiology, 157 (2006) 49-56.
[127] M. Faimali, E. Chelossi, G. Pavanello, A. Benedetti, I. Vandecandelaere, P. De Vos, P. Vandamme, A. Mollica, Electrochemical activity and bacterial diversity of natural marine biofilm in laboratory closed-systems, Bioelectrochemistry, 78 (2010) 30-38.
[128] E. Marsili, J.B. Rollefson, D.B. Baron, R.M. Hozalski, D.R. Bond, Microbial biofilm voltammetry: direct electrochemical characterization of catalytic electrode-attached biofilms, Appl Environ Microbiol, 74 (2008) 7329-7337.
[129] H. Xiao, F. Mansfeld, Evaluation of Coating Degradation with Electrochemical Impedance Spectroscopy and Electrochemical Noise Analysis, Journal of The Electrochemical Society, 141 (1994) 2332-2337.
[130] R.A. Cottis, Interpretation of Electrochemical Noise Data, Corrosion, 57 (2001) 265-285.
[131] C.C. Dupont-Gillain, K.M. Mc Evoy, M. Henry, P. Bertrand, Surface spectroscopy of adsorbed proteins: input of data treatment by principal component analysis, Journal of materials science. Materials in medicine, 21 (2010) 955-961.
[132] C. Poleunis, C. Compere, P. Bertrand, Time-of-flight secondary ion mass spectrometry: characterisation of stainless steel surfaces immersed in natural seawater, J Microbiol Methods, 48 (2002) 195-205.
[133] S.J. Yuan, S.O. Pehkonen, AFM study of microbial colonization and its deleterious effect on 304 stainless steel by Pseudomonas NCIMB 2021 and Desulfovibrio desulfuricans in simulated seawater, Corrosion Science, 51 (2009) 1372-1385.
[134] F. Hook, M. Rodahl, P. Brzezinski, B. Kasemo, Measurements Using the Quartz Crystal Microbalance Technique of Ferritin Monolayers on Methyl-Thiolated Gold: Dependence of Energy Dissipation and Saturation Coverage on Salt Concentration, Journal of colloid and interface science, 208 (1998) 63-67.
[135] B.V. Kjellerup, B.H. Olesen, J.L. Nielsen, K.R. Sowers, P.H. Nielsen, In situ detection of bacteria involved in cathodic depolarization and stainless steel surface corrosion using microautoradiography, Journal of applied microbiology, 105 (2008) 2231-2238.
[136] J.M. Suflita, D.F. Aktas, A.L. Oldham, B.M. Perez-Ibarra, K. Duncan, Molecular tools to track bacteria responsible for fuel deterioration and microbiologically influenced corrosion, Biofouling, 28 (2012) 1003-1010.
[137] W.V. Sigler, C. Miniaci, J. Zeyer, Electrophoresis time impacts the denaturing gradient gel electrophoresis-based assessment of bacterial community structure, J Microbiol Methods, 57 (2004) 17-22.
[138] I. Neria-Gonzalez, E.T. Wang, F. Ramirez, J.M. Romero, C. Hernandez-Rodriguez, Characterization of bacterial community associated to biofilms of corroded oil pipelines from the southeast of Mexico, Anaerobe, 12 (2006) 122-133.
[139] B.S. Stevenson, H.S. Drilling, P.A. Lawson, K.E. Duncan, V.A. Parisi, J.M. Suflita, Microbial communities in bulk fluids and biofilms of an oil facility have similar composition but different structure, Environmental microbiology, 13 (2011) 1078-1090.
[140] A. Agrawal, K. Vanbroekhoven, B. Lal, Diversity of culturable sulfidogenic bacteria in two oil-water separation tanks in the north-eastern oil fields of India, Anaerobe, 16 (2010) 12-18.
[141] H.K. Ly, F. Harnisch, S.F. Hong, U. Schroder, P. Hildebrandt, D. Millo, Unraveling the interfacial electron transfer dynamics of electroactive microbial biofilms using surface-enhanced Raman spectroscopy, ChemSusChem, 6 (2013) 487-492.
[142] C. Rubio, C. Ott, C. Amiel, I. Dupont-Moral, J. Travert, L. Mariey, Sulfato/thiosulfato reducing bacteria characterization by FT-IR spectroscopy: a new approach to biocorrosion control, J Microbiol Methods, 64 (2006) 287-296.
[143] S.E. Coetser, T.E. Cloete, Biofouling and biocorrosion in industrial water systems, Critical reviews in microbiology, 31 (2005) 213-232.
[144] S.R. Hiibel, L.P. Pereyra, L.Y. Inman, A. Tischer, D.J. Reisman, K.F. Reardon, A. Pruden, Microbial community analysis of two field-scale sulfate-reducing bioreactors treating mine drainage, Environmental microbiology, 10 (2008) 2087-2097.
[145] J.S. Dickschat, Quorum sensing and bacterial biofilms, Natural product reports, 27 (2010) 343-369.
[146] C. Hubert, G. Voordouw, Oil field souring control by nitrate-reducing Sulfurospirillum spp. that outcompete sulfate-reducing bacteria for organic electron donors, Appl Environ Microbiol, 73 (2007) 2644-2652.
[147] A.J.M. Muyzer G Fau - Stams, A.J. Stams, The ecology and biotechnology of sulphate-reducing bacteria, Nat Rev Microbiol, 6 (2008) 14.
[148] V.V. Zinkevich, I.B. Beech, Screening of sulfate-reducing bacteria in colonoscopy samples from healthy and colitic human gut mucosa, FEMS microbiology ecology, 34 (2000) 147-155.
[149] J.D. Cline, Spectrophotometric Determination of Hydrogen Sulfide in Natural Waters, Limnology and Oceanography, 14 (1969) 454-458.
[150] A. Aguilera, V. Souza-Egipsy, P. San Martin-Uriz, R. Amils, Extraction of extracellular polymeric substances from extreme acidic microbial biofilms, Appl Microbiol Biotechnol, 78 (2008) 1079-1088.

[151] F. Höök, M. Rodahl, P. Brzezinski, B. Kasemo, Energy Dissipation Kinetics for Protein and Antibody−Antigen Adsorption under Shear Oscillation on a Quartz Crystal Microbalance, Langmuir, 14 (1998) 5.
[152] S. Kjelleberg, S. Molin, Is there a role for quorum sensing signals in bacterial biofilms?, Curr Opin Microbiol, 5 (2002) 254-258.
[153] I. Majumdar, F. D'Souza, N.B. Bhosle, Microbial exopolysaccharides: Effect on corrosion and partial chemical characterization, J Indian Inst. Sci., 79 (1999) 11.
[154] J.J.G. Moura, P. Gonzalez, I. Moura, G. Fauque, Dissimilatory nitrate and nitrite ammonification by sulphate-reducing eubacteria, in: L.L. Barton, W.A. Hamilton (Eds.) Sulphate-reducing Bacteria, Cambridge University Press, 2007.
[155] H. Ma, X. Cheng, G. Li, S. Chen, Z. Quan, S. Zhao, L. Niu, The influence of hydrogen sulfide on corrosion of iron under different conditions, Corrosion Science, 42 (2000) 14.
[156] L.R. Hilbert, T. Hemmingsen, L.V. Nielsen, S. Richter, When can Electrochemical Techniques give Reliable Corrosion Rates on Carbon Steel in Sulfide Media?, in: Corrosion2005, USA, 2005.
[157] F. Kuang, J. Wang, L. Yan, D. Zhang, Effects of sulfate-reducing bacteria on the corrosion behavior of carbon steel, Electrochimica Acta, 52 (2007) 6084-6088.
[158] Z.H. Dong, T. Liu, H.F. Liu, Influence of EPS isolated from thermophilic sulphate-reducing bacteria on carbon steel corrosion, Biofouling, 27 (2011) 487-495.
[159] A.M. Belu, D.J. Graham, D.G. Castner, Time-of-flight secondary ion mass spectrometry: techniques and applications for the characterization of biomaterial surfaces, Biomaterials, 24 (2003) 3635-3653.
[160] J.L.S. Lee, I.S. Gilmore, M.P. Seah, Quantification and methodology issues in multivariate analysis of ToF-SIMS data for mixed organic systems, Surface and Interface Analysis, 40 (2008) 1-14.
[161] E.S.F. Berman, L. Wu, S.L. Fortson, K.S. Kulp, D.O. Nelson, K.J. Wu, Chemometric and statistical analyses of ToF-SIMS spectra of increasingly complex biological samples, Surface and Interface Analysis, 41 (2009) 97-104.
[162] M. Henry, P. Bertrand, Surface composition of insulin and albumin adsorbed on polymer substrates as revealed by multivariate analysis of ToF-SIMS data, Surface and Interface Analysis, 41 (2009) 105-113.
[163] D.J. Graham, D.G. Castner, Multivariate analysis of ToF-SIMS data from multicomponent systems: the why, when, and how, Biointerphases, 7 (2012) 49.
[164] J.C. Ingram, W.F. Bauer, R.M. Lehman, S.P. O'Connell, A.D. Shaw, Detection of fatty acids from intact microorganisms by molecular beam static secondary ion mass spectrometry, J Microbiol Methods, 53 (2003) 295-307.
[165] H. Jungnickel, E.A. Jones, N.P. Lockyer, S.G. Oliver, G.M. Stephens, J.C. Vickerman, Application of TOF-SIMS with chemometrics to discriminate between four different yeast strains from the species Candida glabrata and Saccharomyces cerevisiae, Anal Chem, 77 (2005) 1740-1745.
[166] A. Rossi, B. Elsener, G. Hähner, M. Textor, N.D. Spencer, XPS, AES and ToF-SIMS investigation of surface films and the role of inclusions on pitting corrosion in austenitic stainless steels, Surface and Interface Analysis, 29 (2000) 460-467.
[167] B. Garg, S.-L. Lei, S.-C. Liu, T. Bisht, J.-Y. Liu, Y.-C. Ling, Rapid identification of trimethyl and triethyl amines using sulphonic acidic ionic liquids: A time-of-flight secondary ion mass spectrometry study of fragmentation reactions, Analytica Chimica Acta, 757 (2012) 48-55.
[168] N. Akar, B. Asar, N. Dizge, I. Koyuncu, Investigation of characterization and biofouling properties of PES membrane containing selenium and copper nanoparticles, Journal of Membrane Science, 437 (2013) 216-226.
[169] E. Zhang, L. Yang, Microstructure, mechanical properties and bio-corrosion properties of Mg–Zn–Mn–Ca alloy for biomedical application, Materials Science and Engineering: A, 497 (2008) 111-118.
[170] P.G. Rouxhet, N. Mozes, P.B. Dengis, Y.F. Dufrêne, P.A. Gerin, M.J. Genet, Application of X-ray photoelectron spectroscopy to microorganisms, Colloids and Surfaces B: Biointerfaces, 2 (1994) 347-369.
[171] A.M. Baty, P.A. Suci, B.J. Tyler, G.G. Geesey, Investigation of Mussel Adhesive Protein Adsorption on Polystyrene and Poly(octadecyl methacrylate) Using Angle Dependent XPS, ATR-FTIR, and AFM, Journal of Colloid and Interface Science, 177 (1996) 307-315.
[172] P.G. Rouxhet, M.J. Genet, XPS analysis of bio-organic systems, Surface and Interface Analysis, 43 (2011) 1453-1470.
[173] J. Osán, J. de Hoog, P. Van Espen, I. Szalóki, C.U. Ro, R. Van Grieken, Evaluation of energy-dispersive x-ray spectra of low-Z elements from electron-probe microanalysis of individual particles, X-Ray Spectrometry, 30 (2001) 419-426.
[174] P. Van Espen, in: R. Grieken, A. Markowicz (Eds.) Handbook of X-ray spectrometry: methods and techniques, Marcel Dekker, 1993.
[175] G.F. Bastin, J.M. Dijkstra, H.J.M. Heijligers, PROZA96: an improved matrix correction program for electron probe microanalysis, based on a double Gaussian φ(ρz) approach, X-Ray Spectrometry, 27 (1998) 3-10.

[176] G. Boon, G. Bastin, Quantitative Analysis of Thin Specimens in the TEM Using a ?(?z)-Model, Microchimica Acta, 147 (2004).
[177] T. Kyotani, Identification of individual Si-rich particles derived from Kosa aerosol by the alkali elemental composition, Bulletin of the Chemical Society of Japan, 74 (2001) 723 -729
[178] E. Tokareva, A. Pranovich, B. Holmbom, Characteristic fragment ions from lignin and polysaccharides in ToF–SIMS, Wood Sci Technol, 45 (2011) 767-785.
[179] D.T. Wright, A. Oren, Nonphotosynthetic Bacteria and the Formation of Carbonates and Evaporites Through Time, Geomicrobiology Journal, 22 (2005) 27-53.
[180] O. Braissant, A.W. Decho, C. Dupraz, C. Glunk, K.M. Przekop, P.T. Visscher, Exopolymeric substances of sulfate-reducing bacteria: Interactions with calcium at alkaline pH and implication for formation of carbonate minerals, Geobiology, 5 (2007) 401-411.
[181] P.T. Visscher, J.F. Stolz, Microbial mats as bioreactors: populations, processes, and products, Palaeogeography, Palaeoclimatology, Palaeoecology, 219 (2005) 87-100.
[182] P. Saravanan, S. Jayachandran, Preliminary characterization of exopolysaccharides produced by a marine biofilm-forming bacterium Pseudoalteromonas ruthenica (SBT 033), Letters in Applied Microbiology, 46 (2008) 1-6.
[183] M. Toyofuku, B. Roschitzki, K. Riedel, L. Eberl, Identification of Proteins Associated with the Pseudomonas aeruginosa Biofilm Extracellular Matrix, Journal of Proteome Research, 11 (2012) 4906-4915.
[184] I.B. Beech, L. Hanjagsit, M. Kalaji, A.L. Neal, V. Zinkevich, Chemical and structural characterization of exopolymers produced by Pseudomonas sp. NCIMB 2021 in continuous culture, Microbiology, 145 (1999) 1491-1497.
[185] R. Stadler, W. Fuerbeth, K. Harneit, M. Grooters, M. Woellbrink, W. Sand, First evaluation of the applicability of microbial extracellular polymeric substances for corrosion protection of metal substrates, Electrochimica Acta, 54 (2008) 91-99.
[186] R. Stadler, L. Wei, W. Fürbeth, M. Grooters, A. Kuklinski, Influence of bacterial exopolymers on cell adhesion of Desulfovibrio vulgaris on high alloyed steel: Corrosion inhibition by extracellular polymeric substances (EPS), Materials and Corrosion, 61 (2010) 1008–1016.
[187] R. Gubner, I.B. Beech, The effect of extracellular polymeric substances on the attachment of Pseudomonas NCIMB 2021 to AISI 304 and 316 stainless steel, Biofouling, 15 (2000) 25-36.
[188] V. Aguie-Beghin, Y. Adriaensen, N. Peron, M. Valade, P. Rouxhet, R. Douillard, Structure and chemical composition of layers adsorbed at interfaces with champagne, Journal of agricultural and food chemistry, 57 (2009) 10399-10407.
[189] Y.F. Dufrêne, A. van der Wal, W. Norde, P.G. Rouxhet, X-ray photoelectron spectroscopy analysis of whole cells and isolated cell walls of gram-positive bacteria: comparison with biochemical analysis, J Bacteriol, 179 (1997) 1023–1028.
[190] F. Ahimou, C.J. Boonaert, Y. Adriaensen, P. Jacques, P. Thonart, M. Paquot, P.G. Rouxhet, XPS analysis of chemical functions at the surface of Bacillus subtilis, Journal of colloid and interface science, 309 (2007) 49-55.
[191] L. Leone, J. Loring, S. Sjöberg, P. Persson, A. Shchukarev, Surface characterization of the Gram-positive bacteriaBacillus subtilis-an XPS study, Surface and Interface Analysis, 38 (2006) 202-205.
[192] C.J.P. Boonaert, P.G. Rouxhet, Surface of Lactic Acid Bacteria: Relationships between Chemical Composition and Physicochemical Properties, Appl Environ Microbiol, 66 (2000) 2548-2554.
[193] C.M. Pradier, C. Rubio, C. Poleunis, P. Bertrand, P. Marcus, C. Compère, Surface Characterization of Three Marine Bacterial Strains by Fourier Transform IR, X-ray Photoelectron Spectroscopy, and Time-of-Flight Secondary-Ion Mass Spectrometry, Correlation with Adhesion on Stainless Steel Surfaces, The Journal of Physical Chemistry B, 109 (2005) 9540-9549.
[194] H.C. van der Mei, J. de Vries, H.J. Busscher, X-ray photoelectron spectroscopy for the study of microbial cell surfaces, Surface Science Reports, 39 (2000) 1-24.
[195] M. DuBois, K.A. Gilles, J.K. Hamilton, P.A. Rebers, F. Smith, Colorimetric Method for Determination of Sugars and Related Substances, Anal Chem, 28 (1956) 350-356.
[196] T.M.C.C. Filisetti-Cozzi, N.C. Carpita, Measurement of uronic acids without interference from neutral sugars, Analytical Biochemistry, 197 (1991) 157-162.
[197] M.M. Bradford, A rapid and sensitive method for the quantitation of microgram quantities of protein utilizing the principle of protein-dye binding.
[198] K. Burton, A Studyof the Conditions and Mechanism of the Diphenylamine Reaction for the Colorimetric Estimation of Deoxyribonucleic Acid, Biochem. J., 62 (1956) 315-323.
[199] N. Dyballa, S. Metzger, Fast and sensitive colloidal coomassie G-250 staining for proteins in polyacrylamide gels, Journal of visualized experiments : JoVE, (2009).
[200] C. Sohlenkamp, I.M. López-Lara, O. Geiger, Biosynthesis of phosphatidylcholine in bacteria, Progress in Lipid Research, 42 (2003) 115-162.

[201] Y.F. Dufrêne, C.J.P. Boonaert, P.G. Rouxhet, Surface analysis by X-ray photoelectron spectroscopy in study of bioadhesion and biofilms, in: J.D. Ron (Ed.) Methods in Enzymology, Academic Press, 1999, pp. 375-389.
[202] J. Zhou, Q. He, C.l. Hemme, A. Mukhopadhyay, K. Hillesland, A. Zhou, Z. He, J.D. Van Nostrand, T.C. Hazen, D.A. Stahl, J.D. Wall, A.P. Arkin, How sulphate-reducing microorganisms cope with stress: lessons from systems biology, Nat Rev Microbiol, 9 (2011) 1740-1534.
[203] V. Zinkevich, I. Bogdarina, H. Kang, M.A.W. Hill, R. Tapper, I.B. Beech, Characterisation of exopolymers produced by different isolates of marine sulphate-reducing bacteria, International Biodeterioration & Biodegradation, 37 (1996) 163-172.
[204] C.M.C.F. Silveira, Development of electrochemical nitrite biosensors using cytochrome c nitrite reductase from Desulfovibrio desulfuricans ATCC 27774, in: Chemistry, Universidade Nova de Lisboa, Lisbon, 2011, pp. 238.
[205] S. Ray, A.G. Shard, Quantitative analysis of adsorbed proteins by X-ray photoelectron spectroscopy, Anal Chem, 83 (2011) 8659-8666.
[206] D.G. Castner, B.D. Ratner, Biomedical surface science: Foundations to frontiers, Surface Science, 500 (2002) 28-60.
[207] M.M. Browne, G.V. Lubarsky, M.R. Davidson, R.H. Bradley, Protein adsorption onto polystyrene surfaces studied by XPS and AFM, Surface Science, 553 (2004) 155-167.
[208] R. Michel, D.G. Castner, Advances in time-of-flight secondary ion mass spectrometry analysis of protein films, Surface and Interface Analysis, 38 (2006) 1386-1392.
[209] F. Caruso, D.N. Furlong, P. Kingshott, Characterization of Ferritin Adsorption onto Gold, Journal of colloid and interface science, 186 (1997) 129-140.
[210] R. Schumacher, The Quartz Microbalance: A Novel Approach to the In-Situ Investigation of Interfacial Phenomena at the Solid/Liquid Junction [New Analytical Methods (40)], Angewandte Chemie International Edition in English, 29 (1990) 329-343.
[211] D.A. Elias, J.M. Suflita, M.J. McInerney, L.R. Krumholz, Periplasmic cytochrome c3 of Desulfovibrio vulgaris is directly involved in H2-mediated metal but not sulfate reduction, Appl Environ Microbiol, 70 (2004) 413-420.
[212] R.O. Louro, Proton thrusters: overview of the structural and functional features of soluble tetrahaem cytochromes c3, Journal of biological inorganic chemistry : JBIC : a publication of the Society of Biological Inorganic Chemistry, 12 (2007) 1-10.
[213] M.V. Pattarkine, J.J. Tanner, C.A. Bottoms, Y.H. Lee, J.D. Wall, Desulfovibrio desulfuricans G20 tetraheme cytochrome structure at 1.5 Angstrom and cytochrome interaction with metal complexes, Journal of molecular biology, 358 (2006) 1314-1327.
[214] M. Brugna, M.T. Giudici-Orticoni, S. Spinelli, K. Brown, M. Tegoni, M. Bruschi, Kinetics and interaction studies between cytochrome c3 and Fe-only hydrogenase from Desulfovibrio vulgaris hildenborough, Proteins: Structure, Function, and Bioinformatics, 33 (1998) 590-600.
[215] J.M. Odom, H.D. Peck, Hydrogenase, Electron-Transfer Proteins, and Energy Coupling in the Sulfate-Reducing Bacteria Desulfovibrio, Annu Rev Microbiol, 38 (1984) 551-592.
[216] R.D. Bryant, W. Jansen, J. Boivin, E.J. Laishley, J.W. Costerton, Effect of hydrogenase and mixed sulfate-reducing bacterial populations on the corrosion of steel, Appl Environ Microbiol, 57 (1991) 2804-2809.
[217] C. Chatelus, P. Carrier, P. Saignes, M.F. Libert, Y. Berlier, P.A. Lespinat, G. Fauque, J. Legall, Hydrogenase activity in aged, nonviable Desulfovibrio vulgaris cultures and its significance in anaerobic biocorrosion, Appl Environ Microbiol, 53 (1987) 1708-1710.
[218] F. Höök, M. Rodahl, P. Brzezinski, B. Kasemo, Energy Dissipation Kinetics for Protein and Antibody−Antigen Adsorption under Shear Oscillation on a Quartz Crystal Microbalance, Langmuir, 14 (1998) 729-734.
[219] G. Sauerbrey, Verwendung von Schwingquarzen zur Wägung dünner Schichten und zur Mikrowägung, Z. Physik, 155 (1959) 206-222.